UCC

University College Cork, Ireland
Coláiste na hOllscoile Corcaigh

Correlated electron transport across atomic and molecular tunnel junctions

Shane Mc Dermott

BSC

Thesis submitted for the degree of
Doctor of Philosophy

NATIONAL UNIVERSITY OF IRELAND, CORK

SCHOOL OF SCIENCE

DEPARTMENT OF PHYSICS

TYNDALL NATIONAL INSTITUTE

January 2018

Head of Department:	Professor John McInerney
Supervisor:	Professor Jim Greer

Contents

List of Figures

List of Tables

List of Publications

1. S.McDermott, C.B. George, G.Fagas, J.C. Greer, and M.A. Ratner, "Tunnel currents across silane diamines/dithiols and alkane diamines/dithiols: A comparative computational study," *The Journal of Physical Chemistry C*, vol.113, no.2, pp.744-750, 2008

2. I.Yeriskin, S.McDermott, R.J. Bartlett, G.Fagas, and J.C. Greer, "Electronegativity and Electron Currents in Molecular Tunnel Junctions†," *J. Phys. Chem. C*, vol.114, pp.20564-20568, Sep 2010

3. S.McDermott and J.C. Greer, "Many-electron scattering applied to atomic point contacts," *J. Phys.: Condens. Matter*, vol.24, p.125602, Mar. 2012

I, Shane Mc Dermott, certify that this thesis is my own work and has not been submitted for another degree at University College Cork or elsewhere.

_____

Shane Mc Dermott

Acknowledgements

I'd like to thank my family and Ted McGowan for their support. Also would like thank my supervisor Jim Greer and everyone in the ETG group for their help.

Abstract

As transistors continue to miniaturise the importance of describing electronics on an atomic scale increases. A molecular junction consists of a molecule connected to to metal electrodes via linker molecules and may be thought of as the prototype system for electronics on a few nanometre length scale. For charge transport calculations such systems are usually treated with a single particle approximation such as NEGF + DFT non-equilibrium Green's function plus density functional theory. Typical single particle treatmentsare incomplete due to approximations made in the treatment of the electronic structure leading to discrepancies between theory and experiment by orders of magnitude, believed to be due to electron correlation. A solution to this is an accurate many body treatment of charge transport explicitly accounting for electron correlation. In this thesis the comparison of many body method MECS (Many Electron Correlated Scattering) to experiment and single particle methods, in particular the (NEGF+DFT) is performed. Comparison with single particle methods is established for alkane-based and silane-based molecular junctions utilising both thiol and amine linker molecules. In addition, components of the method such as electrostatic behaviour and screening, electronegativity, sensitivity to boundary conditions, and the level of treatment of electron correlation are tested. Comparisons with single particle methods yield agreement for systems with a lower degree of electron correlation such as alkane-based molecular junctions, with a larger disagreement between single particle and MECS methods for the moderately correlated silane-based junctions. A complex band structure analysis was performed on silane and alkane junctions with an emphasis on the dependence with respect to the linker molecules was undertaken to further investigate energy level alignment and demonstrate how alignment is affected by end groups. Electrostatic calculations have been used to investigate and quantify the effects of the screening effect on

point contact and molecular junction voltages focussing on the screening length into the metal contacts was performed. This allows for more accurate estimates of the applied voltage across the junctions. The application of single particle open system boundary conditions through the use of the Wigner function is shown to be robust with respect to electrode dimensions and geometry, and is demonstrated to have little impact on the current for molecular junctions. Electronegativity calculations consist of a hexatriene-di-thiol model system with variable treatment of the electron correlation in comparison with conventional electronic structure treatments and demonstrate that correcting ionisation potentials and electron affinities with electron correlation leads to inreasing the overlap to the exact one-electron reduced density matrix thereby improving theoretical predictions of electron currents on the nanoscale.

Chapter 1

Introduction

Microelectronics has continued on the path of minaturisation of transistors for improvements in circuit performance and cost per function over the last 50 years. The transition to quantum scale devices is desired, where the principal aim is to design transistors on atomic scale lengths.

These junctions could include logic and memory and could allow for higher device density on chip while increasing function and lowering cost per unit. Molecular junctions provide a theoretical and experimental laboratory that allows for exploration of atomic scale limits that allows for the continuation of Moore's law [1] into the atomic scale.

A molecular junction consists of a molecule placed between two electrodes (usually metal). The molecule can be organic, inorganic or a polymer chain and is attached to the electrodes via linker molecules. A principal aim of the development of molecular electronics is to utilise molecular junctions to improve common transistor components in devices. Electronic processes at the molecular level differ from mesoscopic scale devices not just in length scale but also in physical operation. This presents both theoretical and experimental challenges. A requirement is that molecular junctions can be easily reproduced and are stable while performing the diverse functionality of conventional computational architecture. From a materials point of view molecular devices are constructed from the bottom up atomic scale using small molecular components to form larger devices. This is in contrast to the top-down traditional method where larger devices are minaturised. Therefore new difficulties arise regarding how to create molecular devices from single molecules in addition to many new challenges(i.e. integration into large scale complex architectures and theoretically modelling the behaviour of junctions accurately).

Despite these difficulties molecular electronics offer many opportunities. These devices operate in the quantum regime where the small dimensions of devices give rise to unexpected phenomena with potential for new device applications. This

offers the possibility of powerful nanoelectronics technology in the near future.

Possible applications include molecular photochromic switchs which open or close depending on the frequency of electromagnetic radiation incident upon it, with resistance increasing by up to three orders of magnitude in the closed position [2, 3]. Such molecular switches could be arranged in arrays to implement logic operations. However due to the mechanical nature of the molecular switches the switching speed is limited. In contrast by using a transistor that relies on charge transfer greatly improves switching speeds and should in principle be achievable. The first example of a molecular transistors was proposed in 1988 [4]. In these devices a high degree of flexibility and control may be achievable where molecules are arranged in one two or three transistor terminal circuits to serve as building components for a variety of digital logic functions (i.e. an inverter, a NOR logic gate, random access memory (RAM) cell [5, 6]), and rectifier [7, 8].

Molecular electronics could be also used in the implementation of memristors. Memristors are two terminal devices that are based on resistive switching [9]. Another alternative approach to molecular electronics systems include spintronics which uses both open and closed spin shells to form spin devices [10, 11, 12]. Indeed the incredible number of possible molecules leads to a high potential for a large number of interesting structures yet to be discovered. In addition, molecular junctions also give the opportunity to investigate and understand the electron transfer mechanisms of relevance to biology and chemistry [13, 14] within a controlled experimental environment. In order to develop molecular electronics, the fundamental science of molecular junctions must be better understood to develop design paradigms.

Current research in molecular electronics is directed towards determining conductance across molecular junctions. In electronics, conductance (G) across a

junction is determined from the current (I) and applied voltage (V).

$$G = \frac{dI}{dV} \tag{1.1}$$

At the atomic scale, conductance is quantized as predicted by Landauer [15]. For molecular and low dimensional systems, the conductance is given by the Landauer formula

$$G = \frac{2e^2}{h} MT \tag{1.2}$$

where M is the number of modes ($M = 1, 2, 3..$ etc), T is the transmission, h is Planck's constant and e is the elementary unit of electric charge of a single-electron $1.602 \times 10^{19} C$. Typically gold or platinum electrodes are used in molecular junction experiments to avoid oxidation.

The two main experimental methods for measuring current within molecular junctions are by using electrochemical [16, 17], mechanical break junction methods [18, 19] and electromigration break junctions [20]. These methods can facilitate fast measurement producing large amounts of data. This data can be used for statistical analysis to gain insight into geometry and charge transport mechanisms. Mechanical break junctions involve two electrodes which are slowly stretched with microactuators deforming the geometry while measuring the conductance. As the junction is being stretched apart the junction goes through various geometry transformations with a corresponding conductance for each new geometry. Onedifficulty is determining the exact geometry configuration for a measured conductance. Electromigration break junctions exploit the effect of electromigration which causes ions to move in the presence of an applied field due to both the direct effect of an applied filed and the electron 'wind' due to scattering of oppositely charged electrons to modify junction geometry. Electrochemical junctions involve the use of a reference gate electrode in addition to the source and drain to control molecular orbital band gaps. By applying a

positive or negative charge to the reference gate (counter) electrode the position of the Fermi level relative to the HOMO Highest occupied molecular orbital and the LUMO Lowest occupied molecular orbital can be modified and the resulting current measured. Thus electrochemical gating yields conductance curves based on the gate potential which reflect the molecular energy levels of the system.

Modelling in contrast allows one to craft and study specific relaxed geometries according to commonly used electronic structure formalisms. With modelling it is possible to determine the bonding and orbitals for a junction in addition to its current voltage profile. Comparisons between theory and experiment can prove difficult for molecular junction as the corresponding experimental atomic configuration for each conductance value for a given molecule is as yet not fully understood. This uncertainty can lead to difficulties in comparison between experiment and theoretical calculations, however when achieved a wealth of information concerning charge transport in nanostructures can be extracted.

Traditional approaches to modelling electron transport at the atomic scale rely on single-particle (electron) approximations such as Hartree Fock (HF) [21] or more commonly Density Functional Theory (DFT) [22]. The Hartree Fock method is the best approximation to the ground state energy of a system of interacting electrons when treating the many-electron wavefunction as a single Slater determinant. This is solved utilising the variational method where starting from an initial guess the system energy is minimised with respect to the individual electron wavefunctions (or orbitals) leading to lowest lying energy state within the Slater determinant approximation.

Single electron approximations treat electron-electron interactions using a mean field approximation where the presence of all electrons is treated as an averaged field. This neglects individual electron-electron interactions, which taken as a sum, are defined as electron correlation (i.e. the difference between the single-electron

mean field approximation and the complete (full) non-relativistic energy including all electron-electron interactions and multi-reference configurations). The Hartree Fock method is a starting point for most post single-particle methods which account for electron correlation such as configuration interaction, coupled cluster, and GW.

Density functional theory draws from the fact that many ground state properties of a many electron system can be determined from the electron density. Density functional theory utilises functionals solely of the electron density to determine the total energy. Approximations are introduced into density functional theory in the functionals describing electron exchange and correlation.

For conventional electron transport calculation for molecular junctions, single-particle methods are used in conjunction with Non-Equilibrium Greens Function (NEGF) methods [23] and can provide accurate results for many systems. While NEGF is in principle a many-body method, in practice however it is typically applied at a single-particle level.

Previous work involving DFT/NEGF has led to questions over the effect of correlation energy on conductance with some conductance values differing by orders of magnitude relative to experimental values [24, 25]. Therefore deducing correlated effects on transport methods is critical in determining the cause of divergence between experiment and theoretical calculations. The approximate treatment of electron exchange and correlation in DFT is believed to lead to a poor description of the energy level alignments between electrodes and molecules within single molecule junctions.

MECS or Many Electron Correlated Scattering is a many-body transport method [26, 27]. MECS utilises configuration interaction (CI) based methods to account for the correlation energy (e.g., Monte Carlo configuration interaction (MCCI)). Using MCCI generated configurations to determine the many-body wavefunction,

MECS employs a scattering based formalism to determine correlated transport across molecular junctions. The MECS method relies on the realisation that open boundary conditions can be applied to many body systems by utilising the Wigner function transform [28, 29] in conjunction with the one-body reduced density matrix RDM.

The Wigner function is a quasi probability distribution which allows for the application of single-particle open boundary conditions to the MECS method. Initially using the MECS method the many electron wavefunction is obtained and used to determine the RDM reduced density matrix. Applying the Wigner-Weyl transform [30] to the RDM reduced density matrix transforms the RDM from a Hilbert space representation to a phase space (postion and momentum) Wigner function representation necessary to apply boundary conditions. Thus the Wigner-Weyl transformation allows for the application of single-particle boundary conditions to the many-electron wavefunction.

Conventional approaches and approximations to electron transport can in many cases accurately determine the current, but there is no systematic way of knowing when and why they fail [24]. With many-electron wavefunctiion methods, one can apply perturbation theory or configuration interaction to improve results and the degree of approximation. The MECS method with a many-body treatment therefore seeks to treat the transport calculations with the highest degree of accuracy. The development and application of the MECS method aims to provide a many-body benchmark to determine which approximations are valid and why various treatment of charge transport can fail.

MCCI generates random single and double excitations relative to a trial many-electron wavefunction and reaches a solution using the variational method keeping only those excitations with large contributing coefficients while discarding the rest. This process is repeated to obtain a configuration interaction vector of

dominant configurations. Since MCCI generates single and double excitations from the current vector and not just the reference state, it can therefore in principal capture any excited level so long as it sigificantly contributes to the wavefunction. Due to this feature MCCI is not excitation limited as is the case for most traditional CI approaches.

The current implementation of MECS is a finite sized system where the boundary conditions are applied to the electrodes. Boundary conditions are imposed via Wigner distribution functions to apply single-particle open system boundary conditions to the many-electron wavefunction. Constraints are applied to the many electron wave function by constraining the value of the Wigner function for incoming momenta in the electrodes to mimic the effect of the electron reservoirs. The Wigner function constrains electron momentum flow to the scattering region to mimic the behaviour of a molecular junction contacted to two electron reservoirs (i.e. electrodes).

The aim of this thesis is the application and testing of the MECS method. In particular the aim is to establish and benchmark MECS for a variety of systems that have reproducible electrical measurements, or that are well understood theoretically, or both. A motivation for development of the MECS method is its ability to act as a means for benchmarking other quantum transport approaches to determine which approximations are valid and under what conditions. The following benchmarks are tested during the course of this thesis:

- The quantum of conductance: This is well documented experimentally in the literature [31, 32]. The quantum of conductance has been determined by number of electron transport calculation methods and as such it represents an established benchmark in quantum transport. In this work, point contacts were used to model the quantum of conductance.

- Electrode-molecule coupling: Of interest is how MECS performs within the

strongly coupled limit(i.e. systems where the electrode-molecule interaction is large). Point contacts are an example of a system with strong coupling. Similarly, weakly coupled systems consist of systems where the coupling and charge transfer between the molecule and electrodes are small (e.g. in molecular junctions such as aromatic molecules, alkane and silane based systems coupled to metal junctions through linker molecules).

- Weakly-correlated systems: MECS is benchmarked in the weakly correlated system limit. This allows comparison between the MECS method and weakly correlated experimental systems such as alkane junctions. MECS is diectly compared against single-electron codes such as NEGF/DFT.

- Moderately-correlated system: Further investigation into systems of increasing correlation was investigated. Starting from the weakly correlated systems (alkanes), MECS is applied to a system with a higher degree of correlation (silanes) to test its divergence with uncorrelated electron transport calculation methods. As MECS is applied to a more correlated system, divergence between correlated and uncorrelated methods (NEGF/DFT) would be expected.

- Electrostatics: The behaviour of electrostatics within the electrodes is of interest to understand how an applied voltage polarises a junction. To study the voltage drop across a point contact, the Poisson equation is used to determine the electrostatic potential and how it is determined by an applied electric field.

- Wigner functions and boundary conditions: A topic of further interest is the different components of the MECS system and their application to finite cluster models. Boundary conditions are imposed via Wigner function at

selected regions in the electrode referred to as Wigner planes. Finite geometry effects and their interaction with boundary conditions are investigated. The effect of the finite geometry approximation on the current and stability of the Wigner function with respect to electrode site is shown.

- Electronegativity: Electronegativity describes a system's affinity for electrons. An independent particle model is employed and compared to calculations utilising non-equilibrium Greens functions (NEGF). The reduced density matrices of the model wavefunction with second order correlation corrections and the one-electron Green's function with second order self-energies are known to be equivalent [33, 34]. The current can be deduced from the reduced density matrix. Using a correlated model in conjunction with conventional electron structure treatment, the relationship between single-particle electronegativity and the resultant current transport can be deduced. In this work as electron correlation is increased its corresponding effect on electronegativity and electron transport is determined.

- Validation: MECS was compared to experimental transport results for both point contacts and alkanes. Reproducible experimental results shows that the MECS method can accurately describe systems in the strong to intermediate coupling regime. Comparison of the MECS method with established single-particle theoretical methods both benchmarks MECS with the literature state of the art and provides possible evidence for the divergence of results for correlated systems.

The following is an overview of the chapters in this thesis.

- Chapter 2: The quantum of conductance is determined for metallic point contacts using the MECS method. Electrostatic tests were carried out on

point contacts to determine the effect of electrostatic screening on the voltage and resultant current. The stability of the Wigner functions in the finite electrode limit is tested and the effect of varying geometry is investigated. Comparison of the theoretical MECS calculation to the experimentally verified quantum of conductance is performed with numerical error arising out of approximations that are quantified and examined.

- Chapter 3: Contains the comparison of the MECS method to single-particle methods such as NEGF for alkanes and silanes. The molecules are connected to the electrodes using two linker molecule sets: amines (NH_2) and thiols (S) combined with the alkanes and silanes giving rise to a total of four systems. Comparison between MECS and NEGF is performed for all systems and is compared for theory and experiment on the alkanes. The effect of linker molecules are studied with the help of a simple barrier model and complex bandstructure analysis. A energy level alignment is determined and in conjunction with bandstructure is utilised to explain differences in conductance.

- Chapter 4: The effects of electronegativity on molecules and transport is studied. A correlated independent particle model is created and compared to conventional electronic structure/transport calculations. The effect of electronegativity on charge transfer, energy level alignments and electron currents is shown where relationship between the single-particle electronegativity and voltage current profile is analysed. A relation between electron correlation and electronegativity, and hence transport is determined.

- Conclusion: The results and benchmarks achieved through the course of this work are stated and described. In depth analysis of results is discussed with implications for future theoretical and experimental work are considered.

Finally conclusions are drawn and future improvements to the method are discussed.

References

[1] G. E. Moore, "Cramming more components onto integrated circuits," *Electronics*, vol. 38, April 1965.

[2] T. Kudernac, N. Katsonis, W. R. Browne, and B. L. Feringa, "Nano-electronic switches: Light-induced switching of the conductance of molecular systems," *J. Mater. Chem.*, vol. 19, pp. 7168–7177, Oct. 2009.

[3] F. Nickel, M. Bernien, D. Krüger, J. Miguel, A. J. Britton, L. M. Arruda, L. Kipgen, and W. Kuch, "Highly efficient and bidirectional photochromism of spirooxazine on au(111)," *The Journal of Physical Chemistry C*, vol. 122, no. 14, pp. 8031–8036, 2018.

[4] A. Aviram, "Molecules for memory, logic, and amplification," *J. Am. Chem. Soc.*, vol. 110, pp. 5687–5692, Aug. 1988.

[5] A. Bachtold, P. Hadley, T. Nakanishi, and C. Dekker, "Logic Circuits with Carbon Nanotube Transistors," *Science*, vol. 294, pp. 1317–1320, Nov. 2001.

[6] B. Kandasamy, G. Ramar, L. Zhou, S.-T. Han, S. Venkatesh, S.-C. Cheng, Z. Xu, C.-C. Ko, and V. A. L. Roy, "Polypyridyl chromium(iii) complexes for non-volatile memory application: impact of the coordination sphere on memory device performance," *J. Mater. Chem. C*, vol. 6, pp. 1445–1450, 2018.

[7] A. Aviram and M. A. Ratner, "Molecular rectifiers," *Chemical Physics Letters*, vol. 29, pp. 277–283, Nov. 1974.

[8] M. S. Johnson, C. L. Horton, S. Gonawala, C. N. Verani, and R. M. Metzger, "Observation of current rectification by a new asymmetric iron(iii) surfactant in a eutectic gain|lb monolayer|au sandwich," *Dalton Trans.*, pp. –, 2018.

[9] L. Chua, "Resistance switching memories are memristors," *Appl. Phys. A*, vol. 102, pp. 765–783, Jan. 2011.

[10] S. Datta and B. Das, "Electronic analog of the electro-optic modulator," *Applied Physics Letters*, vol. 56, pp. 665–667, Feb. 1990.

[11] I. Zutic, J. Fabian, and S. D. Sarma, "Spintronics: Fundamentals and applications," *Reviews of Modern Physics*, vol. 76, pp. 323–410, Apr. 2004. arXiv: cond-mat/0405528.

[12] A. Cornia and P. Seneor, "Spintronics: The molecular way," *Nat. Mater.*, vol. 16, p. 505, Apr 2017.

[13] A. M. Kuznetsov and J. Ulstrup, *Electron Transfer in Chemistry and Biology: An Introduction to the Theory (Wiley Series in Theoretical Chemistry)*. Wiley, Feb. 1999.

[14] J. Blumberger, "Recent advances in the theory and molecular simulation of biological electron transfer reactions," *Chemical Reviews*, vol. 115, no. 20, pp. 11191–11238, 2015. PMID: 26485093.

[15] R. Landauer, "Spatial Variation of Currents and Fields Due to Localized Scatterers in Metallic Conduction," *IBM Journal of Research and Development*, vol. 1, pp. 223–231, July 1957.

[16] A. F. Morpurgo, C. M. Marcus, and D. B. Robinson, "Controlled fabrication of metallic electrodes with atomic separation," *Applied Physics Letters*, vol. 74, no. 14, p. 2084, 1999.

[17] B. Capozzi, Q. Chen, P. Darancet, M. Kotiuga, M. Buzzeo, J. B. Neaton, C. Nuckolls, and L. Venkataraman, "Tunable charge transport in single-molecule junctions via electrolytic gating," *Nano Letters*, vol. 14, no. 3, pp. 1400–1404, 2014. PMID: 24490721.

[18] J. Moreland and J. W. Ekin, "Electron tunneling experiments using Nb-Sn "break" junctions," *Journal of Applied Physics*, vol. 58, pp. 3888–3895, Nov. 1985.

[19] R. Frisenda, L. Parlato, M. Barra, H. S. van der Zant, and A. Cassinese, "Single-molecule break junctions based on a perylene-diimide cyano-functionalized (pdi8-cn2) derivative," *Nanoscale Research Letters*, vol. 10, p. 305, Jul 2015.

[20] D. Demarchi, P. Civera, G. Piccinini, M. Cocuzza, and D. Perrone, "Electrothermal modelling for EIBJ nanogap fabrication," *Electrochimica Acta*, vol. 54, pp. 6003–6009, Oct 2009.

[21] D. R. Hartree and W. Hartree, "Self-Consistent Field, with Exchange, for Beryllium," *Proceedings of the Royal Society of London. Series A, Mathematical and Physical Sciences*, vol. 150, no. 869, pp. 9–33, 1935.

[22] P. Hohenberg and W. Kohn, "Inhomogeneous electron gas," *Physical review*, vol. 136, no. 3B, p. B864, 1964.

[23] L. V. Keldysh and others, "Diagram technique for nonequilibrium processes," *Sov. Phys. JETP*, vol. 20, no. 4, pp. 1018–1026, 1965.

[24] M. A. Reed, C. Zhou, C. J. Muller, T. P. Burgin, and J. M. Tour, "Conductance of a Molecular Junction," *Science*, vol. 278, pp. 252–254, Oct. 1997.

[25] M. Thoss and F. Evers, "Perspective: Theory of quantum transport in molecular junctions," *The Journal of Chemical Physics*, vol. 148, no. 3,

p. 030901, 2018.

[26] P. Delaney and J. C. Greer, "Correlated Electron Transport in Molecular Electronics," *Physical Review Letters*, vol. 93, p. 036805, July 2004.

[27] P. Delaney and J. C. Greer, "Quantum electronic transport in a configuration interaction basis," *Int. J. Quantum Chem.*, vol. 100, pp. 1163–1169, Dec. 2004.

[28] E. Wigner, "On the Quantum Correction For Thermodynamic Equilibrium," *Phys. Rev.*, vol. 40, pp. 749–759, June 1932.

[29] W. R. Frensley, "Boundary conditions for open quantum systems driven far from equilibrium," *Rev. Mod. Phys.*, vol. 62, pp. 745–791, July 1990.

[30] H. Weyl, "Quantenmechanik und Gruppentheorie," *Zeitschrift fur Physik*, vol. 46, pp. 1–46, Nov. 1927.

[31] H. Ohnishi, Y. Kondo, and K. Takayanagi, "Quantized conductance through individual rows of suspended gold atoms," *Nature*, vol. 395, pp. 780–783, Oct. 1998.

[32] T. Jasper-Tönnies, A. Garcia-Lekue, T. Frederiksen, S. Ulrich, R. Herges, and R. Berndt, "Conductance of a freestanding conjugated molecular wire," *Phys. Rev. Lett.*, vol. 119, p. 066801, Aug 2017.

[33] B. T. Pickup and O. Goscinski, "Direct calculation of ionization energies: I. Closed shells† Supported by the Swedish Natural Sciences Research Council.," *Molecular Physics*, vol. 26, no. 4, pp. 1013–1035, 1973.

[34] E. R. Davidson, "Properties and uses of natural orbitals," *Reviews of Modern Physics*, vol. 44, no. 3, p. 451, 1972.

Chapter 2

Many-electron scattering applied to atomic point contacts

2.1   Abstract

Electron transport in a strong coupling regime is investigated by applying the many-electron correlated scattering (MECS) method to an atomic point contact model. Comparing the theoretical calculations to the quantum of conductance obtained experimentally for these systems allows for the error associated with the numerical implementation of the MECS method to be estimated and attributed to different components of the calculations. Errors associated with implementing the scattering boundary conditions and determination of the applied voltage in a finite explicit electrode models are assessed, and as well the the impact on the basis set description on predicting the conductance is examined in this weakly correlated limit. The MECS calculation for the atomic point contact results in a conductance of $0.6G_0$ in reasonable agreement with measurements for gold point contacts where approximately the conductance quantum G_0 is obtained. The analysis indicates the error attributable to numerical approximations and the explicit electrode model introduced in the calculations should not exceed 40% of the total conductance, whereas the effect of electron-electron correlations even in this weakly correlated regime can result in as much as a 30% change in the predicted conductance.

2.2   Introduction

Many-electron correlated scattering (MECS) is a quantum transport method that relies on use of the Wigner distribution function to apply single-particle scattering boundary conditions to a many-electron wave function [1, 2]. The method has been applied to describe tunnelling in single molecule junctions consisting of benzene dithiol (BDT) [1], alkane dithiols [3], alkane diamines [4], silane dithiols and silane diamines [5]. In each case, the predicted current-voltage characteristics are in good agreement with available experimental data [6, 7, 8, 9, 10]. For these single

molecule tunnel junctions, a range of experimentally determined conductances and several conductance peaks can appear; the explicit atomic configurations corresponding to different conductance values has not been fully unravelled. Hence direct comparison to experiment can be difficult, although it should be mentioned that there is an improvement in the agreement between measured conductances in, for example, the case of BDT [6, 7, 8], and for the cases where amine linker molecules are used to bond the molecule to the metal electrodes for which well-defined conductance peaks result [9, 10]. However, comparison of the MECS calculations to date with experiment have been for molecular tunnel junctions in a weak coupling regime, as the molecules studied are bonded to electrodes via a linker group (-thiol, -amine) resulting in large contact resistances [3, 4].

Theoretically, the single-particle limit of the MECS method for a single ideal conducting channel with unity transmission, or in the strong coupling limit, has been studied for a simple analytical model yielding the well-known result of the conductance quantum [11, 12]. Here we consider a single conducting channel by considering an explicit atomic model of a gold atomic point contact. Gold point contacts have been well characterised experimentally with observation of conductance quantisation in several measurements [13, 14, 15, 16, 17, 18, 19]. Comparing to these systems where the conductance value is well established theoretically and experimentally allows exploration of MECS in a strong coupling limit and permits an assessment of the explicit finite electrode models used in the calculations and errors associated with the numerical implementation of the theory.

Relatively little work has been performed studying the effect of atomic orbital expansions on prediction of electron currents in single-particle models [20, 21], and even less is known on the role of many-electron expansions about the single-particle model [22]. In this study, we consider the problem from the standpoint of the many-electron expansion in spin-coupled Slater determinants. Hartree-Fock

orbitals are used as single-particle basis states. As a voltage is applied across the junction, the junction polarises. A new set of self-consistent orbitals can be recalculated for each new voltage bias point, or equivalently a single configuration interaction (CI) expansion about the zero electric field self-consistent field solution

$$|\Psi> = \prod_{i=1}^{N} \prod_{m=N+1}^{M} (1 + C_i^m a_m^\dagger a_i)|\Phi_0 > \tag{2.1}$$

can be performed. Here $|\Phi_0>$ is the zero voltage Hartree-Fock determinant, i is the index for occupied single-electron states in $|\Phi_0>$, N is the number of electrons, m is the index for unoccupied single-electron states, M is the number of single-electron states included in a finite expansion, $a^\dagger, a$ are the electron electron creation and annihilation operators, and the C_i^m are the CI expansion coefficients for singly-excited determinants. Thouless' theorem states that any $|\Psi>$ of the form eq. 2.1 is itself a single determinant (strictly, for $M \to \infty$). Optimising the CI coefficients C_i^m for an expansion including only singly-excited determinants allows us to explore the single-particle limit of the MECS method [3]. Adding higher order excitations into a CI expansion allows us to estimate the role of increasing electron correlations beyond a mean field solution.

Atomic point contacts are somewhat trivial examples for Green's functions or single-electron scattering approaches to quantum transport in that it is only necessary within these methods to calculate the transmission of an electron impinging on the junction at the Fermi energy. For a single atomic state strongly coupled to the two leads, it is inferred from a unity or near unity transmission that the conductance from Landauer's formula is $2e^2/h$, where e is the electron charge and h is Planck's constant. In the case of many-electron scattering, the one-electron reduced density matrix is obtained from a full many-electron density matrix and the current density is obtained from the one-electron reduced density

matrix in the direction of current flow as

$$J_z(\mathbf{r}) = \frac{e\hbar}{2mi}[\partial_z - \partial_{z'}]\rho(\mathbf{r}, \mathbf{r}')|_{\mathbf{r},\mathbf{r}'}, \tag{2.2}$$

where ρ is the density matrix, z is a Cartesian coordinate along the direction of current flow, $\mathbf{r}, \mathbf{r}'$ are position vectors, e and m are the electron charge and mass, respectively, $i = \sqrt{-1}$ and $\hbar$ is Planck's constant divided by 2π. Hence to accurately determine the conductance, an accurate determination of the one-electron reduced density matrix and the applied voltage across the junction is required. Thus atomic point contacts pose a stringent test case for a MECS determination of the conductance. In the following, the junction electrostatics, sensitivity of the boundary conditions to the selection of the explicit electrode model, and the effect of the many-electron expansion on the electron current are studied. It will be demonstrated that the conductance quantum can be approximately determined using MECS in an explicit atomistic junction model, thus allowing an evaluation of the accuracy of the method with respect to computational approximations.

2.3   Method

2.3.1   MECS transport calculations

The numerical implementation of the MECS procedure has been previously presented [2, 23] and here a brief outline of the method is given for reference. Scattering boundary conditions are applied to model electrodes acting as electron reservoirs with open system boundary conditions usually expressed as conditions on the occupation of single-electron wave functions in electron reservoirs, each locally in equilibrium. For correlated many-electron calculations, there is a need to

apply the single-particle boundary conditions to a many-electron density matrix. A difficulty arises in that these boundary conditions are expressed in terms of single-particle energies and occupations as Fermi-Dirac distributions in the reservoirs along with the reservoir (local) Fermi levels. The single-particle energies and occupations have no direct counterparts for a correlated many-electron density matrix. A formulation of open system boundary conditions that provides a similar description to the single-particle scattering boundary conditions to model the electron reservoirs is a fundamental feature of MECS and relies on the use of the Wigner function to apply momentum constraints to mimic the behaviour of electron reservoirs [24]. The electrodes attached to the scattering region are taken to act as leads in equilibrium with electron reservoirs; see fig. 2.1. The scattering boundary conditions can then be re-expressed in terms of the equilibrium momenta of the electrons flowing inwards to the scattering site. As these distributions are characteristic of the reservoirs and leads independently of voltage, the inward electron momentum flow is held fixed to equilibrium values as voltage is applied between the electrodes. Simultaneously, the reservoirs must be able to absorb any distribution of electrons flowing or scattering out from the molecules without disturbing the net inward flow of electrons [25].

Formulation and application of the scattering boundary conditions in the MECS approach uses a many-electron or configuration interaction (CI) expansion, and the N-electron density matrix on the scattering region is determined from the N-electron wave function. From the N-electron density matrix, a reduced one-electron density matrix is obtained and re-expressed using the Weyl transformation to yield the one-electron Wigner distribution function

$$\rho_N \rightarrow \rho_1, \quad \text{with} \quad \text{Tr}(\rho_1) = N$$

$$f_W(\mathbf{q}, \mathbf{p}) = \int_{-\infty}^{+\infty} d\mathbf{r} \, \exp(-i\mathbf{p}\mathbf{r}/\hbar)\rho_1(\mathbf{q} - \mathbf{r}/2; \mathbf{q} + \mathbf{r}/2), \qquad (2.3)$$
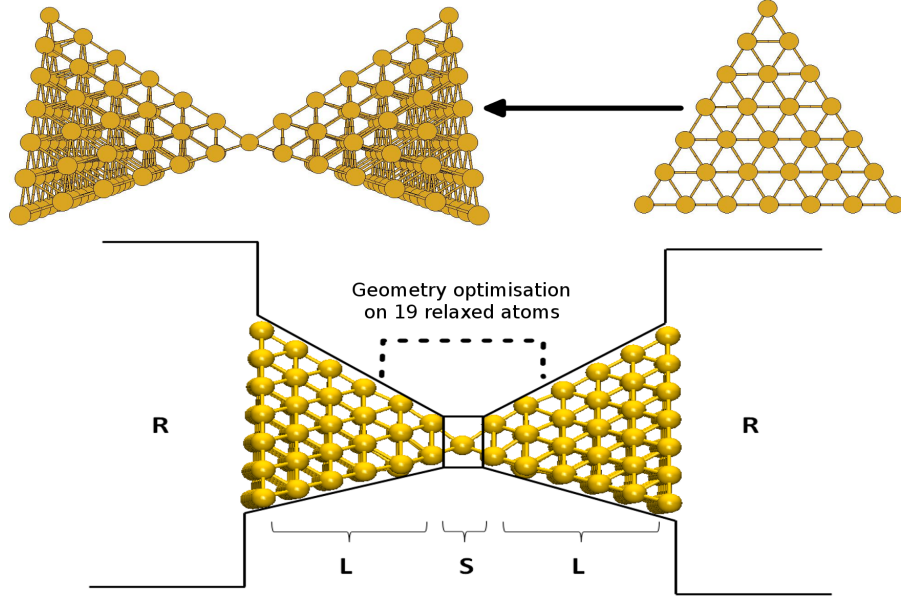
Figure 2.1: Atomistic model for gold point contact. In the figure, the electrodes
are schematically partitioned into a reservoir (R) connected to a scat-
tering site (S) by leads (L) in equilibrium with the electron reservoirs.

where ρ_N is the N-electron density matrix on the scattering region, ρ_1 is the
one-electron reduced density matrix, f_W is the Wigner distribution function, and
$\mathbf{p}, \mathbf{q}$ are the Wigner phase space variables. The use of the Wigner function to
apply scattering boundary conditions to single-particle quantum transport
problems is well-known and details of its use to formulate scattering boundary
conditions can be found in [24].

The many-electron density matrix on the scattering region and including an
explicit portion of the electrodes is determined by using the CI method for the
many-electron Coulomb Hamiltonian. In this approach, an N-electron wave
function is represented as a sum over configuration state functions (or CSFs, also
known as an expansion in spin-projected Slater determinants)

$$|\Psi> = \sum_A c_A |\Phi_A>, \tag{2.4}$$

where the $|\Phi_A>$ are the CSFs and A is the index over many-electron

configurations. Any many-body wave function can be written as an infinite sum of Slater determinants, and this method can in principle deliver an exact solution to the many-electron Schrödinger equation. The usefulness of CI is that truncated sums of well-chosen configurations can give accurate results for any electronic property with a controllable approximation to the electron correlation energy: namely, the number of terms in the length of the expansion. To perform a calculation, a set of single-electron orbitals that are used to build occupied configurations for the finite set used in the expansion are chosen. The CI method proceeds by finding the ground and excited states of a quantum system by obtaining stationary points of the energy by varying the CI expansion coefficients. In practice, the set of configurations to be selected for an accurate description of the problem is key to a successful treatment of a correlated problem: Monte Carlo configuration interaction [26, 27] has been used to optimise the set of CSFs included in the many-electron expansion. Using this approach, an initial trial CI vector is chosen and random single and double substitutions are made with respect to this guess. The variational problem is solved with this expanded vector, and those configurations that contribute significantly to the wave function are retained based on the magnitude of their corresponding normalised expansion coefficients. This sequence is iterated until the calculation converges with respect to the acceptance threshold for new configurations; the method is outlined in table 1. Note that the method always works with a compact CI vector, is not excitation limited as higher excitations become included into the trial vector at each new iteration, and inherently has importance sampling of the CI space built-in, as only those excitations accessible via single and double substitutions relative to the current trial vector are accessible. This last fact implies that the algorithm always works with a substantially reduced space, yet can recover any portion of the correlation energy desired by lowering the acceptance criterion for CSFs. This approach is used to select important configurations at zero bias voltage for the

Table 2.1: MCCI procedure after ref. [28]

		$K = 0$.
(0)	Initialize	Define the starting vector $\lvert\Psi_0\rangle = \sum\limits_{i=1}^{N_0} c_A \lvert\Psi_A\rangle$;
		Repeat steps (1)-(4) until convergence of the vector length N_A and the energy E
		$K = K + 1$
(1)	Branching	Generate $\lvert\Psi_R\rangle = \hat{\alpha}_R \lvert\Psi_A\rangle$ $1 \le A \le N_A^{K-1}$; N_A^{K-1} $+1 \le R \le N_{K-1} + N_{\mathrm{new}}$;
		where $\hat{\alpha}_R \in \{0, \hat{a}_m^\dagger \hat{a}_i, \hat{a}_m^\dagger \hat{a}_n^\dagger \hat{a}_i \hat{a}_j\}$
		$\lvert\Psi^K\rangle = \sum\limits_{A=1}^{N_{K-1}+N_{\mathrm{new}}} c_A \lvert\Psi_A\rangle$,
(2)	Matrix generation	Generate Hamiltonian $\mathbf{H}$ and overlap $\mathbf{S}$ matrices in the CSF basis.
(3)	Diagonalisation	Solve $\mathbf{Hc} = \mathbf{Sc}E$.
(4)	Pruning	IF $\lvert c_A \rvert >$ threshold THEN retain $\lvert\Psi_A\rangle$ ELSE reject $\lvert\Psi_A\rangle$;
		$\lvert\Psi^K\rangle = \sum\limits_{A=1}^{N_K} c_A \lvert\Psi_A\rangle$, where $N_K \le N_{K-1} + N_{\mathrm{new}}$,
(5)	Converged	$E^K = \langle\Psi^K \rvert \hat{H} \lvert\Psi^K\rangle / < \Psi^K \lvert \Psi^K >$.

ground state and for several low-lying excited states. The configurations selected in this manner then are merged together and serve as the basis set for the scattering calculations as voltage is applied across the junction.

In the scattering calculations, additional constraints, those arising from imposition of open system boundary conditions, are required and there is not an associated linear eigenvalue problem. Another means for approaching the variational formulation is required to determine the constraints associated with imposing the boundary conditions. The many-body wave function for the current-carrying state induced by the applied electric field and satisfying the reservoir boundary conditions is solved for by treating the variational problem as a constrained optimisation using the penalty function method [2]

$$\mathcal{L}[\lvert\Psi\rangle, \lambda_i, \sigma] = \langle\Psi \rvert H + \mathcal{E}z \lvert\Psi\rangle - \sum_{i=1}^n \lambda_i \mathcal{C}_i[\lvert\Psi\rangle] + \frac{1}{2}\sigma \sum_{i=1}^n \mathcal{C}_i^2[\lvert\Psi\rangle]. \qquad (2.5)$$

The stationary points of $\mathcal{L}$ are sought, H is the many-electron Hamiltonian on the

scattering region, $\mathcal{E}$ is an external electric field applied along the junction axis z, the $\mathcal{C}_i$ are the constraints imposing the scattering boundary conditions (for details see [1, 2, 3, 11, 12]), and the last term is the penalty function introduced to aid in the numerical optimisation. The λ_i are the Lagrangian multipliers used to enforce the boundary conditions as constraints, and σ is a numerical parameter associated with the penalty function to improve convergence and to avoid ill conditioning during the search for the stationary points of eq. 2.5. The CSFs in our calculations are built from real molecular orbitals and to generate a current carrying state it is required that the CI expansion coefficients are allowed to be complex-valued. The constraints require that the values for the Wigner function deduced from the many-electron wave function obtained in eq. 2.5 match those calculated from the equilibrium wave function at the points in Wigner phase space chosen to model the behaviour of the electron reservoirs. For a description of electron reservoirs, it is required to identify incoming electrons from the left and right, and apply these conditions to the reduced one-electron density matrix. A plane perpendicular to the net current flow is chosen within the left electrode. The Wigner function for incoming momentum is determined for the incoming electrons located at all points on this plane. To simplify the analysis, the planar distribution is integrated over the in-plane position co-ordinates. With this function, the net inward momentum flow from the left contact can be specified assuming that the Wigner function is constrained in a region where it well approximates a classical distribution function. The Wigner function is first computed from the initial equilibrium (no applied voltage) many-electron problem on the scattering region, and evaluated for a chosen number of momenta values $p_i > 0$ in the left electrode. A similar procedure for the right electrode is performed with the distinction that the electrons incoming from the right are those with $p_i < 0$. The constraints for the left lead are expressed as

$$f_{\Psi\Psi^*}(q_L, p_i > 0) - f_{V=0}(q_L, p_i > 0) = 0, \qquad (2.6)$$

where $f_{\Psi\Psi^*}$ is the Wigner function calculated from the many-electron wavefunction on the scattering region as voltage is applied and $f_{V=0}$ is the equilibrium or zero voltage Wigner function. Note the condition $p_i > 0$ enforces that only the incoming momentum values are constrained. Similarly for the right lead the constraints are

$$f_{\Psi\Psi^*}(q_R, p_i < 0) - f_{V=0}(q_R, p_i < 0) = 0, \tag{2.7}$$

whereby the constraints are only applied for $p_i < 0$ to enforce that only the incoming momentum from the right is constrained. As the outgoing electrons in the left or right leads are not constrained, the scattering region is free to reflect as many electrons as needed to make the constrained energy stationary. Once the constrained minimisation problem is solved, the current is calculated from the probability current density $J_z(\mathbf{r})$ given by eq. 2.2. This current density is integrated over the plane normal to the net flow to obtain the total electron current passing through the molecule.

2.3.2 Details of the electronic structure calculations

To obtain a set of single-particle orbitals used to build the CSFs for the CI expansion, a Hartree-Fock calculation is performed [29]. The structure we use to explicitly model the atomic point contact consists of (111)-oriented gold atoms (fig. 2.1). The tip of each electrode is modelled as a triangular based pyramid with C_{2v} symmetry. Geometry optimisation (minimisation of the energy with respect to nuclear coordinates) is performed on a truncated section of the geometry containing 39 atoms. Of the 39 atoms, 10 atoms in each back plane are constrained and the central 19 are allowed to relax during the geometry optimisation. The single-particle basis set employed in the geometry optimisation is a split valence with polarisation (SV(P)) used in conjunction with an 60 electron effective core potential [30]. This central relaxed structure is then re-inserted into to the full

(111)-oriented gold atom structure. To generate the orthogonal single-particle basis set used to construct the many-electron expansion functions, the CRENBS basis set for the gold atoms is used [31] in conjunction with a 78 electron effective core potential (ECP). The CRENBS basis set consist of s and p orbitals to describe the band arising from the gold $6s$ state. The seven central atoms in the structure (central atom plus first plane of atoms in each electrode) are complemented with a single d function. The electrode geometry is similar to that used in previous calculations on the alkanes and silanes [5] but has been extended by an additional back plane of gold atoms. The overall symmetry of the structure is C_{2v} and the Hartree-Fock electronic ground state has symmetry described by the b_1 irreducible representation of C_{2v}.

To generate CSFs used in the many-electron CI expansion for the transport calculations, the Monte Carlo configuration interaction technique or MCCI [26, 27] method is used to generate the first six electron states with symmetry of both the b_1 and a_2 irreducible representations in C_{2v}. A threshold for the CI normalised expansion coefficients of $7{\times}10^{-3}$ is used to select important configurations. These twelve electronic states are concatenated along with all possible singly substituted configurations with respect to the Hartree-Fock ground states of b_1 and a_2 symmetry. This choice of configurations for the many-electron expansion allows for a description of the polarisation of the atomic point contact as the b_1 and a_2 symmetric states couple as an electric field is applied along the principal C_{2v} axis, and induce a voltage difference between the left and right electrodes. The requirement to couple the excited states can be readily understood from a second order perturbation correction to the energy

$$\Delta E^{(2)} = e^2 \mathcal{E}^2 \sum_{I \neq 0} \frac{|\langle \Psi_I | z | \Psi_0 \rangle|^2}{E_I - E_0} \tag{2.8}$$

describing the quadratic energy dependence as the external electric field induces a

dipole moment. The perturbation expansion is about the zero external field many-body ground state and couples to the many-electron excited states through the dipole matrix elements $\langle \Psi_I | z | \Psi_0 \rangle$. Eq. 2.8 highlights the motivation for adding the configurations associated with the excited many-body states into the CI expansion: they are required to provide the flexibility in the expansion for the scattering region to polarise as voltage is applied. Note, from a zeroth order wavefunction of b_1 symmetry, only the a_2 excited states will contribute due to the field applied along the z-axis coupling these states to the zeroth order wave function.

2.4 Analysis

2.4.1 Electric field screening

As an electric field is applied, the electrodes are driven out of equilibrium with respect to one another due to the potential difference governed by left (μ_L) and right (μ_R) chemical potentials as measured within the electrodes. The potential imbalance introduces a difference in the charge density between the electrodes resulting in the formation of surface dipoles at the interface between the electrodes and the scattering region, in this case a single gold atom. Standard practice in most electron transport computations is to include an external electric field in the scattering region Hamiltonian to mimic the action of physical electrodes on the scattering region (a notable exception to this is the method of Ke *et al* [32]). To understand the role of the external field in atomic point contacts, it is useful to consider the depiction of the scattering region as presented in fig. 2.2. As a voltage difference is applied between the left and right electrodes, the fact that electrostatic screening is efficient in metals implies that for the quasi-equilibrium regions of the electrodes, the electric field will be zero within the electrodes and

consequently, the electric field is zero within an order of the screening distance, or equivalently the voltage is constant within the electrodes. Thus all of the voltage drop is approximately across the scattering region plus two screening lengths into the electrodes. Typical screening lengths in metals are less than 0.1 nanometre, hence any charge imbalance in the electrodes resides at the surface of the metal. The opposite polarity of the surface-induced charges between the electrodes gives rise to an electric field across the region situated between the electrodes; a situation depicted in fig. 2.2 as field lines connecting the electrode surfaces and the scattering site. Alternatively, one can apply an external electric field and the junction will polarise in response to the field, and surface charges will be induced at the surface of the electrodes. In the MECS procedure, charges rearrange as the many-electron expansion coefficients are found subject to the open system boundary conditions and in the presence of the externally applied electric field. The voltage can then be obtained from the combined field arising from the applied field and polarised charge distribution in the scattering region [33]. The model of electrode behaviour we are describing is consistent with standard formulations of quantum electronic transport [12].

To study the voltage across the point contact, the classical electrostatic potential resulting from solving Poisson's equation from the junction's self-consistent charge density [29] is used to calculate the difference between the electrostatic potential with and without the application of the external electric field. The resulting potential profile reflects the voltage induced by the applied field and is depicted for several values of external field in fig. 2.3a with the voltage averaged over planes normal to the junction axis. In order to estimate the induced voltage drop across the contact region, the resulting one-dimensional electrostatic potential profile is then averaged over the 'constant' voltage region within the electrode regions. The difference between the potentials in the left and right electrodes is taken as the applied voltage. In previous applications of the MECS method, the external
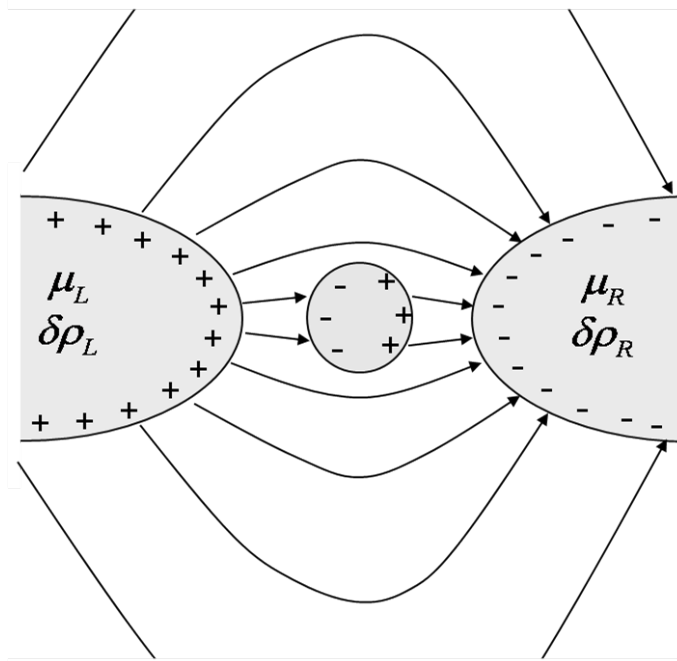
Figure 2.2: Pictorial representation of the voltage induced across an electrode model as an external electric field is applied.

electric field was simply integrated between the planes in the electrodes where the Wigner function constraints are imposed- note this distance is typically significantly larger than a screening length, resulting in an overestimation of the voltage for those calculations. This approximation introduces a relatively small error for molecular tunnel junctions as the length of the molecules is in turn significantly larger than the lengths into the electrodes, hence the calculated voltage is dominated by the length of the molecule in the junction. Atomic point contacts are more sensitive to these considerations than molecular junctions due to the fact that the length of the junction is essentially a single atom plus the screening lengths into the electrodes. In fig. 2.3c, the relationship of the voltage arising across the junction as a function of the external field is displayed- the slope yields the effective junction distance relating voltage to external electric field. We obtain an estimate for the effective junction distance of $d = 0.43$ nanometres enabling us to estimate the voltage drop in the point contact given the value of the external applied electric field. The distance obtained can be compared to the

screening length and atomic dimensions of the gold atom. We extract an estimate of the screening length in the gold electrodes as the distance from the edge of the contact to where the voltage profile becomes approximately constant in fig. 2.3a, where the 'edge' of the contacts is defined as the backplane atomic coordinates plus 0.179 nanometre (the radius of a gold atom). With this definition, the screening length is found to be approximately 0.04 to 0.08 nanometre, comparable to predictions from the Thomas-Fermi model of less than an Ångström for gold. Hence the effective junction distance, as physically intuitive, is approximately the length across the central atom to the surface of the two electrodes or the scattering region as shown in fig. 2.1. Also seen in fig. 2.3a at the centre of the point contact, the screening effect breaks down between the single central atom and the first plane of the electrodes, a surface dipole arise due to charges accumulating on the surface of the point contact as schematically represented in fig. 2.2.

2.4.2   Wigner function constraints and finite lead approximations

To implement the scattering boundary conditions within the MECS method, a region in the electrodes at which the momentum constraints are to be imposed must be chosen; typically this is selected in the 'middle' of the explicit electrode model [11]. An explicit atomic region is used to model the point contact and the Wigner constraints are applied within the explicit atomic region. In this picture, small atomic electrodes leading (or 'leads') to the point contact are considered to be in equilibrium with electron reservoirs, and that the electrons exiting the leads into the electron reservoirs are not reflected. This assumption allows us to assume the incoming electrons from the left and right leads are equilibrated with respect to the left and right electron reservoirs, respectively. This allows us to neglect the details of the electron reservoir/lead interface and to calculate conductance
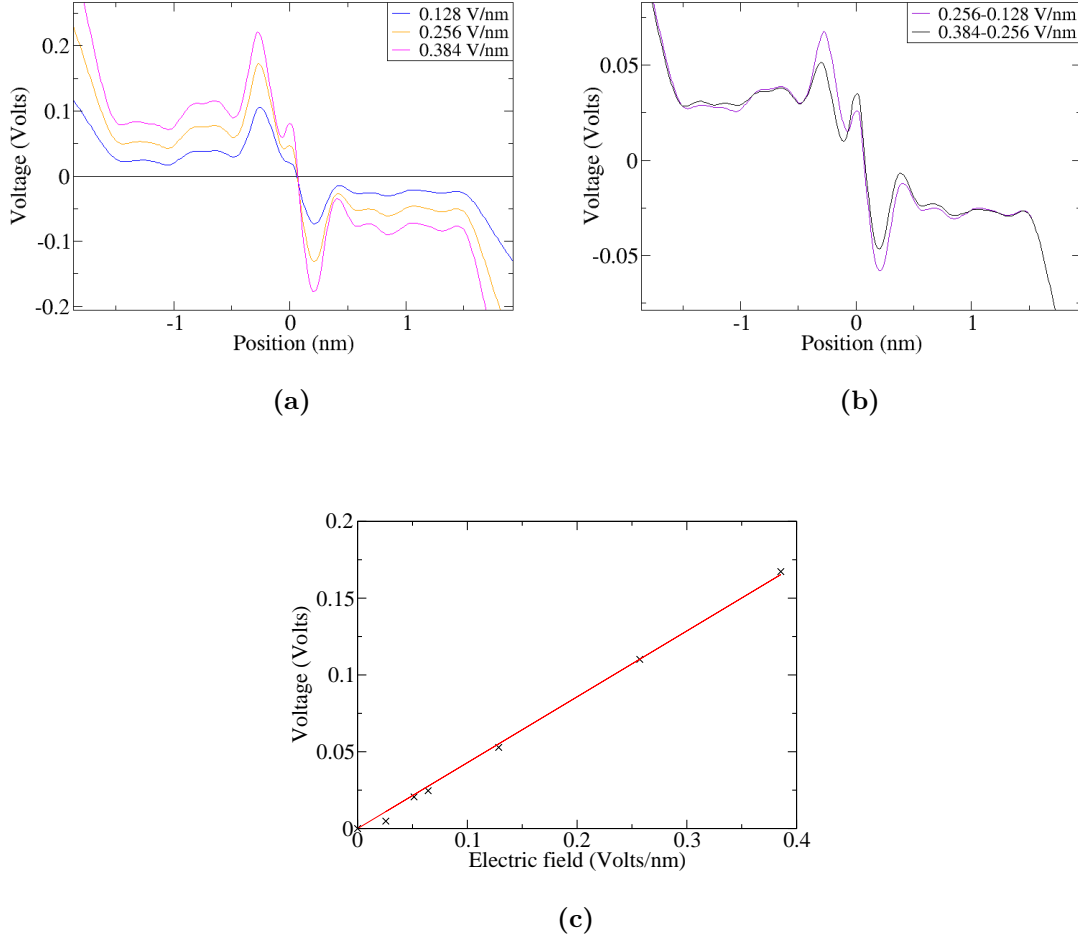
Figure 2.3: (a) One dimensional representation of the voltage for a series of applied external electric fields. Of note are the voltage 'plateaus' within the contacts as a result of electrostatic screening. Surface dipoles form in the centre of the point contact between the electrodes and the single atom scattering site. (b) Plot of the difference between successive voltage profiles for increments in electric field of 0.128 V/nm. The voltage differences as the electric field is increased are approximately the same indicating a linear regime. The magnitude of the surface dipole increases with increasing electric field. (c) The linear relationship between the voltage difference and applied electric field yields the effective distance across which the voltage drop occurs.

between the two leads [34]. Thus it is sufficient to constrain the incoming

momentum distributions to be characteristics of the leads, if the assumption that

the leads are in equilibrium with electron reservoirs holds.

The one-electron reduced density matrix displays a rapid decay with distance in

metals [35]. This allows for a decoupling of the density matrix between the
electrodes and allows the electrodes to be treated independently. The one-electron
Wigner function is a transformed representation of the one-electron density matrix,
and we investigate the effect of finite metal electrode models on the Wigner
distribution function as sampled in the plane where the scattering boundary
conditions are applied. For symmetric electrodes and at zero voltage bias across
the junction, the Wigner distributions in the two electrodes are identical and the
net momentum flow balances to zero current. As an external field is applied, the
distributions of the momenta incoming to the scattering region are fixed to their
zero bias distribution and the outflow of the momenta become asymmetric between
the left and right electrodes due to scattering, thus yielding a net current flow.

In fig. 2.4a, four atomic scale models for the leads are shown. The first is a typical
electrode used in the explicit atomic region in the scattering calculations, the next
models are extended by adding repeating unit cells consisting of 41 atoms to the
back plane of the electrode. The Wigner distribution function calculated as a
planar average for each of these electrode models is plotted in fig. 2.4c. In each
case the Wigner plane is placed at the same position relative to the tip of the
electrode and is situated between the last two planes of atoms in the electrode
shown at the top of fig. 2.4a. The distributions agree well for larger momentum
values although there is some discrepancy at lower momenta, in particular with the
smallest electrode displaying a smaller magnitude in the distribution for low
momenta. However, the smaller magnitude components do not significantly
contribute to the current as demonstrated in fig. 2.4e where the product $p\,f(p,q)$ is
displayed where $f(p,q)$ is the Wigner function and (p,q) are the Wigner momenta
and position variables, respectively. The similar behaviour for the four electrode
models for the relative magnitudes for the incoming momenta indicates that there
are small differences in the equilibrium distributions between the different
electrode models, hence their overall behaviour in terms of scattering boundary

conditions is similar in each case.

Next the interaction between the electrodes is considered; the two electrodes should decouple to ensure that each can be equilibrated independently. In fig. 2.4b, the left and right electrodes are considered simultaneously by examining the effect on the right electrode due to different left electrode configurations. Fig. 2.4d, shows that the Wigner distribution in the right electrode is stable against the variations in the geometry of the left electrode. It is also seen as a consequence that the net momentum inflow for the right electrode is stable against changes in the left electrode as seen in fig. 2.4f. Hence the required independence of the electrodes in the model is established.

Finally, we note ongoing work whereby the self-energies of semi-infinite electrodes are replaced by energy-independent complex absorbing potentials (CAPs) [25] that enable inclusion of larger electrode structures into a CI treatment by the addition of complex valued, energy independent single body operator. Similar treatments of electrodes using CAPs are being considered within other transport frameworks [36, 37].

2.5   Current voltage characteristics

The calculated current-voltage characteristics from MECS for the point contact are given in fig. 2.5. A resistance of 20.6 kΩ is obtained where the voltages applied in typical break junction experiments are considered for values where the current-voltage characteristics are linear. The calculated resistance corresponds to a conductance of $0.6G_0 \pm 0.24G_0$ for the model point contact of fig 2.1 in units of the conductance quantum G_0, which compares well with the experimentally reported values of 0.3 - 0.8G_0, $\sim 1G_0$, $\sim 1G_0$, 0.85 - 0.90G_0, 0.7 - 1.0G_0, 0.88 - 0.97G_0, and $(1.0 \pm 0.4)G_0$ in refs. [13, 14, 15, 16, 17, 18, 19], respectively. Our

(a)

(b)

(c)

(d)

(e)

(f)
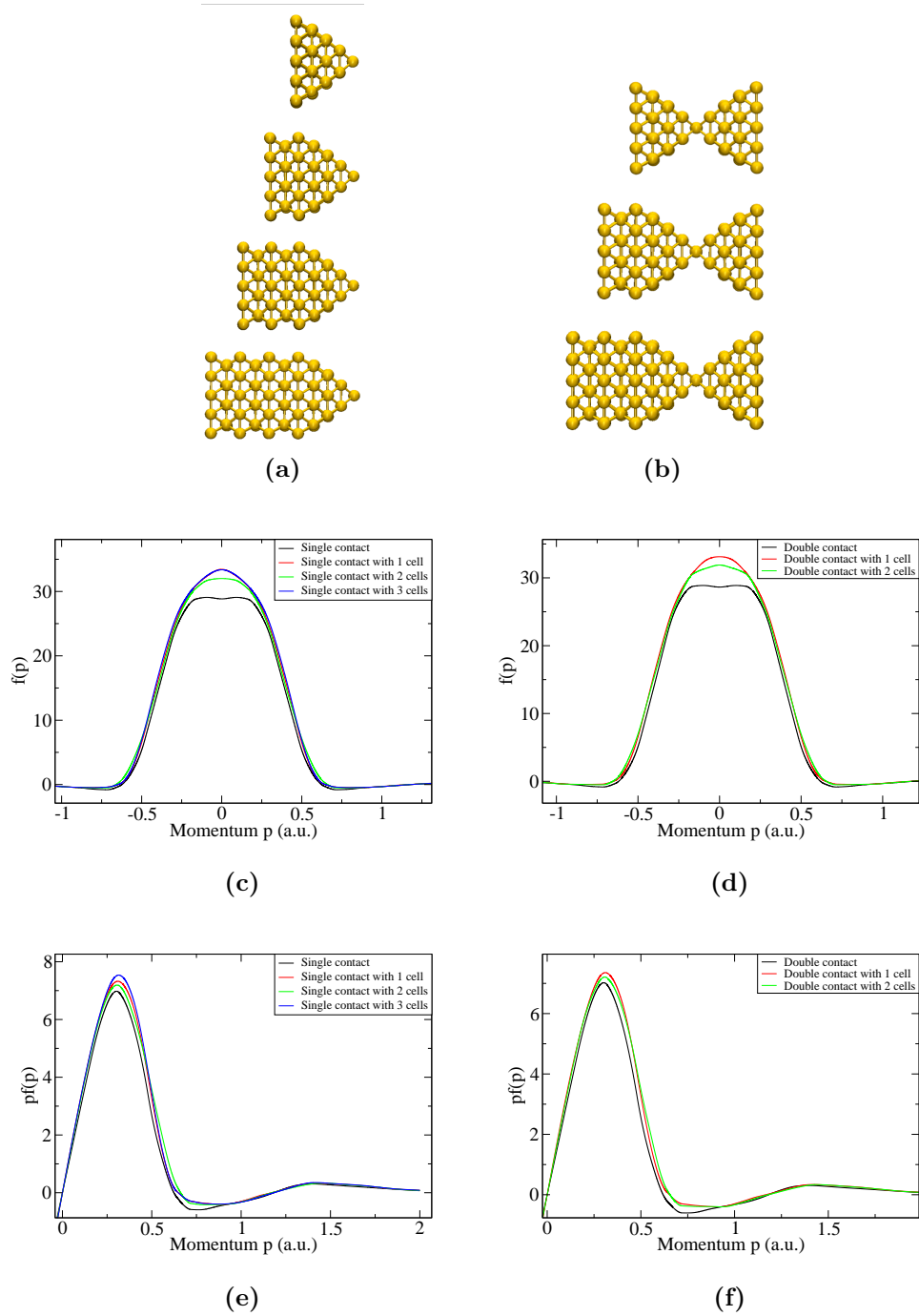
Figure 2.4: (a) A single sided electrode geometry with the tip contact at the top, and with increasing number of additional lead cells. (c) Wigner function for the electrode geometries in (a) calculated within the electrode tip. (e) the Wigner function multiplied by momentum. The lower values of momenta do not significantly contribute to the net inward momentum flow. (b) Two sided electrode model with the left electrode model extended by additional lead unit cells. (d) Wigner function calculated within the right electrode tip. (f) As in the case for the one sided electrode model, the small contributions due to lower values of momenta reveals that the boundary conditions describing the equilibrium momentum flow are relatively insensitive the exact electrode model, and that the two electrodes decouple.

voltage error is estimated from fig. 2.3a) as the difference between the respective
maximum and minimum values between the left and right potentials within the
region where screening is observed at a given applied electric field. The error in our
predicted current is estimated as the difference between the maximum and
minimum values for the current as a function of position across the junction at a
given bias point; see fig. 2.6a. We mention that several point contact geometries
have been tested, with smaller and larger electrodes, and with differing atomic
arrangements where the atomic arrangement has not been optimised. In none of
these cases was a conductance value found exceeding the conductance quantum, or
indeed the value of $0.6\ G_0$ found for the optimised structure. The fact that a lower
value for conductance is found for non-optimised junctions is consistent with the
expectation of increased scattering in non-ideal junctions [13, 18]. Hence we
conclude that the MECS approach is capable of approximately reproducing the
conductance quantum, within identified numerical errors, through explicit
calculation of the full density matrix on the scattering region. This validates the
approach for a new coupling regime as previous MECS calculations have, as
mentioned, studied molecular tunnel junctions with weak coupling between the
metallic electrodes and the scattering site.

In fig. 2.6a, the current profile calculated as a function of distance across the
junction is displayed showing the percentage deviation in the current for a range of
voltage biases between 2 to 10 mV. Current conservation is imposed for currents
entering and exiting the scattering region [12], but no local current constraints are
imposed. Hence local current oscillations are seen indicating that the
many-electron expansion function on the junction is not a complete set and the
variational nature of the calculation allows for local violations of current
continuity. However, as demonstrated in fig. 2.6a the percentage change in the
current for a range of voltages remains approximately constant as voltage across
the junction is increased.
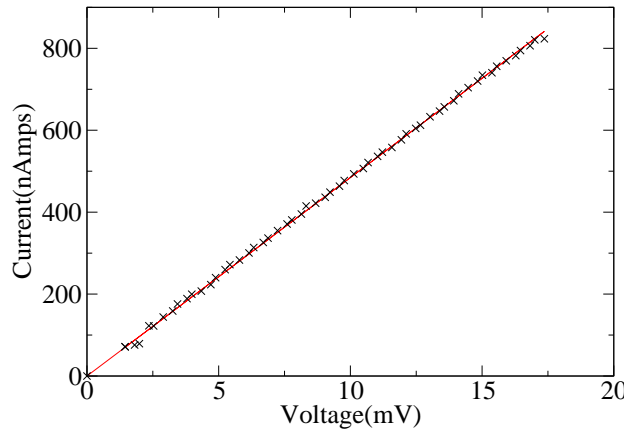
Figure 2.5: Current voltage characteristic yielding a resistance of 20.6 kΩ or equivalently a conductance of 0.63 G_0 over a 15 mV range

In fig. 2.6b, the effect of extending the CI basis by adding the configurations needed to describe higher energy many-electron states is investigated. As can be seen, adding the lower excitations introduces some change in the current relative to basis for the 'ground state' which includes the configurations from the two lowest energy many electron states of b_1 and a_2 symmetry, along with the singly excited configurations relative to the Hartree-Fock determinants for each symmetry. Higher energy excitations are added pairwise by symmetry into the expansion vector. A significant change is seen when adding the sixth excited states of b_1 and a_2 symmetry. The ability to polarise the junction as a voltage is applied requires coupling to lowest lying excitations as in eq. 2.8, and in particular should include the excited states that couple strongly through dipole matrix elements to the ground state as bias across the junction is applied. This is demonstrated in fig. 2.6b where the lowest energy b_1 and a_2 states (plus single excitations) and with the sixth excitations of b_1 and a_2 symmetry included in the CI basis is given. The current in this case is seen to be comparable to the current calculated in the basis with the first six excitations of b_1 and a_2 symmetry included. The current predicted from the CI expansion consisting of the lowest energy states (and

(a)

(b)
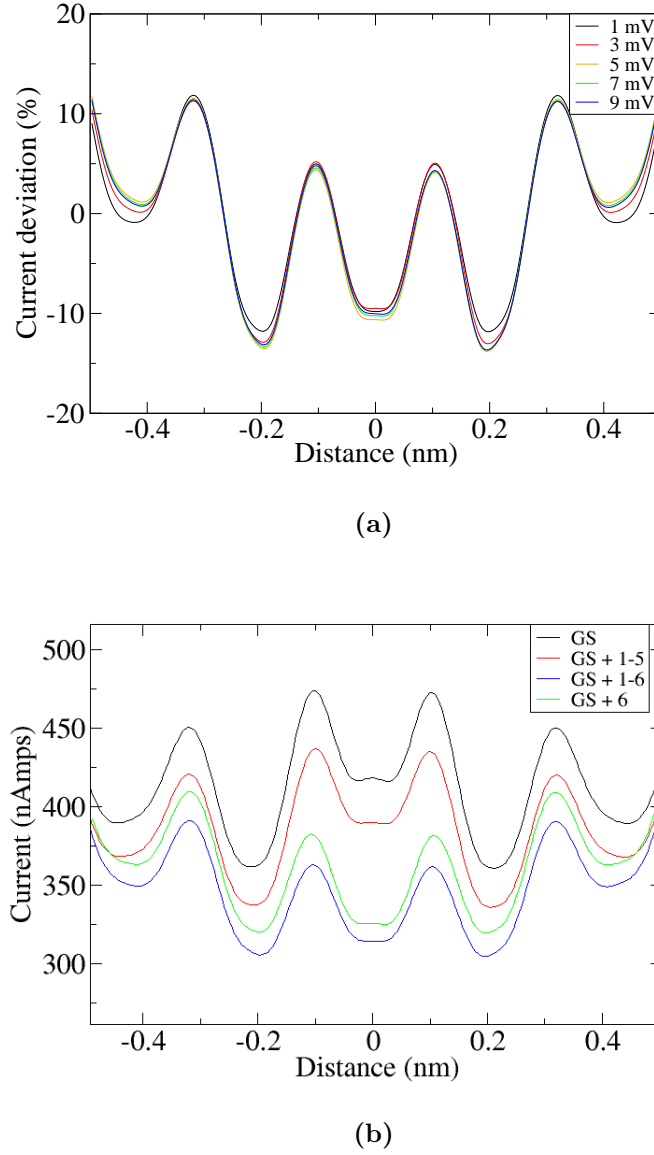
Figure 2.6: (a) Current stability across current carrying region expressing as $\frac{\Delta I}{I}$ as a percentage at 1,3,5,7 and 9 mV. The variation of the current over the scattering region due to finite basis effects is approximately a constant percentage of the total current magnitude. (b) Comparison of the current across scattering region for different many-electron expansions. GS indicates the ground states of b_1 and a_2 symmetry and including all single excitations with respect to these states. GS+ m - n denotes the many electron expansion including GS with the addition of all unique configurations from the first m through n many electron excited states of b_1 and a_2 symmetry ordered by energy. The greatest change to the current is obtained by adding the 6th excitations, revealing that these states couple to the ground state more strongly as an electric field is applied across the junction than the lower lying excitations. Hence it is more important to capture the effect of the states in the many particle expansion that polarise with applied bias than to include all low lying excitations. Voltage bias across the junction is 7mV.

singles) with the inclusion of the first five excitation pairs in b_1 and a_2 symmetry does a relatively poor job of capturing the effects of correlations relative to including only the sixth excitations 'GS + 6'. Hence including the sixth excited states has a greater effect than including the first five excited states. Thus, from the calculations displayed in fig. 2.6b, it is demonstrated that it is more important to include the strongest dipole coupled excitations as opposed to simply choosing the energetically lowest lying states.

2.6 Conclusions

A study of atomic point contacts using the MECS method has been presented. The calculations represent an extension of the MECS cases studied to date to include strong coupling. It is demonstrated that, within reasonable errors due to approximations related to finite atomic electrodes, estimation of the voltage and current, and single and many-electron basis sets, that the method may be applied in the strong coupling limit. It is interesting to note, even in what is believed to be essentially a single-particle regime, our calculations suggest that electron-electron correlations can account for up to a 30% reduction in the current magnitude. Atomic point contacts represent a stringent test case for the MECS method in that accurate measurement of the voltage drop across the junction and an accurate representation of the one-electron density matrix are required to calculate conductances explicitly. The results can be seen to complement recent analytical study of the MECS method for many-(non-interacting) electrons and demonstrates physical predictions using the method can be obtained on realistic atomic and molecular models of tunnel junctions with controllable errors.

2.7   Acknowledgements

References

[1] P. Delaney and J. C. Greer, "Correlated Electron Transport in Molecular Electronics," *Physical Review Letters*, vol. 93, p. 036805, July 2004.

[2] P. Delaney and J. C. Greer, "Quantum electronic transport in a configuration interaction basis," *International Journal of Quantum Chemistry*, vol. 100, pp. 1163–1169, Dec. 2004.

[3] G. Fagas, P. Delaney, and J. C. Greer, "Independent particle descriptions of tunneling using the many-body quantum transport approach," *Physical Review B*, vol. 73, no. 24, p. 241314, 2006.

[4] G. Fagas and J. C. Greer, "Tunnelling in alkanes anchored to gold electrodes via amine end groups," *Nanotechnology*, vol. 18, no. 42, p. 424010, 2007.

[5] S. McDermott, C. B. George, G. Fagas, J. C. Greer, and M. A. Ratner, "Tunnel currents across silane diamines/dithiols and alkane diamines/dithiols: A comparative computational study," *The Journal of Physical Chemistry C*, vol. 113, no. 2, pp. 744–750, 2008.

[6] M. A. Reed, C. Zhou, C. J. Muller, T. P. Burgin, and J. M. Tour, "Conductance of a Molecular Junction," *Science*, vol. 278, pp. 252–254, Oct. 1997.

[7] E. Lörtscher, H. B. Weber, and H. Riel, "Statistical Approach to Investigating Transport through Single Molecules," *Physical Review Letters*, vol. 98,

p. 176807, Apr. 2007.

[8] C. A. Martin, D. Ding, H. S. J. v. d. Zant, and J. M. v. Ruitenbeek, "Lithographic mechanical break junctions for single-molecule measurements in vacuum: possibilities and limitations," *New Journal of Physics*, vol. 10, no. 6, p. 065008, 2008.

[9] L. Venkataraman, J. E. Klare, I. W. Tam, C. Nuckolls, M. S. Hybertsen, and M. L. Steigerwald, "Single-Molecule Circuits with Well-Defined Molecular Conductance," *Nano Letters*, vol. 6, pp. 458–462, Mar. 2006.

[10] F. Chen, X. Li, J. Hihath, Z. Huang, and N. Tao, "Effect of Anchoring Groups on Single-Molecule Conductance: Comparative Study of Thiol-, Amine-, and Carboxylic-Acid-Terminated Molecules," *Journal of the American Chemical Society*, vol. 128, pp. 15874–15881, Dec. 2006.

[11] J. C. Greer, P. Delaney, and G. Fagas, "Comment on "Electron transport through correlated molecules computed using the time-independent Wigner function: Two critical tests"," *Physical Review B*, vol. 82, p. 087301, Aug. 2010.

[12] J. C. Greer, "Variational method with scattering boundary conditions imposed by the Wigner distribution," *Physical Review B*, vol. 83, p. 245413, June 2011.

[13] E. Scheer, N. Agraït, J. C. Cuevas, A. L. Yeyati, B. Ludoph, A. Martín-Rodero, G. R. Bollinger, J. M. van Ruitenbeek, and C. Urbina, "The signature of chemical valence in the electrical conduction through a single-atom contact," *Nature*, vol. 394, pp. 154–157, July 1998.

[14] L. G. C. Rego, A. R. Rocha, V. Rodrigues, and D. Ugarte, "Role of structural evolution in the quantum conductance behavior of gold nanowires during stretching," *Physical Review B*, vol. 67, p. 045412, Jan. 2003.

[15] J. L. Costa-Krämer, N. García, and H. Olin, "Conductance quantization histograms of gold nanowires at 4 K," *Physical Review B*, vol. 55, pp. 12910–12913, May 1997.

[16] V. Rodrigues and D. Ugarte, "Metal nanowires: atomic arrangement and electrical transport properties," *Nanotechnology*, vol. 13, no. 3, p. 404, 2002.

[17] A. Halbritter, S. Csonka, G. Mihály, O. I. Shklyarevskii, S. Speller, and H. van Kempen, "Quantum interference structures in the conductance plateaus of gold nanojunctions," *Physical Review B*, vol. 69, p. 121411, Mar. 2004.

[18] A. I. Yanson, G. R. Bollinger, H. E. van den Brom, N. Agraït, and J. M. van Ruitenbeek, "Formation and manipulation of a metallic wire of single gold atoms," *Nature*, vol. 395, pp. 783–785, Oct. 1998.

[19] J. Kröger, H. Jensen, and R. Berndt, "Conductance of tip–surface and tip–atom junctions on Au(111) explored by a scanning tunnelling microscope," *New Journal of Physics*, vol. 9, no. 5, p. 153, 2007.

[20] C. W. Bauschlicher Jr., J. W. Lawson, A. Ricca, Y. Xue, and M. A. Ratner, "Current–voltage curves for molecular junctions: the effect of Cl substituents and basis set composition," *Chemical Physics Letters*, vol. 388, pp. 427–429, Apr. 2004.

[21] C. Herrmann, G. C. Solomon, J. E. Subotnik, V. Mujica, and M. A. Ratner, "Ghost transmission: How large basis sets can make electron transport calculations worse," *The Journal of Chemical Physics*, vol. 132, p. 024103, Jan. 2010.

[22] J. C. Greer, "Electronic current density expanded in natural orbitals," *Molecular Physics*, vol. 106, pp. 1363–1367, June 2008.

[23] P. Delaney and J. C. Greer, "Classical computation with quantum systems," *Proceedings of the Royal Society of London A: Mathematical, Physical and*

Engineering Sciences, vol. 462, pp. 117–135, Jan. 2006.

[24] W. R. Frensley, "Boundary conditions for open quantum systems driven far from equilibrium," *Reviews of Modern Physics*, vol. 62, pp. 745–791, July 1990.

[25] T. M. Henderson, G. Fagas, E. Hyde, and J. C. Greer, "Determination of complex absorbing potentials from the electron self-energy," *The Journal of Chemical Physics*, vol. 125, p. 244104, Dec. 2006.

[26] J. C. Greer, "Estimating full configuration interaction limits from a Monte Carlo selection of the expansion space," *The Journal of chemical physics*, vol. 103, no. 5, pp. 1821–1828, 1995.

[27] J. C. Greer, "Monte Carlo Configuration Interaction," *Journal of Computational Physics*, vol. 146, pp. 181–202, Oct. 1998.

[28] W. Győrffy, R. Bartlett, and J. Greer, "Monte Carlo configuration interaction predictions for the electronic spectra of Ne, CH2, C2, N2, and H2o compared to full configuration interaction calculations," *The Journal of Chemical Physics*, vol. 129, p. 064103, Aug. 2008.

[29] R. Ahlrichs, M. Bär, M. Häser, H. Horn, and C. Kölmel, "Electronic structure calculations on workstation computers: The program system turbomole," *Chemical Physics Letters*, vol. 162, pp. 165–169, Oct. 1989.

[30] D. Andrae, U. Häußermann, M. Dolg, H. Stoll, and H. Preuß, "Energy-adjustedab initio pseudopotentials for the second and third row transition elements," *Theoretica chimica acta*, vol. 77, pp. 123–141, Mar. 1990.

[31] R. Ross, J. Powers, T. Atashroo, W. Ermler, L. LaJohn, and P. Christiansen, "Ab initio relativistic effective potentials with spin–orbit operators. IV. Cs through Rn," *The Journal of Chemical Physics*, vol. 93, pp. 6654–6670, Nov. 1990.

[32] S.-H. Ke, H. U. Baranger, and W. Yang, "Electron transport through molecules: Self-consistent and non-self-consistent approaches," *Physical Review B*, vol. 70, p. 085410, Aug. 2004.

[33] M. Brandbyge, J.-L. Mozos, P. Ordejón, J. Taylor, and K. Stokbro, "Density-functional method for nonequilibrium electron transport," *Physical Review B*, vol. 65, p. 165401, Mar. 2002.

[34] S. Datta, *Electronic Transport in Mesoscopic Systems*. Cambridge University Press, May 1997.

[35] X. Zhang and D. A. Drabold, "Properties of the density matrix from realistic calculations," *Physical Review B*, vol. 63, p. 233109, May 2001.

[36] J. A. Driscoll and K. Varga, "Calculation of self-energy matrices using complex absorbing potentials in electron transport calculations," *Physical Review B*, vol. 78, p. 245118, Dec. 2008.

[37] B. G. Cook, P. Dignard, and K. Varga, "Calculation of electron transport in multiterminal systems using complex absorbing potentials," *Physical Review B*, vol. 83, p. 205105, May 2011.

Chapter 3

Tunnel Currents across Silane Diamines/Dithiols and Alkane Diamine/Dithiols:A Comparative Computational Study

3.1   Abstract

Two different first-principles methods, one based on density functional theory
combined with Green's functions and the other on a configuration interaction
method, are used to calculate the electronic transport properties of alkane and
silane chains terminated by amine end groups in metal-molecule-metal junctions.
The low voltage conductance is found to decay exponentially with increasing
length in both systems, and decay constants are obtained from the different
methods. Both methods predict smaller conductance values and steeper decay in
the alkane-bridged junctions compared with the silane-bridged junctions, but
quantitative differences in the decay constants obtained from the two formalisms
arise. These differences are attributed to the treatment of the energy-level
alignments in the tunnel junctions as well as the treatment of correlation within
the molecular chains. Additionally, end-group effects for both the alkane and the
silane chains are studied using both a simple tunnel barrier model and complex
band-structure calculations. These results are used to explain differences observed
in conductance decay constants in amine- and thiol-linked junctions obtained from
the two transport methods; the results further highlight the importance of accurate
energy-level alignment between the electrode and molecular states.

3.2   Introduction

As a central problem of molecular electronics, the process of electron transport
through single molecules between metallic electrodes has been achieved
experimentally and studied theoretically [1, 2, 3]. The desire to create junctions
with tailored functionalities has led to work examining the roles that end groups,
molecular energy levels, and contact geometries play in determining the transport
properties of these systems [4, 5, 6, 7, 8, 9, 10, 11, 12, 13, 14]. In particular, recent

studies have examined physical tunnel junctions in which alkanes of varying

lengths are bonded between gold electrodes via amine or thiol linkers

[5, 10, 15, 16, 17, 18, 19, 20, 21]. These junctions exhibit an exponential decrease

in low-voltage conductance, G, with increasing bridging molecular length, l (given

in angstroms or the number of methylene units), as is reasonable for conductance

far from any injection resonance. This behavior is described by:

$$G(l) = G_C exp(-\beta l) \tag{3.1}$$

which is characterized by two parameters: the contact resistance $R_C = \frac{1}{G_C}$ and the

inverse decay length β [22]. The inverse decay length determines how tunnel

conductance and resistance scale with increasing molecular length. The contact

resistance is obtained in the limit $l \longrightarrow 0$ and determines the resistance associated

with the bonding of the end groups to the metal electrodes or contacts. However,

the contact resistance is strongly dependent on the exact configuration of the

metal-molecule bonding site [4, 8, 9], so it will not be discussed in depth in this

chapter (cf. Supporting Information Appendix C).

Most theoretical treatments of conductance in single-molecule junctions up to this

point have been based on density functional theory (DFT) combined with a

nonequilibrium Green's function (NEGF) formalism [23]. The NEGF/DFT

formalism recently has been questioned, however, over concerns that

exchange-correlation effects are leading to spurious conductance values

[24, 25, 26, 27, 28, 29, 30], sometimes described incorrectly by orders of magnitude.

[24] To avoid issues related to exchange-correlation approximations in DFT, a new

transport formalism was recently developed [31, 32]. The method uses a

configuration interaction (CI) method [33, 34] to calculate the electronic structure

of the junction, and transport properties are calculated using the Wigner function

within open boundary conditions under constraint of the maximum entropy

principle. To compare the two methodologies, four test systems were chosen. The amine- and thiol-linked systems were selected as a means to compare the effect of different end groups on conductance, whereas the silane and alkane chains were selected to compare the effects of different chemical backbones and degrees of correlation on the transport. The increased correlation in the silane chains is related to the σ-bond delocalization that has been studied extensively in peralkylated oligosilane chains [35, 36]. The photophysics of these oligosilane chains has indicated that their excitation energies are lower than those of alkane chains, and the size of the band gap in silanes may lead to interesting conductance properties such as a decay length between that of alkanes and π-conjugated systems.

3.3 Computational Methods and Theory

3.3.1 Junction Geometries

Calculations are performed on tunnel junctions consisting of single molecules spanning a gap between two metal clusters. The molecules considered within this study are alkanes and silanes, and both deprotonated thiol $(-S-)$ and amine (NH_2-) end groups are used to bond the molecular chains $(-CH_2-)_n$ and $(-SiH_2-)_n$ to the gold electrodes. A typical geometry is shown in figure 3.1. For thiol end groups, the electrodes are modeled as a 19 gold atom cluster, allowing the thiol to bond to a 3-atom (hollow) site. [37, 38] For amine-gold bonding, a 20-atom cluster is used, allowing the $-NH_2-$ linker group to bond to a single gold apex atom. [20, 39] Details of the generation of the $Au_{19} - S - (CH_2)_n - S - Au_{19}$ and $Au_{19} - S - (SiH_2)_n - S - Au_{19}$ model structures can be found in ref [37], and $Au_{20} - NH_2 - (CH_2)_n - NH_2 - Au_{20}$ model structures are described in ref [39].
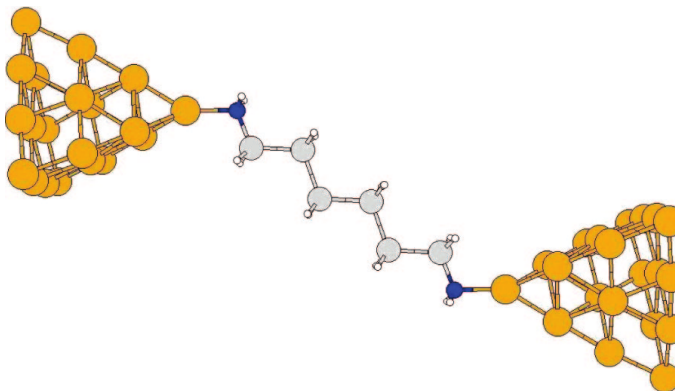
Figure 3.1: Representative tunnel junction model: depicted is the $Au_{20} - NH_2 - (SiH2)_6 - NH_2 - Au_{20}$ junction. An additional 5×5 layer of gold atoms (not shown) is placed on either side of the above junction for the NEGF/DFT calculations to allow for periodic DFT calculations.

For the comparisons presented in this work, additional tunnel junctions $Au_{20} - NH_2 - (SiH_2)_n - NH_2 - Au_{20}$, with n=4,6,8, and 10, are generated; a typical junction model is shown for n=6 in 3.1. For silanes with amine end groups, molecular geometries are relaxed in the model junction with DFT calculations using the B3-LYP hybrid exchange/correlation functional [40, 41] as implemented in the TURBOMOLE program system. [42] A split-valence polarized SV(P) basis set [43] is used for all atoms. This treats all electrons in the molecular chain and the linkers and 19 valence electrons on each atom in the gold clusters. The remaining gold electrons are treated by an effective core potential (ECP). [44]

3.3.2   Transport Methods

Model geometries for the alkanes and silanes terminated with amine $(-NH_2-)$ end groups are used in subsequent transport calculations where electronic currents are calculated using an NEGF/DFT formalism as implemented in ATK2.0. [45] In the NEGF/DFT calculations, the $Au_{20} - NH_2 - (SiH_2)_n - NH_2 - Au_{20}$ and $Au_{20} - NH_2 - (CH_2)_n - NH_2- Au_{20}$ structures are each placed between single layers of 25 gold atoms on either side to allow for periodic DFT calculations. The DFT calculations are performed using the local density approximation (LDA)

parametrized by Perdew and Zunger [46] with a single-ζ plus polarization basis set used for gold atoms and a double-ζ plus polarization basis set used for all other atoms.

Using the same atomic coordinates and reduced CRENBS ECP basis set with one active electron per gold atom, aug-cc-pVDZ basis for all carbon atoms, and relativistic Si-ECP (SEFIT,DF) basis set [47] with four active electrons per silicon atom, electron transport calculations are repeated using methods [31, 32] in which the electronic structure of the tunnel junction is represented by a many-electron or configuration interaction (CI) expansion. [33, 34] We compare the NEGF/DFT transport results with these many-electron correlated scattering (MECS) calculations for the alkanes with amine end groups performed in ref [39] and with MECS calculations performed within this work for the $Au_{20} - NH_2 - (SiH_2)_n - NH_2 - Au_{20}$ junctions. For the MECS studies, structures optimized at the DFT level are used to generate a set of Hartree-Fock orbitals in TURBOMOLE. [42] These orbitals are used as the single-particle basis to generate the many-body bases for the CI calculations. To reduce the size of the configuration space in our many-body approach,ECPs leaving only the gold 6s electron [48] and the silicon $3s^2\,3p^2$ valence electrons [47] explicitly treated are used in generating the Hartree-Fock orbitals. The Hartree-Fock orbital set is truncated by excluding all virtual orbitals with eigenvalues greater than 9.0 eV. This truncation was performed to limit the CI space where 9.0 eV was chosen as orbitals higher than this energy will not contribute to the current. The truncated molecular orbital set is used with the Monte Carlo configuration interaction (MCCI) selection procedure [33, 34] to generate a many-electron basis set for the explicitly correlated transport calculations. A coefficient selection threshold of $c_{min} = 10^{-3}$ is used to generate CI vectors in the A_g singlet ground-state and the first excited singlet state in B_u symmetry. As voltage is applied, these two many-body states couple and allow the junction to polarize. The CI expansion

vectors for the tunnel junctions with varying silane lengths contain from 5000 to 10,000 configuration state functions (CSFs). This level of correlation has been shown to be accurate for reproducing intermediate range electron correlations [49] that dominate correlation energies and seems adequate for molecular transport calculations. [31, 32, 37, 39] These short CI expansions capture a large percentage of the correlation energy (resulting in accurate descriptions of electronic spectra [50, 51]) as required to determine relative energy levels accurately in molecular junctions. MCCI allows for a select choice of highly contributing configurations with a large proportion of the correlation energy in a compact CI expansion. As an example to compute an equivalent full CI calculation it would require vast number of CSFs in the hundreds of thousands as illustrated by the equation A.15.

3.3.3 Tunnel Barrier Model

To gain a better understanding of end-group effects on the decay value β in alkane and silane systems, a simple tunnel barrier model is considered and complex band structures are calculated. In the tunnel barrier model, the tunnel current through a rectangular barrier can be written as:

$$I \propto exp\left[-2l\sqrt{2\frac{m^*}{\hbar^2}\Phi_b}\right] \tag{3.2}$$

where l is the molecular length, m^* represents the effective mass of the charge carriers, and Φ_b is the barrier height. The barrier heights are estimated using the B3-LYP hybrid exchange correlation functional. Optimized structures from the earlier DFT/B3-LYP calculations are used. The highest occupied molecular orbital (HOMO) and lowest unoccupied molecular orbital (LUMO) energy levels for the alkane and silane diamines and dithiols bonded to the gold contacts are approximated by Kohn-Sham eigenvalues. Their energies are measured relative to the Fermi energy, which is taken to be the experimental work function for gold

surfaces of $F = -5.1eV$. [52] The potential energy barrier for electrons is approximated by the offset between the Fermi level and the LUMO state, whereas for hole transport the HOMO/Fermi-level offset is used to approximate the tunnel barrier height. Bandstructures of 1D alkane and polysilane chains are computed to extract electron and hole effective masses from conduction and valence bands, respectively, via $m^* = (\hbar)^2(d^2E/dk^2)^{-1}$ evaluated at the band edge. The bandstructures are calculated by generating hydrogen-terminated molecules composed of either 20 $-CH_2-$ or $-SiH_2-$ units. DFT/B3-LYP calculations using the SV(P) basis set [43] are performed. From this calculation, a Kohn-Sham Hamiltonian matrix is extracted from the chain center to reduce finite length effects using four alkane or silane units. An infinite molecular wire is then generated by periodically repeating the extracted Hamiltonian matrix, yielding infinite chains with a primitive cell that is double the normal size, yielding a lattice constant $2a$. Additionally, complex band structures are calculated to obtain more accurate values (as compared to the simple tunnel barrier model) for the exponential decay of the various chains. [53, 54, 55] Complex band-structure calculations yield the characteristic length of wave function decay for states in an energy gap along the molecular chains in a similar fashion to the decay exponent from the wave function inside the potential barrier. The nonresonant tunneling probability through a unit cell with lattice constant $2a$ is proportional to $e^{-2\beta a}$, or equivalently $e^{-4|Im(k)|a}$, where $k(E)$ is the momentum wavevector. The decay length β can be determined using $\beta(E) = 2\mathrm{Im}k(E)$, and its value is dependent on the location of the Fermi level. The position of the Fermi level is determined using the same HOMO/Fermi-level offset discussed above for the simple tunnel barrier model.

3.4   Computational Results and Discussion

3.4.1   Fermi-Level Alignment

The alignment of the Fermi level relative to the bridging molecule's HOMO and
LUMO in a metal-molecule-metal junction is extremely sensitive to charge transfer
at the metal-molecule interface. [56, 57, 58] The use of DFT to describe the band
alignment in metal-molecule-metal junctions has been studied widely,
[24, 25, 26, 27, 28, 29, 30, 54, 56, 59, 60, 61, 62, 63] and self-interaction errors as
well as a lack of surface polarization response have been shown to yield incorrect
transport properties, even in single-molecule junctions. In light of these issues, we
have chosen to determine the alignment of the Fermi energy with the same
procedure used for the Fermi-level alignment in the tunnel barrier model and the
complex band-structure calculations described in Section 3.3. Conductance values
are determined using the equation for zero bias conductance:

$$G = G_0 T(E_F) \tag{3.3}$$

where G_0 is the fundamental unit of conductance, $2e^2/h = 77.5\mu S$, and $T(E_F)$ is
the transmission at the Fermi energy. Plots of the transmission for the alkane and
silane diamines can be seen in Figures 3.2 and 3.3. In Figure 3.2, the alkane
system shows a broad peak in the transmission plot in the HOMO-LUMO gap that
can be attributed to metal-induced gap states (MIGS) from the Au_{20} clusters. [64]
Because the Fermi level is sufficiently far from the bridging molecule's HOMO and
LUMO, the decay constant β is relatively constant for a range of Fermi-energy
shifts. In Figure 3.3, the silane system shows markedly different transmission
properties. The HOMO-LUMO gap is much smaller than in the alkane case, and β
and the conductance are much more dependent on the exact choice of Fermi level.
The final Fermi energy for the alkane systems lies approximately 3-4 eV above the
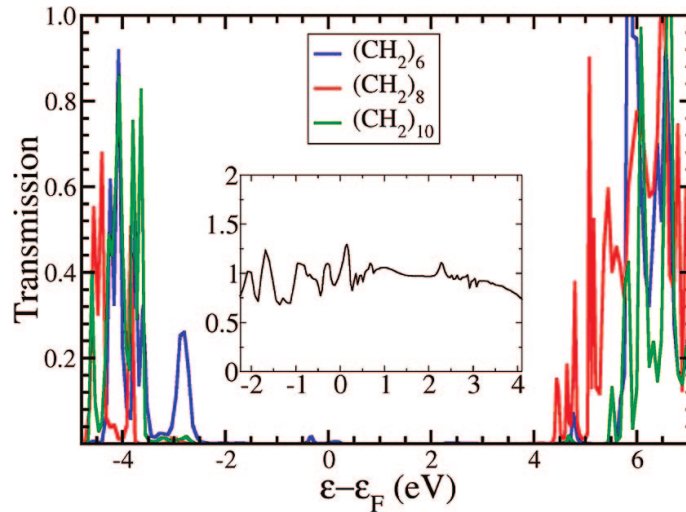
Figure 3.2: Transmission vs energy shifted from the Fermi energy for alkane diamines obtained from NEGF/DFT calculations. The inset shows a plot of the β decay values (per $-CH_2-$) vs a shift in the choice of the Fermi energy.
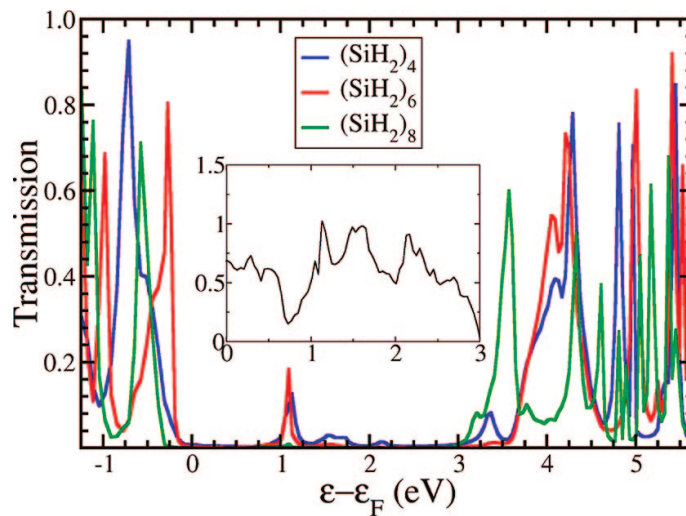

Figure 3.3: Transmission vs energy shifted by the Fermi energy for silane diamines obtained from NEGF/DFT calculations. The peaks in transmission near 1 eV are attributed to metal induced gap states (MIGS). The inset shows a plot of the β decay values vs a shift in the alignment of the Fermi energy. The β decay value varies greatly depending on the Fermi-level band alignment.

HOMOs for the three alkyl chains; this compares well with the 3 eV separation between the Fermi energy and alkyl chain valence band edge predicted by Prodan and Car. [54]

3.4.2   Conductance Results

For alkane diamine tunnel junctions, the change in resistance as a function of the alkane length as predicted by different calculations is shown in Figure 3.4. Previous data from ref [39] using the MECS method [31, 32] and results from our NEGF/DFT calculations using the same geometry as in the MECS study are shown. For comparison, experimental results from Venkataraman et al. [20] are also shown. From Figure 3.4, it is readily seen that the calculations are in good agreement with the experimental results for the alkane diamine tunnel junctions. Previous calculations using the MECS method for the alkane diamine [39] and alkane dithiol [37] junctions found $\beta_C = 0.98/CH_2$ ($\beta = 0.76\text{Å}^{-1}$) and $\beta_C = 0.50/CH_2$ ($\beta = 0.39\text{Å}^{-1}$), respectively. Our NEGF/DFT approach found $\beta_C = 1.01/CH_2$ ($\beta = 0.78\text{Å}^{-1}$) for the alkane diamine junctions, compared to $\beta_C = 0.93/CH_2$ from Wohlthat et al. [65] using an NEGF/DFT approach and $\beta_C = 0.82/CH_2$ from a semianalytical estimation by Prodan et al. [54] Earlier works by Muller, [11] Kaun et al., [66] and Basch et al. [4] report β_C values of $1.24/CH_2$, $0.95/CH_2$, and $1.0/CH_2$ respectively for the alkane dithiol systems studied using the NEGF/DFT formalism.

These are in good agreement with the measurements made for these tunnel junctions [5, 16, 17, 20, 21, 67, 68, 69] as seen in Table 3.1. The contact geometry used in ref [11] for the alkane dithiol system differs from those used in ref [4] and ref [66]; in ref [11], the dithiol linkers are bound to coordinatively unsaturated gold atoms above Au(111) surfaces (similar to the contact geometry for the amine-linked systems in this study), as opposed to the contact geometries in ref [4] and ref [66] in which the sulfur atoms lie above hollow sites on the gold surface. The above-atom geometry in ref [11] yields a 25% larger β_C value as compared with the above hollow-site binding geometries, thus illustrating the sensitivity of the transport properties to the exact junction geometry. Changing the $S - Au$
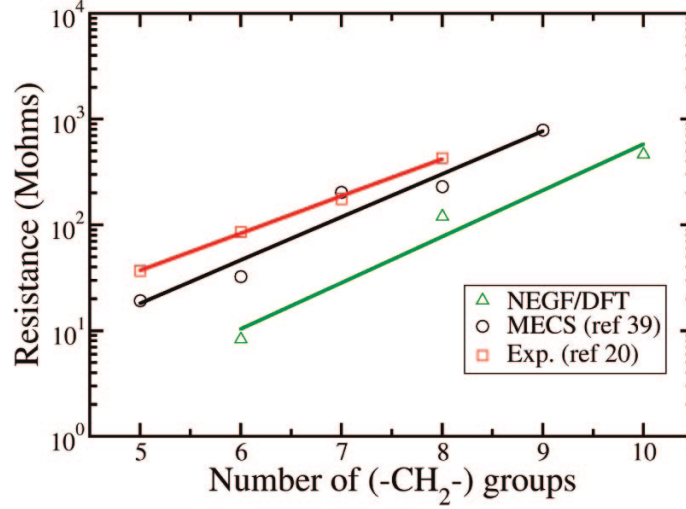
Figure 3.4: Resistance vs number of $-CH_2-$ groups in the alkane diamine systems. The theoretical results (NEGF/DFT and MECS) show good agreement with the experimental results [20] for this system with similar β decay values (calculated from the slopes of the lines of least squares and given in Table 3.1).

Table 3.1: Experimental and Theoretical Decay Values β_C for Both Alkane Dithiols and Alkane Diamines

Amine End Group			
reference	$\beta_C(per-CH_2-)$	reference	$\beta_C(per-CH_2-)$
[5](experiment,HC[a])	0.81 ± 0.01	[65] (theory)	0.93
[5](experiment,LC)	0.88 ± 0.03	MECS (ref [39])	0.98
[20] (experiment)	0.91 ± 0.03	NEGF/DFT (this work)	1.01
[54] (theory)	0.82		
Thiol End Group			
reference	$\beta_C(per-CH_2-)$	reference	$\beta_C(per-CH_2-)$
[4] (theory)	1.0	[17] (experiment, LC)	0.45 ± 0.09
[5] (experiment, HC)	1.02 ± 0.14	[21] (experiment)	1.0 ± 0.05
[5] (experiment, LC)	1.08 ± 0.12	[66] (theory)	0.95
[9](experiment)	1.07 ± 0.05	[67] (experiment)	0.57 ± 0.03
[11] (theory)	1.24	[68] (experiment)	0.68 - 0.79
[16] (experiment)	1.0	[69] (experiment)	0.52 ± 0.05
[17] (experiment, HC)	0.96 ± 0.15	MECS (ref [37])	0.50
[17] (experiment, MC)	0.94 ± 0.05		

[a] For experimental data with multiple peaks in the conductance histogram, peaks are separated as HC for high conductance, MC for medium conductance, and LC for low conductance.
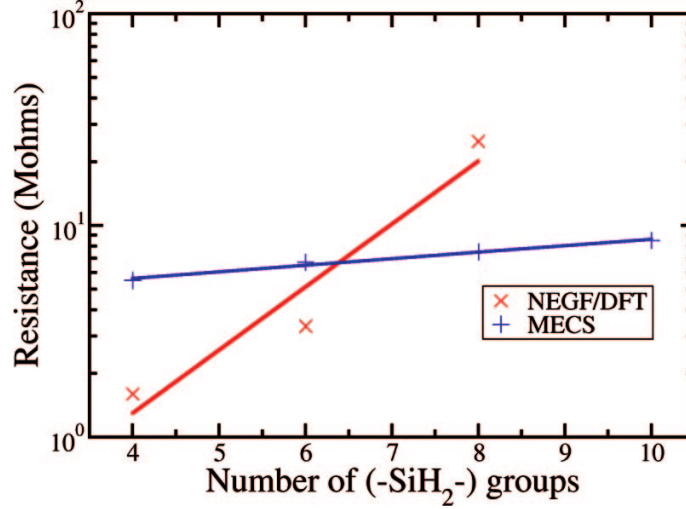
Figure 3.5: Resistance vs number of $-SiH_2-$ groups in the silane diamine systems. The NEGF/DFT results show a steeper slope and hence a larger β value than the MECS results ($\beta_{Si} = 0.69/SiH_2$ for the NEGF/DFT calculations compared with $\beta_{Si} = 0.14/SiH_2$ for the MECS method).

binding geometry from above hollow site to above-atom has a comparable effect to changing the linking atom. MECS calculations for the silane diamine junction yield a decay length $\beta_{Si} = 0.14/SiH_2$ ($\beta = 0.07\text{Å}^{-1}$), whereas our NEGF/DFT calculations for the same junction yield $\beta_{Si} = 0.69/SiH_2$ ($\beta = 0.35\text{Å}^{-1}$); the calculated resistances are plotted in Figure 3.5. Previously reported calculations for silane dithiol tunnel junctions with the CI transport approach yield $\beta_{Si} = 0.18/SiH_2$ ($\beta = 0.09\text{Å}^{-1}$). [37] While to the best of our knowledge silane tunnel junctions have not been studied experimentally, methylated oligosilane chains in donor-bridge-acceptor (D-B-A) systems have been shown to exhibit a bridge attenuation factor of $\beta_{Si} = 0.37/Si$ ($\beta = 0.16\text{Å}^{-1}$), [70] which falls in between our calculated values. The decay factor from electron-transfer data is obtained via a formula similar to eq 3.1: [71]

$$k = k_0 exp(-\beta R_{DA}) \tag{3.4}$$

where k_0 is the rate constant at the reference distance, β is the length decay factor, and R_{DA} is the distance between the donor and acceptor minus the

reference distance. In general, β values calculated from eq 3.4 will be dependent on the inter-site coupling strengths along the bridging molecule as well as the LUMO and energy differences between the bridge and the donor. [72, 73] Interestingly, the β decay factor reported for the oligosilanes is closer to those reported for polyyne ($\beta = 0.10\text{Å}^{-1}$) and polyene ($\beta = 0.08\text{Å}^{-1}$) bridges [74] than those for alkanes. It should be noted, however, that β values below $\sim 0.2\text{Å}^{-1}$ in D-B-A systems may indicate a multistep hopping mechanism as opposed to a single-step tunneling mechanism; [75] the mechanism of charge transfer in silane chains would thus be somewhat ambiguous, whereas the mechanism in polyyne and polyene would likely be best described by hopping. Regardless of the mechanism, combined with the observed reduction in β relative to alkane chains seen in our calculations, these comparisons from electron-transfer data highlight the importance of σ-conjugation for transport in silanes. The reduced HOMO-LUMO gap in the silane chains due to the effects of σ-conjugation causes the decrease in β relative to the alkane chains, and it also could lead to the differences in the MECS and NEGF/ DFT results. Correlation in silane chains has been shown to be greater than in alkane chains, [37] and the different treatments of correlation in the MECS and NEGF/DFT methods should therefore be more visible in the silane results.

3.4.3   Tunnel Barrier Model and Complex Band-Structure Results

Using the MECS approach, the inverse decay lengths for alkanes with different end groups differ by approximately a factor of 2, with $\beta_C = 0.98/\text{CH}_2$ for the alkane diamines and $\beta_C = 0.50/\text{CH}_2$ for the alkane dithiols. This is in contrast with experimental results, which indicate a steeper decay for the thiol end group. [5] This difference can be understood by considering the simple model of tunnel currents through a rectangular potential barrier described in eq 3.2. The HOMO

Table 3.2: : Electron and Hole Effective Masses for Infinite Length Alkane and
Silane Chains as Extracted from Band-Structure Calculations

	alkane	silane
m_e^*	$3.03 m_e{}^a$	$0.22 m_e$
m_h^*	$0.30 m_e$	$0.31 m_e$

$^a m_e$ denotes the free electron mass
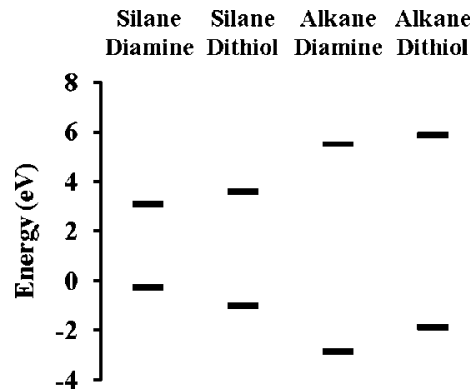
Figure 3.6: Molecular frontier energy levels for the hexane and hexasilane bonded
to gold clusters via amine and thiol end groups. Energies levels are
approximated by the Kohn-Sham eigenvalues from the DFT/B3LYP
calculations described in the text. The zero of energy is taken to
be the Fermi level approximated as the work function of gold (-5.1
eV).[52] The band gaps of the silane chains are much smaller than the
band gaps of the alkane chains, leading to lower β decay values for the
silanes.

and LUMO energies for the molecules between metal clusters are approximated as
Kohn-Sham frontier orbital energies for alkane diamine and dithiol, and for silane
diamine and dithiol, and are plotted relative to the Fermi energy in Figure 3.6.
Bandstructures of extended 1D alkane (compare to refs [54] and [55]) and silane
chains were also calculated and are plotted in Figures 3.7 and 3.8, respectively.
The electron and hole effective masses are extracted from the bandstructures as
described earlier and shown in Table 3.2.

The calculated effective mass for electrons in the alkanes is roughly three times the
free-electron mass m_e and approximately an order of magnitude larger than the
calculated effective mass for holes in alkanes of $0.3 m_e$. The energy-level offsets for
the hexanes (and hexasilanes) with the two different end groups considered in this
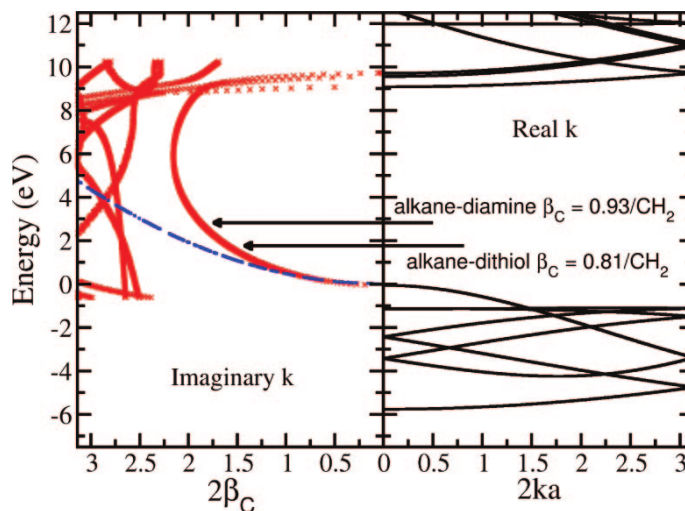
Figure 3.7: Band structure of the alkane chain for propagating states (solid lines)
in the right panel and complex wavevectors of decaying wave functions
(red crosses) in the left panel. The zero of the energy is taken at the top
of the valence band with arrows indicating where the position of the
Fermi energy should be located in alkane-based tunnel junctions with
amine or thiol linkers. Only the complex wave vectors that lie within
the HOMO-LUMO gap are shown. These correspond to two times
the inverse decay length β_C of the probability density per $-CH_2-$
unit. The prediction of the rectangular potential barrier for alkanes is
plotted with a blue dashed line for comparison.

work are displayed in Figure 3.6. The LUMO offsets relative to the Fermi level for
these systems present a barrier of over 5 eV for tunneling electrons, whereas holes
see a barrier of less than 3 eV. This is in agreement with the effective mass data in
Table 3.2 for the alkane system, and we conclude that the electronic current across
the alkanes is dominated by hole transport, as in other tunnel junctions. [58],[66]

Ignoring electrons as charge carriers, the hexane HOMO level offset relative to the
Fermi level is used to approximate the tunnel barrier height, and for the purposes
of our simple model analysis we assume that this is a representative barrier height
for all of the alkane lengths considered. For the alkane diamines, the
HOMO-Fermi-level offset is 2.83 eV, close to the previously reported value of 3 eV,
[54] and larger than the estimated HOMO-Fermi offset for alkane dithiols of 1.84
eV computed in an earlier work. [37] These energy offsets are marked by the
arrows in Figure 3.7. By the position of the arrows in Figure 3.7, we see that this
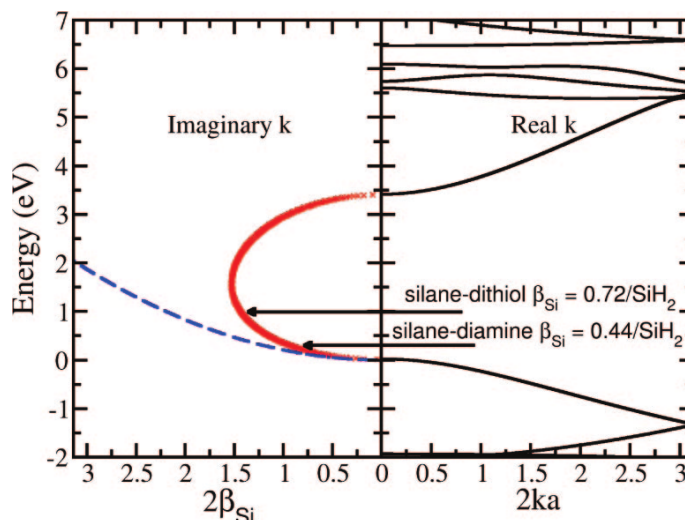
Figure 3.8: Similar to Figure 3.7, but for silicon hydride chains and silane- based tunnel junctions with amine or thiol linkers. The substantially decreased HOMO-LUMO gap size in the silanes, compared to the alkanes (Figure 3.7), makes the values of β_{Si} more sensitive to small differences in the Fermi-level alignment.

simple potential barrier model qualitatively agrees with the MECS results, which predict a larger β value for the amine- linked alkanes compared to the thiol-linked ones (in contrast to the experimental results). Using the tunnel barrier model and the previous discussion of Fermi-level alignment, one can understand why the disagreement with experiment occurs. A moderate shift of the Fermi level away from the HOMO of the alkane dithiol could potentially change the predicted trend of the β decay values. This shift could occur with a more exact treatment of the electronic charge transfer between the molecule and the metal surface [56] or by treating systems with slightly different contact geometries at the metal-molecule interface. [11] Complex band-structure calculations for alkane diamines (Figure 3.7) yielded an inverse decay length of $\beta_C = 0.93/CH_2$, which is in surprisingly good agreement with the direct calculations of the tunnel current. The inverse decay length for alkane dithiols of $\beta_C = 0.81/CH_2$ is lower than the decay value $\beta_C = 1.0/CH_2$ obtained by Tomfohr et al. [55] As with the simple potential barrier model, this is likely due to the different techniques used in determining the position of the Fermi level relative to the HOMO and LUMO of the alkane chain.

The size of the difference between the decay values highlights the sensitivity of the method to Fermi-level alignment. An additional source of disagreement between experimental results and the complex band-structure results could arise from the neglect of the sulfur contribution to the molecular HOMO in the band- structure model (cf. Supporting Information Appendix C). [53, 76] The simple model of electron tunneling through a potential barrier can also be applied to provide a better understanding of the silane systems. The inverse decay lengths β obtained for silanes from the MECS transport calculations are similar in Silane and Alkane Diamines/Dithiols magnitude with $\beta_{Si} = 0.14/\text{SiH}_2$ ($\beta = 0.07\text{Å}^{-1}$) for silane diamines and $\beta_{Si} = 0.18/\text{SiH}_2$ ($\beta = 0.09\text{Å}^{-1}$) for silane dithiols. Because of the reduction of the silane band gap relative to the alkane band gap, we are limited to a qualitative discussion of the observed values of β; the smaller band gap makes the tunnel currents much more sensitive to the approximations made to estimate the tunnel barriers. For the silanes, electron and hole effective masses are of the same order of magnitude with an electron effective mass equal to $0.22m_e$, compared to the hole effective mass of $0.31m_e$. It is found that there is some molecular contribution to the HOMOs of the gold cluster-derived states, which lie around 1.01 and 0.27 eV below the Fermi energy for hexasilane with thiol and amine linkers, respectively. In this case, the Fermi level is not in a midgap position, but the molecular HOMO states are aligned close to the Fermi level (as seen from Figure 3.6). This suggests that the transport is predominately through the HOMO state of the molecule with hole transport dominating the current. The larger potential barrier for hole transport in the silane dithiol systems is consistent with a slightly higher value of β for the thiol-bridged silanes relative to the amine terminated silanes. Complex band-structure calculations for silanes confirm the predictions of the simple square barrier analysis, as shown in Figure 3.8. The silane complex band structures yield $\beta_{Si} = 0.44/\text{SiH}_2$ for the diamine linked and $\beta_{Si} = 0.72/\text{SiH}_2$ for the dithiol linked. The discrepancies between the NEGF/DFT,

complex band structure, and MECS results are likely related to the increased importance of correlation in the silane systems and the differences in how the transport methods compute the electronic structure of the systems (DFT with the LDA/PZ exchange correlation functional for NEGF, DFT with the B3-LYP hybrid exchange correlation functional for band structure, and CI for MECS). The trend observed for the reduction in the β values for the silanes relative to the alkanes is consistent with the simple tunnel barrier model and the complex band-structure analysis. However, the analysis also points out that the exact β values for the silanes are sensitive to small errors in the energy-level alignments. This can be seen in Figure 3.8 where the complex band connecting the valence and conduction bands of the silane systems falls away more steeply from the band edges than the analogous complex band for the alkanes in Figure 3.7.

3.5   Conclusions

A comparative study between an NEGF/DFT method and an MECS formalism for transport in oligoalkane and oligosilane single-molecule transport junctions has been conducted. Conductance values of metal-molecule-metal junctions in which gold electrodes are bridged by alkane and silane diamines and dithiols have been computed using both methods, and the results were interpreted using both a simple potential barrier model and complex band-structure calculations. Conductance results from both the NEGF/DFT and MECS methods and from experiment agree well for the alkane diamine system. For the alkane dithiol system, inverse decay lengths calculated from MECS and NEGF/DFT methods disagree. The source of the disagreement is likely from the different methods used for handling charge transfer at the metal-molecule interface, which has a strong effect on the band alignment. In the case of silane diamine, the NEGF/DFT method yields a higher value for the inverse decay length β compared to the MECS results. The values fall

on either side of the experimental result estimated from electron-transfer reactions. [70] The discrepancy in β values between the two methods could be due in part to the different techniques used to treat correlation between the two formalisms.

The energy-level alignment is found to be critical in all systems for accurately determining end-group effects and inverse decay lengths. Of the four systems studied, the alkane diamine junctions seem to have the most tolerance for error in band alignment, partly due to the large HOMO-LUMO gap and partly due to the nature of the charge transfer between the gold electrode and amine linker. Because the silanes have smaller HOMO-LUMO gaps, errors in the band alignment for these systems are magnified and the inverse decay length is found to be extremely dependent on the exact Fermi-energy position. In both methods, the silane inverse decay length is found to be lower than that of the alkane decay value, indicating that σ-bond delocalization may be another means by which to tailor molecular electronic properties, serving as an intermediate between π-conjugated and nonconjugated systems. This could serve as another potential tool in the tool kit of molecular transport engineering.

3.6   Acknowledgments

Supporting Information Available (Appendix C): A table of contact resistances extrapolated from experimental results compared with contact resistances calculated by the NEGF/DFT and MECS methods is available, and a plot of the partial density of states (PDOS) projected on one of the linking sulfur atoms in a

hexanedithiol bridging molecule is provided to demonstrate the contribution of the sulfur atoms to the molecular HOMO in a tunnel junction. This material is available free of charge via the Internet at http://pubs.acs.org.

References

[1] G. Cuniberti, G. Fagas, and K. Richter, "Introducing molecular electronics: A brief overview," in *Introducing molecular electronics*, pp. 1–10, Springer, 2006.

[2] A. Nitzan and M. A. Ratner, "Electron transport in molecular wire junctions," *Science*, vol. 300, no. 5624, pp. 1384–1389, 2003.

[3] N. J. Tao, "Electron transport in molecular junctions," *Nature nanotechnology*, vol. 1, no. 3, pp. 173–181, 2006.

[4] H. Basch, R. Cohen, and M. A. Ratner, "Interface geometry and molecular junction conductance: Geometric fluctuation and stochastic switching," *Nano letters*, vol. 5, no. 9, pp. 1668–1675, 2005.

[5] F. Chen, X. Li, J. Hihath, Z. Huang, and N. Tao, "Effect of anchoring groups on single-molecule conductance: comparative study of thiol-, amine-, and carboxylic-acid-terminated molecules," *Journal of the American Chemical Society*, vol. 128, no. 49, pp. 15874–15881, 2006.

[6] A. Grigoriev, J. Sköldberg, G. Wendin, and v. Crljen, "Critical roles of metal-molecule contacts in electron transport through molecular-wire junctions," *Physical Review B*, vol. 74, no. 4, p. 045401, 2006.

[7] G. Kim, S. Wang, W. Lu, M. Buongiorno Nardelli, and J. Bernholc, "Effects of end group functionalization and level alignment on electron transport in

molecular devices," *The Journal of chemical physics*, vol. 128, no. 2, p. 024708, 2008.

[8] M. H. Lee, G. Speyer, and O. F. Sankey, "Electron transport through single alkane molecules with different contact geometries on gold," *physica status solidi (b)*, vol. 243, no. 9, pp. 2021–2029, 2006.

[9] X. Li, J. He, J. Hihath, B. Xu, S. M. Lindsay, and N. Tao, "Conductance of single alkanedithiols: conduction mechanism and effect of molecule- electrode contacts," *Journal of the American Chemical Society*, vol. 128, no. 6, pp. 2135–2141, 2006.

[10] C. A. Martin, D. Ding, H. S. van der Zant, and J. M. van Ruitenbeek, "Lithographic mechanical break junctions for single-molecule measurements in vacuum: possibilities and limitations," *New Journal of Physics*, vol. 10, no. 6, p. 065008, 2008.

[11] K.-H. Müller, "Effect of the atomic configuration of gold electrodes on the electrical conduction of alkanedithiol molecules," *Physical Review B*, vol. 73, no. 4, p. 045403, 2006.

[12] Y. Xue and M. A. Ratner, "Microscopic study of electrical transport through individual molecules with metallic contacts. II. Effect of the interface structure," *Physical Review B*, vol. 68, no. 11, p. 115407, 2003.

[13] Y. Xue and M. A. Ratner, "End group effect on electrical transport through individual molecules: A microscopic study," *Physical Review B*, vol. 69, no. 8, p. 085403, 2004.

[14] X.-Y. Zhu, *Charge transport at metal- molecule interfaces: a spectroscopic view*. ACS Publications, 2004.

[15] L. A. Bumm, J. J. Arnold, T. D. Dunbar, D. L. Allara, and P. S. Weiss, "Electron transfer through organic molecules," *The Journal of Physical*

Chemistry B, vol. 103, no. 38, pp. 8122–8127, 1999.

[16] S.-Y. Jang, P. Reddy, A. Majumdar, and R. A. Segalman, "Interpretation of stochastic events in single molecule conductance measurements," *Nano letters*, vol. 6, no. 10, pp. 2362–2367, 2006.

[17] C. Li, I. Pobelov, T. Wandlowski, A. Bagrets, A. Arnold, and F. Evers, "Charge transport in single Au| alkanedithiol| Au junctions: coordination geometries and conformational degrees of freedom," *Journal of the American Chemical Society*, vol. 130, no. 1, pp. 318–326, 2008.

[18] J. R. Petta, D. G. Salinas, and D. C. Ralph, "Measurements of discrete electronic states in a gold nanoparticle using tunnel junctions formed from self-assembled monolayers," *Applied Physics Letters*, vol. 77, no. 26, pp. 4419–4421, 2000.

[19] M. Suzuki, S. Fujii, S. Wakamatsu, U. Akiba, and M. Fujihira, "Self-assembly of thiolates with alicyclic moieties on Au (111)," *Nanotechnology*, vol. 15, no. 4, p. S150, 2004.

[20] L. Venkataraman, J. E. Klare, I. W. Tam, C. Nuckolls, M. S. Hybertsen, and M. L. Steigerwald, "Single-molecule circuits with well-defined molecular conductance," *Nano Letters*, vol. 6, no. 3, pp. 458–462, 2006.

[21] B. Xu and N. J. Tao, "Measurement of single-molecule resistance by repeated formation of molecular junctions," *Science*, vol. 301, no. 5637, pp. 1221–1223, 2003.

[22] S. H. Choi, B. Kim, and C. D. Frisbie, "Electrical resistance of long conjugated molecular wires," *Science*, vol. 320, no. 5882, pp. 1482–1486, 2008.

[23] S. Datta, *Quantum transport: atom to transistor.* Cambridge University Press, 2005.

[24] F. Evers, F. Weigend, and M. Koentopp, "Conductance of molecular wires and transport calculations based on density-functional theory," *Physical Review B*, vol. 69, no. 23, p. 235411, 2004.

[25] S.-H. Ke, H. U. Baranger, and W. Yang, *Role of the exchange-correlation potential in ab initio electron transport calculations*. AIP, 2007.

[26] M. Koentopp, K. Burke, and F. Evers, "Zero-bias molecular electronics: Exchange-correlation corrections to Landauer's formula," *Physical Review B*, vol. 73, no. 12, p. 121403, 2006.

[27] J. B. Neaton, M. S. Hybertsen, and S. G. Louie, "Renormalization of molecular electronic levels at metal-molecule interfaces," *Physical review letters*, vol. 97, no. 21, p. 216405, 2006.

[28] K. S. Thygesen, "Impact of Exchange-Correlation Effects on the I V Characteristics of a Molecular Junction," *Physical review letters*, vol. 100, no. 16, p. 166804, 2008.

[29] C. Toher, A. Filippetti, S. Sanvito, and K. Burke, "Self-interaction errors in density-functional calculations of electronic transport," *Physical review letters*, vol. 95, no. 14, p. 146402, 2005.

[30] C. Toher and S. Sanvito, "Effects of self-interaction corrections on the transport properties of phenyl-based molecular junctions," *Physical Review B*, vol. 77, no. 15, p. 155402, 2008.

[31] P. Delaney and J. C. Greer, "Quantum electronic transport in a configuration interaction basis," *International journal of quantum chemistry*, vol. 100, no. 6, pp. 1163–1169, 2004.

[32] P. Delaney and J. C. Greer, "Correlated electron transport in molecular electronics," *Physical review letters*, vol. 93, no. 3, p. 036805, 2004.

[33] J. C. Greer, "Estimating full configuration interaction limits from a Monte Carlo selection of the expansion space," *The Journal of chemical physics*, vol. 103, no. 5, pp. 1821–1828, 1995.

[34] J. C. Greer, "Monte Carlo Configuration Interaction," *Journal of Computational Physics*, vol. 146, pp. 181–202, Oct. 1998.

[35] H. A. Fogarty, D. L. Casher, R. Imhof, T. Schepers, D. W. Rooklin, and J. Michl, "For reviews consult Ref. 2a and 2d and Pure Appl," *Chem*, vol. 75, p. 999, 2003.

[36] R. D. Miller and J. Michl, "Polysilane high polymers," *Chemical Reviews*, vol. 89, no. 6, pp. 1359–1410, 1989.

[37] G. Fagas, P. Delaney, and J. C. Greer, "Independent particle descriptions of tunneling using the many-body quantum transport approach," *Physical Review B*, vol. 73, no. 24, p. 241314, 2006.

[38] J. A. Larsson, M. Nolan, and J. C. Greer, "Interactions between thiol molecular linkers and the Au13 nanoparticle," *The Journal of Physical Chemistry B*, vol. 106, no. 23, pp. 5931–5937, 2002.

[39] G. Fagas and J. C. Greer, "Tunnelling in alkanes anchored to gold electrodes via amine end groups," *Nanotechnology*, vol. 18, no. 42, p. 424010, 2007.

[40] A. D. Becke, "Density-functional thermochemistry. III. The role of exact exchange," *The Journal of chemical physics*, vol. 98, no. 7, pp. 5648–5652, 1993.

[41] P. J. Stephens, F. J. Devlin, C. Chabalowski, and M. J. Frisch, "Ab initio calculation of vibrational absorption and circular dichroism spectra using density functional force fields," *The Journal of Physical Chemistry*, vol. 98, no. 45, pp. 11623–11627, 1994.

[42] R. Ahlrichs, M. Bär, M. Häser, H. Horn, and C. Kölmel, "Electronic structure calculations on workstation computers: The program system turbomole," *Chemical Physics Letters*, vol. 162, no. 3, pp. 165–169, 1989.

[43] F. Weigend, M. Häser, H. Patzelt, and R. Ahlrichs, "RI-MP2: optimized auxiliary basis sets and demonstration of efficiency," *Chemical physics letters*, vol. 294, no. 1, pp. 143–152, 1998.

[44] R. B. Ross, J. M. Powers, T. Atashroo, W. C. Ermler, L. A. LaJohn, and P. A. Christiansen, "A binitio relativistic effective potentials with spin–orbit operators. IV. Cs through Rn," *The Journal of chemical physics*, vol. 93, no. 9, pp. 6654–6670, 1990.

[45] M. Brandbyge, J.-L. Mozos, P. Ordejón, J. Taylor, and K. Stokbro, "Density-functional method for nonequilibrium electron transport," *Physical Review B*, vol. 65, no. 16, p. 165401, 2002.

[46] J. P. Perdew and A. Zunger, "Self-interaction correction to density-functional approximations for many-electron systems," *Physical Review B*, vol. 23, no. 10, p. 5048, 1981.

[47] G. Igel-Mann, H. Stoll, and H. Preuss, "Pseudopotentials for main group elements (IIIa through VIIa)," *Molecular Physics*, vol. 65, no. 6, pp. 1321–1328, 1988.

[48] P. Fuentealba, H. Stoll, L. v. Szentpaly, P. Schwerdtfeger, and H. Preuss, "On the reliability of semi-empirical pseudopotentials: simulation of Hartree-Fock and Dirac-Fock results," *Journal of Physics B: Atomic and Molecular Physics*, vol. 16, no. 11, p. L323, 1983.

[49] D. Prendergast, M. Nolan, C. Filippi, S. Fahy, and J. C. Greer, "Impact of electron–electron cusp on configuration interaction energies," *The Journal of Chemical Physics*, vol. 115, no. 4, pp. 1626–1634, 2001.

[50] W. Gy\Horffy, R. J. Bartlett, and J. C. Greer, "Monte Carlo configuration interaction predictions for the electronic spectra of Ne, CH 2, C 2, N 2, and H 2 O compared to full configuration interaction calculations," *The Journal of chemical physics*, vol. 129, no. 6, p. 064103, 2008.

[51] J. A. Larsson, L. Tong, T. Cheng, M. Nolan, and J. C. Greer, "A basis set study for the calculation of electronic excitations using Monte Carlo configuration interaction," *The Journal of Chemical Physics*, vol. 114, no. 1, pp. 15–22, 2001.

[52] W. N. Hansen and K. B. Johnson, "Work function measurements in gas ambient," *Surface science*, vol. 316, no. 3, pp. 373–382, 1994.

[53] G. Fagas, A. Kambili, and M. Elstner, "Complex-band structure: a method to determine the off-resonant electron transport in oligomers," *Chemical physics letters*, vol. 389, no. 4, pp. 268–273, 2004.

[54] E. Prodan and R. Car, "Tunneling conductance of amine-linked alkyl chains," *Nano letters*, vol. 8, no. 6, pp. 1771–1777, 2008.

[55] J. K. Tomfohr and O. F. Sankey, "Complex band structure, decay lengths, and Fermi level alignment in simple molecular electronic systems," *Physical Review B*, vol. 65, no. 24, p. 245105, 2002.

[56] R. Stadler and K. W. Jacobsen, "Fermi level alignment in molecular nanojunctions and its relation to charge transfer," *Physical Review B*, vol. 74, no. 16, p. 161405, 2006.

[57] W. Tian, S. Datta, S. Hong, R. Reifenberger, J. I. Henderson, and C. P. Kubiak, "Conductance spectra of molecular wires," *The Journal of chemical physics*, vol. 109, no. 7, pp. 2874–2882, 1998.

[58] Y. Xue, S. Datta, and M. A. Ratner, "Charge transfer and "band lineup" in molecular electronic devices: A chemical and numerical interpretation," *The*

Journal of Chemical Physics, vol. 115, no. 9, pp. 4292–4299, 2001.

[59] M. Koentopp, C. Chang, K. Burke, and R. Car, "Density functional calculations of nanoscale conductance," *Journal of Physics: Condensed Matter*, vol. 20, no. 8, p. 083203, 2008.

[60] S. Y. Quek, L. Venkataraman, H. J. Choi, S. G. Louie, M. S. Hybertsen, and J. B. Neaton, "Amine- gold linked single-molecule circuits: experiment and theory," *Nano Letters*, vol. 7, no. 11, pp. 3477–3482, 2007.

[61] J. R. Reimers, Z.-L. CAI, A. Bilić, and N. S. Hush, "The Appropriateness of Density-Functional Theory for the Calculation of Molecular Electronics Properties," *Annals of the New York Academy of Sciences*, vol. 1006, no. 1, pp. 235–251, 2003.

[62] C. Toher and S. Sanvito, "Efficient atomic self-interaction correction scheme for nonequilibrium quantum transport," *Physical review letters*, vol. 99, no. 5, p. 056801, 2007.

[63] J.-g. Wang, E. Prodan, R. Car, and A. Selloni, "Band alignment in molecular devices: Influence of anchoring group and metal work function," *Physical Review B*, vol. 77, no. 24, p. 245443, 2008.

[64] v. Crljen, A. Grigoriev, G. Wendin, and K. Stokbro, "Nonlinear conductance in molecular devices: molecular length dependence," *Physical Review B*, vol. 71, no. 16, p. 165316, 2005.

[65] S. Wohlthat, F. Pauly, and J. R. Reimers, "The conduction properties of α, ω-diaminoalkanes and hydrazine bridging gold electrodes," *Chemical Physics Letters*, vol. 454, no. 4, pp. 284–288, 2008.

[66] C.-C. Kaun and H. Guo, "Resistance of alkanethiol molecular wires," *Nano letters*, vol. 3, no. 11, pp. 1521–1525, 2003.

[67] X. D. Cui, A. Primak, X. Zarate, J. Tomfohr, O. F. Sankey, A. L. Moore, T. A. Moore, D. Gust, L. A. Nagahara, and S. M. Lindsay, "Changes in the electronic properties of a molecule when it is wired into a circuit," *The Journal of Physical Chemistry B*, vol. 106, no. 34, pp. 8609–8614, 2002.

[68] H. B. Akkerman, P. W. Blom, D. M. De Leeuw, and B. De Boer, "Towards molecular electronics with large-area molecular junctions," *Nature*, vol. 441, no. 7089, pp. 69–72, 2006.

[69] W. Haiss, R. J. Nichols, H. van Zalinge, S. J. Higgins, D. Bethell, and D. J. Schiffrin, "Measurement of single molecule conductivity using the spontaneous formation of molecular wires," *Physical Chemistry Chemical Physics*, vol. 6, no. 17, pp. 4330–4337, 2004.

[70] M. Sasaki, Y. Shibano, H. Tsuji, Y. Araki, K. Tamao, and O. Ito, "Oligosilane Chain-Length Dependence of Electron Transfer of Zinc Porphyrin- Oligosilane- Fullerene Molecules," *The Journal of Physical Chemistry A*, vol. 111, no. 16, pp. 2973–2979, 2007.

[71] G. L. Closs and J. R. Miller, "Intramolecular long-distance electron transfer in organic molecules," *Science*, vol. 240, no. 4851, pp. 440–448, 1988.

[72] M. P. Eng and B. Albinsson, "Non-Exponential Distance Dependence of Bridge-Mediated Electronic Coupling," *Angewandte Chemie International Edition*, vol. 45, no. 34, pp. 5626–5629, 2006.

[73] M. A. Ratner, "Bridge-assisted electron transfer: effective electronic coupling," *Journal of Physical Chemistry*, vol. 94, no. 12, pp. 4877–4883, 1990.

[74] A. Osuka, N. Tanabe, S. Kawabata, I. Yamazaki, and Y. Nishimura, "Synthesis and intramolecular electron-and energy-transfer reactions of polyyne-or polyene-bridged diporphyrins," *The Journal of Organic Chemistry*, vol. 60, no. 22, pp. 7177–7185, 1995.

[75] Y. A. Berlin, F. C. Grozema, L. D. Siebbeles, and M. A. Ratner, "Charge transfer in donor-bridge-acceptor systems: Static disorder, dynamic fluctuations, and complex kinetics," *The Journal of Physical Chemistry C*, vol. 112, no. 29, pp. 10988–11000, 2008.

[76] J. K. Tomfohr and O. F. Sankey, "Simple estimates of the electron transport properties of molecules," *physica status solidi (b)*, vol. 233, no. 1, pp. 59–69, 2002.

Chapter 4

Electronegativity and Electron Currents in Molecular Tunnel Junctions

4.1 Abstract

Electronegativity is shown to control charge transfer, energy level alignments, and electron currents in single-molecule tunnel junctions, all of which are described through the density matrix. Currents calculated from the one-electron reduced density matrix correct to second order in electron-electron correlation are identical to currents obtained from the one-electron Green's function corrected to second order in electron self-energy. A tight binding model of hexa-1,3,5-triene-1,6-dithiol bonded between metal electrodes is introduced and the effect of analytically varying electron-electron correlation on electron currents and electronegativity is examined. The model analysis is compared to electronic structure descriptions of a gold-hexatriene (approximated by different exchange-correlation functionals) and Hartree-Fock states as 0th order approximations to the one-electron Green's function. Comparison between the model calculations and the electronic structure treatment allows us to relate the ability to describe electronegativity within a single-particle approximation to predictions of current-voltage characteristics for molecular tunnel junctions.

4.2 Introduction

Prediction of electron transport across single molecules requires determination of electronic structure in the presence of open boundary conditions, whether using a non-equilibrium statistical or dynamical theory [1, 2, 3, 4, 5, 6]. Statistical approaches concentrate directly on the non-equilbrium density matrix, whereas if the time evolution for a system driven from equilibrium is followed, attention is usually focused on the non-equilibrium Green's functions (NEGF) describing electron propagation. Treating electronic structure within transport theories requires an understanding of the intriguing, but challenging to calculate, effects of

electron-electron correlations. As exact approaches are limited to model systems or
nanostructures with a small number of electrons, attention has focused on
improving addition spectra both in the independent electron approximation [7, 8, 9]
and by many-body treatments through the GW scheme [10, 11, 12]. In the
following, we consider correlation corrections to independent particle models and
relate conditions on the one-electron Green's function and reduced density matrix
for calculation of currents within non-equilibrium theories. Correlation corrections
to the density matrix are shown to correspond to improving ionization potentials
(IPs) and electron affinities (EAs). This leads to a discussion of electron currents
in terms of electronegativity: the impact of the electronegativity on charge
transfer, energy level alignments, and current magnitudes is determined.

4.3   One-electron reduced density matrix and Green's function

Electron currents may be calculated from the one-electron reduced density
matrix [13, 14, 15] as

$$J(\mathbf{r}) = \frac{1}{2i}[\nabla_{\mathbf{r}} - \nabla_{\mathbf{r}'}]\rho(\mathbf{r}, \mathbf{r}')|_{\mathbf{r}'=\mathbf{r}}, \tag{4.1}$$

with J the current density, $\mathbf{r}$ a position vector, and ρ the one-electron reduced
density matrix (RDM); atomic units are implied unless otherwise given. As the
current density operator is a one-body differential operator, to obtain accurate
predictions for electron currents it is necessary to obtain accurate predictions of
the RDM; the error in calculating currents with an approximate RDM has recently
been explored [16]. From another viewpoint, calculation of the current can also
proceed through computation of the one electron retarded and advanced Green's

functions $G_{r,a}$ and application of a Landauer-type formula [17, 18]:

$$I = \frac{1}{\pi} \int d\omega \, [f_L(\omega; \mu_L) - f_R(\omega; \mu_R)] \mathrm{Tr}[\, \Gamma_L(\omega) \, G_a(\omega) \, \Gamma_R(\omega) \, \Lambda \, G_r(\omega) \,], \qquad (4.2)$$

with electron energy ω, $\Gamma_{L,R}$ spectral densities, $f_{L,R}$ energy distributions with $\mu_{L,R}$ chemical potentials in the left (L) and right (R) electron reservoirs, and Λ is the correction due to correlations weighted by the spectral density of the electrodes and electron-electron spectral density on the molecule. The causal Green's function is related to the RDM via the relation

$$\rho(\mathbf{r}, \mathbf{r}') = \frac{1}{2\pi i} \oint d\omega \, G(\mathbf{r}, \mathbf{r}'; \omega), \qquad (4.3)$$

with the complex integration performed along the Coulson contour. We begin by recalling that the reduced density matrix obtained from a many-electron wavefunction corrected to second order in electron correlation is equivalent to the reduced density matrix arising from correcting IPs and EAs in the Green's function to second order in the electron self-energy [19]. Details of the relationship of the one-electron Green's function and the density matrix are given in the Supplemental Information (Appendix D), here a general presentation is given.

A perturbation expansion in λ is written for the many-electron wavefunction:

$$|\Psi> = |\Psi^{(0)}> + \lambda|\Psi^{(1)}> + \lambda^2|\Psi^{(2)}> + \dots \; . \qquad (4.4)$$

For the choice of the Hartree-Fock operator as a 0th order approximation, Brillouin's theorem ensures that the first order wavefunction consists of only double electron excitations, on the other hand the second order term includes single through quadruple excitations. From

$$\rho(\mathbf{r}, \mathbf{r}') = < \Psi | \hat{\psi}^\dagger(\mathbf{r}') \hat{\psi}(\mathbf{r}) | \Psi >, \qquad (4.5)$$

to first order in λ the correction to the 0th order density matrix vanishes [20]. The density matrix to second order is

$$\rho \approx \rho^{(0)} + \lambda^2 \rho^{(2)}. \tag{4.6}$$

In the Green's function formalism, transmission resonances are associated with its poles and can be identified as IPs and EAs. It is well-known that introduction of correlation corrections beyond independent particle models for the Green's function improves the prediction of IPs and EAs [19]. Hence, it is reasonable to assume that if an independent particle picture is chosen to optimize IPs and EAs, it follows that prediction of currents from the NEGF approach will be improved. In this context, a model for transport is measured in terms of reproducing the molecular electronegativity.

The Green's function with second order self-energies $[G^{(2)}(\omega)]^{-1}$ has been studied by Pickup and Goscinski [19]. They obtain the lowest order improvement to Koopmans' IPs and EAs from the poles of the diagonal elements of $G(\omega)$. It is found the self-energy corrects Koopmans' IP ϵ_i through terms describing orbital relaxation and pair correlations; a similar interpretation holds for corrections to the EAs [19]. Within this approximation, it is also possible to determine the density matrix directly from eq. 4.3; the resulting density matrix coincides *exactly* with the density matrix calculated from eq. 4.4 through $O(\lambda^2)$. Hence calculating the density matrix through second order in electron correlation and correcting IPs and EAs with second order self-energies $\Sigma^{(2)}$ will lead to the same predictions for electron current. For moderate electron correlations, improving spectra for independent particle models or explicitly including correlations in the RDM are equivalent [19, 20].

A criterion for selecting an independent particle model for quantum electronic

transport was given as the set of single-particle states yielding an approximate density matrix with maximal overlap to the exact RDM [21]. The single-electron states diagonalizing the RDM are natural orbitals (NOs) [22] and their eigenvalues ρ_i are known as natural occupations. If one asks what is the best finite expansion approximation $\tilde{\rho}$ to the exact RDM

$$\int |\rho - \tilde{\rho}|^2 d\mathbf{r}\,d\mathbf{r}' = \min, \qquad (4.7)$$

it is found that including the first n natural orbitals with the largest occupancies for a truncated expansion fulfils the least squares condition [20]. We consider the couplings between density matrix coefficients by writing

$$\rho = \begin{bmatrix} \rho_{ij} & \rho_{ia} \\ \rho_{ai} & \rho_{ab} \end{bmatrix}, \qquad (4.8)$$

with $(i\,j)$, $(a\,b)$, and $(i\,a)$ denoting occupied-occupied, unoccupied-unoccupied, and occupied-unoccupied spaces respectively, with occupations referred to the 0th order wavefunction. The natural orbitals to second order in electron correlation are given by the eigenfunctions of eq. 4.8. Constructing the "best" independent particle picture in the sense of eq. 4.7 implies occupying a single Slater determinant by the first n_e natural orbitals. We have previously shown numerically that a single determinant composed of the largest occupation number NOs can lead to essentially the same results as a full many-body treatment for tunneling through alkanes [21]. For a single determinant approximation, the density matrix is idempotent ($\rho^2 = \rho$), which occurs since the first n_e occupations are equal to 1 with all others 0. Hence a measure for the quality of a single determinant approximation is how well the eigenvalues of eq. 4.8 approximate the idempotency condition. As the ρ_{ia} couplings between the occupied and unoccupied spaces becomes stronger, the occupations of the 0th order states can become significantly

less than unity. From many-body theory it is well understood what this condition implies: a single determinant or independent particle picture is no longer useful as a 0th order wavefunction. For weak to moderate correlations, the Green's function approach can achieve improved IPs and EAs by a low order approximation to the electron self-energy. As natural occupancies in the 0th order wavefunction become very much less than unity, a perturbation expansion about an independent particle picture loses meaning and even higher order corrections to $|\Psi^{(0)}>$ will not correct IPs and EAs on the molecular region. In a similar context, this is seen as the failing of the GW approximation for systems with multi-determinantal ground states [23] or in strongly correlated electron transport [10, 11, 12]. For strong electron correlations coupled-cluster theory offers a convenient nonperturbative framework from which higher order approximations to the density matrix follow [24], alternatively correlated one particle methods [25, 26] to infinite order can be chosen to yield correct IPs and EAs.

4.4 Electronegativity and electron-electron correlation

The Mulliken electronegativity given as (IP+EA)/2 is a useful measure of charge transfer, and it is charge transfer that determines molecular level alignments relative to electron reservoir energies [27, 28]. Predicting level alignments correctly for molecules bonded between electrodes is essential for accurate current-voltage characteristics [29]. In the Hartree-Fock approximation, charge transfer is under-estimated as hybridization to virtual states is weak. In the local density (LDA) and generalized gradient (GGA) approximations to density functional theory (DFT), charge transfer is over-estimated [30]. These effects are demonstrated for the case of hexa-1,3,5-triene-1,6-dithiol (for ease of notation, we
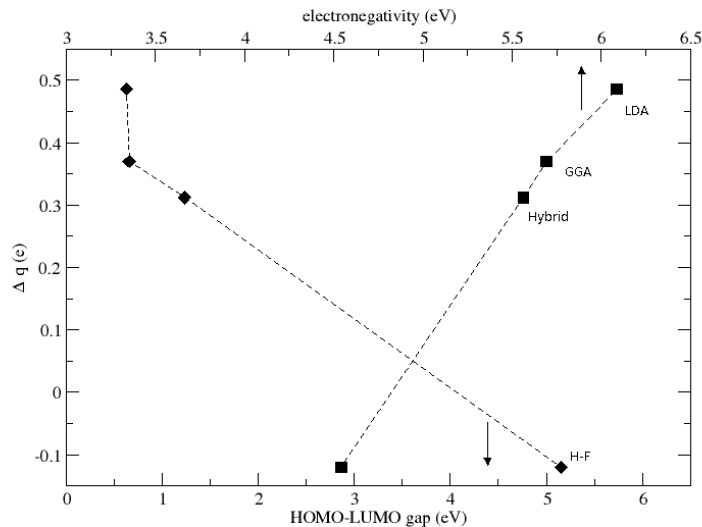
Figure 4.1: Charge transfer versus Highest Occupied and Lowest Unoccupied
(HOMO-LUMO) energy gap and electronegativity for hexatriene
dithiol bonded to linear gold chains. Calculations have been performed
with the TURBOMOLE program system [32, 33]. All calculations
have been performed using the aug-cc-pVDZ basis set for carbon [34]
and split valence polarized valence basis for all other atoms, including
a sixty electron effective core potential for the gold atoms [32, 33].
Calculations have been performed using the Hartree-Fock and den-
sity functional theory calculations using hybrid (B3-LYP), generalized
gradient approximation (GGA/PBE), and local density approximation
(LDA/PW) exchange-correlation functionals.

subsequently refer to hexatriene dithiol) bonded between two linear gold chains in

fig. 4.1 where the highest occupied-lowest unoccupied energy gap in the molecular

orbitals (HOMO-LUMO gap) and molecular electronegativity is given against

charge transfer relative to molecular hexatriene dithiol. For a large HOMO-LUMO

gap or weak electronegativity, charge transfer is small. For small HOMO-LUMO

gaps typical of GGA and LDA, over-estimation of charge transfer is confirmed.

Hybrid functionals correct charge transfer to some extent, but this correction is

not systematic [30] and other approaches to capturing electron-electron

correlations may yield results intermediate to HF and approximate DFT [31].

We introduce a simple correlated model for a molecular chain and investigate the

effect of over- and under-estimation of electronegativity on electron transport. We

use the following model Hamilitonian for an infinite chain:

$$
\begin{aligned}
\hat{H} = \; & - \; \gamma_L \sum_{n<-3} (\hat{c}_n^\dagger \hat{c}_{n-1} + h.c.) + \sum_{n<-3} (\epsilon_L + V_L)\, \hat{c}_n^\dagger \hat{c}_n - \gamma_{LM}(\hat{c}_{-4}^\dagger \hat{b}_{-3} + h.c.) \\
& + \; \sum_{n=-3}^{+3} (\epsilon_M + V_n)\, \hat{b}_n^\dagger \hat{b}_n - \gamma_M(\hat{b}_{-3}^\dagger \hat{b}_{-2} + \hat{b}_{-1}^\dagger \hat{b}_1 + \hat{b}_2^\dagger \hat{b}_3 + h.c.) \\
& - \; \Gamma_M(\hat{b}_{-2}^\dagger \hat{b}_{-1} + \hat{b}_1^\dagger \hat{b}_2 + h.c.) - \gamma_{MR}(\hat{b}_{+3}^\dagger \hat{c}_{+4} + h.c.) \\
& + \; \sum_{n>+3} (\epsilon_R + V_R)\, \hat{c}_n^\dagger \hat{c}_n - \gamma_R \sum_{n>+3} (\hat{c}_n^\dagger \hat{c}_{n+1} + h.c.) \quad (4.9)
\end{aligned}
$$

Six central sites of the chain are labelled -3, -2, -1, 1, 2 ,3 (i.e. there is no 0 site) and are treated as the molecular region with $\hat{b}^\dagger, \hat{b}$ creation and annihilation operators for electrons on the molecule. The electron reservoirs are described by the atomic sites extending towards the left and right away from the central molecular sites with creation and annihilation operators $\hat{c}^\dagger, \hat{c}$ for the reservoir electrons. The site energies are given by $\epsilon_L = \epsilon_R$ and ϵ_M for the reservoir and molecular regions, respectively. The volage applied across the molecular junction is described by the voltages $V_L \neq V_R$ in the reservoirs and the voltage drop V_n across the molecular sites is scaled linearly between the values V_L and V_R. The nearest neighbor interactions are $\gamma_L = \gamma_R$ within the electrode regions, and there are two molecular site-site interaction Γ_M and γ_M representing single and double bonds, respectively, on the molecular region as a simple model for hexatriene dithiol, and $\gamma_{LM} = \gamma_{MR}$ determine the molecule-electrode couplings. The eigenstates of the molecular Hamiltonian are found with the electron-electron self-energy and exact electrode self-energies are introduced describing coupling to the electrodes [35]. The resulting single-electron states are taken as the expansion functions for the correlated version of the model obtained from $\hat{H}_0 \rightarrow \hat{H}_0 + \hat{v}$, with $\hat{v}$ the pairwise perturbation interactions about the mean field solution.

Current-voltage characteristics are calculated using eq. 4.2. We use a simplified form of the self-energy such that the interaction matrix elements are approximated
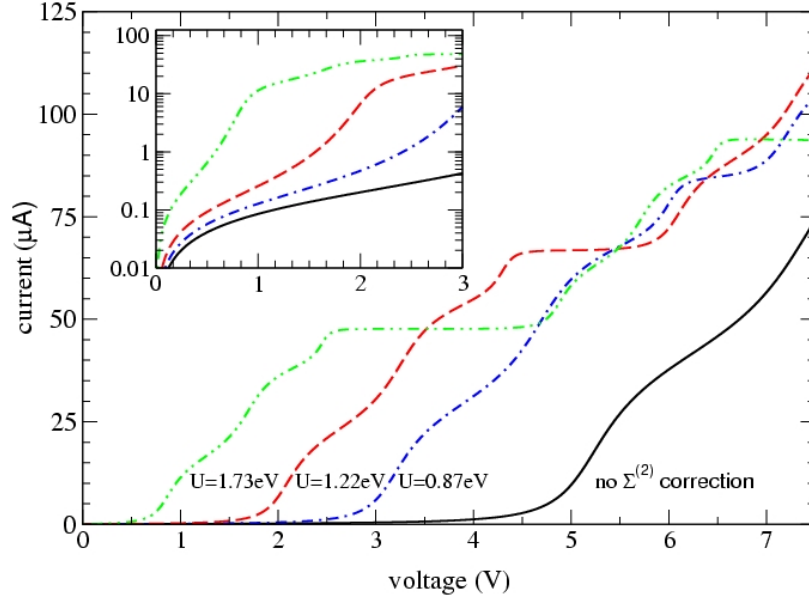
Figure 4.2: Current-voltage characteristics for the model Hamiltonian of eq. 4.9.
$\epsilon_M = 1.0$ eV, $\epsilon_L = \epsilon_R = \epsilon_{\text{Fermi}} = 0.0$, $\gamma_M = 4.54$ eV, $\Gamma_M = 1.5$
eV, $\gamma_L = \gamma_R = 10.0$ eV, $\gamma_{LM} = \gamma_{MR} = 2.4$ eV. Electronegativity is
modified by varying U, with values as labeled within the figure. Inset:
Current-voltage characteristics with current displayed on a logarithmic
scale.

as $< pq||rs > \approx U$. Within the Supplemental Information (Appendix D), the

HOMO-LUMO gap for the molecular region is given as a function of U and

demonstrates that the electronegativity on the molecular region may be

systematically controlled through the electron-electron self-energy. The results for

the current-voltage characteristics from the model are presented in fig. 4.2. The

independent particle or uncorrelated model occurs for $U = 0$ and increasing U

corresponds to increasing electron correlations on the molecular region. At $U = 0$,

currents at low voltages are much lower than when the $\Sigma^{(2)}$ term is allowed to

correct IPs and EAs; in this case, the highest lying occupied states are too low

(IPs too high) and the lowest lying unoccupied single-electron states are too high

(EAs too low) with respect to the Fermi level. Under these conditions neither

occupied or unoccupied states enter into the voltage bias window at low voltages,

and this level of electronic structure treatment corresponds to a Hartree-Fock

approximation. Increasing correlations on the molecular region, the highest

occupied states near the Fermi level enter the bias window at lower values of
voltage, followed by the introduction of the unoccupied states at higher voltage bias
(this sequence is due to the relative position of the Fermi level relative to occupied
and unoccupied states for this example). The correlations on the molecular region
serve to shift up occupied levels relative to the Fermi level leading to reduced IPs,
whereas increasing correlations systematically lower the lowest lying unoccupied
states leading to increased EAs. Increasing correlations continue to reduce the IPs
and increase EAs until eventually electronegativity is overestimated. The impact
on the current-voltage characteristics is that the molecular levels enter the bias
window at very low values of applied voltage resulting in large current magnitudes.
As we will demonstrate in the next section, larger values of U correspond to the
use of LDA exchange-correlation potentials within DFT where the strong
over-estimation of charge transfer is known to occur [30]. There are indications
that GGA and hybrid functionals can be constructed to correct charge transfer,
but these corrections have not been shown to be systematic across a wide range of
systems. Hartree-Fock and Kohn-Sham (using LDA) orbitals are not appropriate
independent particle models for electron transport due to strong under- and
over-estimation of charge transfer, respectively. The results of fig. 4.2 indicates the
impact on current-voltage characteristics for these two extremes.

4.5   DFT and HF transport for hexatriene dithiol

In this section, electron transport calculations are extended for a gold-hexatriene
dithiol-gold tunnel junction using density functional theory and Hartree-Fock
treatments for the electronic structure. In this way, the relationship between
differing electronic structure treatments and model analysis based on increasing
electron-electron correlations of the previous section can be inferred. The electronic
structure calculations in this section have been performed with Fock matrices built

from TURBOMOLE calculations [32, 33] using Hartree-Fock and density functional theory in the local density approximation (LDA/PW), generalized gradient approximation (GGA/BP), and hybrid (B3-LYP) exchange-correlation functional. Green's function transport calculations have been performed with the in-house TIMES scattering program [36] using the tunnel junction Hamiltonians in an atomic orbital basis as extracted from TURBOMOLE. The TURBOMOLE split valence/polarized Gaussian basis sets were used for all atoms on the hexatriene dithiol molecule. In the gold leads, the three gold atoms in each electrode bonding with the sulfur atoms are also treated with a split valence/polarized basis set in conjunction with a 60 electron effective core potential. All other gold atoms are treated with a modified $6s$ orbital basis set used with a 78 electron effective core potential [37]. In fig. 4.3, the atomic model used to describe the tunnel junction is depicted. A full geometry optimization was performed for the junction for each electronic structure treatment. During the Hartree-Fock and DFT electronic structure calculations, an external electric field is applied to mimic the application of a voltage across the molecule. Using gold contact models, the screening depth for the application of the external electric field is calculated and found to be approximately 0.8 Å, consistent with estimates from Thomas-Fermi theory. Hence the clusters employed are large enough to describe the charge transfer due to the molecule bonding to gold with a constant voltage reached within the finite cluster region. The semi-infinite nature of the contact is then described by neutral leads through the electron self-energies in the contact region.

Electron transmission as a function of energy are given in the Supplemental Information (Appendix D) using the various approximations to DFT and the Hartree-Fock approximation. The overestimation of electronegativity within LDA results in a narrow gap around the Fermi energy resulting in a higher density of states with the energy range of interest for electron transport. Conversely, the underestimation of electronegativity within the Hartree-Fock approximation results
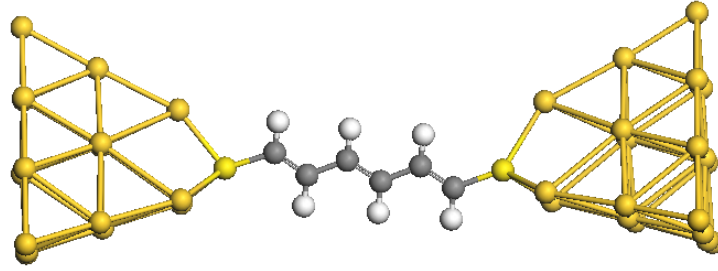
Figure 4.3: Atomistic model of gold-hexatriene dithiol-gold molecular tunnel junc-
tion. The back two planes of gold atoms in the metal contacts are
repeated to model the semi-infinite electrode regions.

in low density of states around the Fermi energy and within a voltage bias window
of a few volts typically considered in molecular electronics. Finally, in fig. 4.4, the
resulting current-voltage characteristics for the hexatriene dithiol tunnel junction
calculated using the different electronic structure treatments is displayed.

The explicit electronic structure treatments of the molecular tunnel junction
confirm the model analysis of the preceeding section. DFT/LDA overestimates
correlations, leading to too large of an electronegativity, and subsequently too large
of a charge transfer between molecule and electrodes. The resulting band
alignments result in an overestimation of the electronic current in the tunnel
junction. Conversely, the Hartree-Fock approximation underestimates correlations,
leading to too small of an electronegativity, and too little charge transfer between
molecule and electrodes. The resulting band alignments result in an
underestimation of the electronic current in the tunnel junction. The GGA and
hybrid approximations tend to lie between the extremes of the LDA and
Hartree-Fock approximations. Similar findings in the context of the effect of
differing exchange-correlation treatments on electronic currents in molecular tunnel
junctions have been reported [38, 39]. However, in the present context, the role of
improving the electronegativity to improve the overlap to the exact RDM is
highlighted.
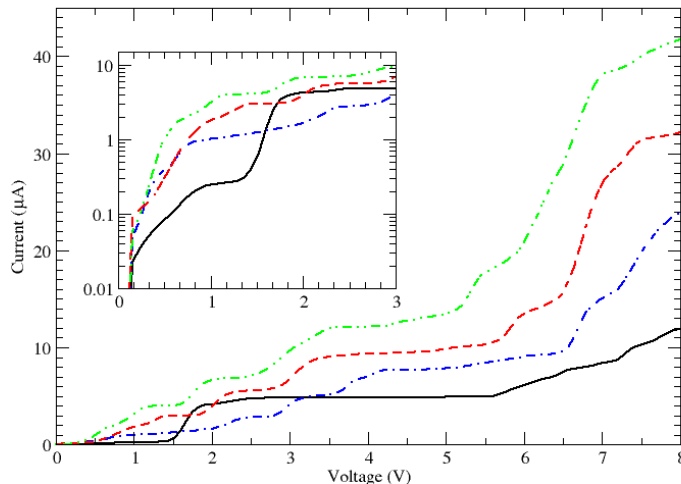
Figure 4.4: Current-voltage characteristics for hexatriene dithiol bonded to gold
using various electronic structure treatments. Green- DFT/LDA, Red-
DFT/GGA, Blue- DFT/hybrid, Black- Hartree-Fock. Inset: Current-
voltage characteristics with current displayed on a logarithmic scale.

4.6 Conclusion

Correcting electronegativity is equivalent to maximizing overlap to the reduced
density matrix: this is true to low orders in electron correlation and of course the
correct electronegativity and density matrix are found at the exact many-body
solution. In general, improving descriptions for the RDM and electronegativity
with the methods described will lead to improved prediction of electron currents in
systems with moderate electron correlations. The best independent particle picture
within this context is a single determinant comprised of natural orbitals; any
attempt to refine single-electron models for transport should lead to electron
wavefunctions that approximate natural orbitals. In the case of Green's function
approaches, moderate electron correlations imply the need to include
electron-electron self-energies to describe quasi-particle propagation. A measure of
the usefulness of a single-particle picture to be used in a transport scheme is its
ability to reproduce the exact molecular electronegativity. The ability of *exact*

DFT to accurately determine electron transport [40] is within the present discussion understood as the ability to provide correct ionization potentials and electron affinitites. For strong correlations, a single determinant wave function is not an adequate approximation to predict IPs and EAs and perturbation corrections about a single reference state fail, thus complicating treatment of molecular junctions with Green's function approaches. However, in all cases, from weak to strong correlations, the criterion to maximize overlap to the exact reduced density matrix will lead to improved predictions for electron currents.

References

[1] E. T. Jaynes, "Information theory and statistical mechanics," *Physical review*, vol. 106, no. 4, p. 620, 1957.

[2] E. T. Jaynes, "Information theory and statistical mechanics. II," *Physical review*, vol. 108, no. 2, p. 171, 1957.

[3] V. P. Kalashnikov and D. N. Zubarev, "On the extremal properties of the nonequilibrium statistical operator," *Physica*, vol. 59, no. 2, pp. 314–320, 1972.

[4] E. T. Jaynes, "The minimum entropy production principle," *Annual Review of Physical Chemistry*, vol. 31, no. 1, pp. 579–601, 1980.

[5] G. Baym and L. P. Kadanoff, "Conservation laws and correlation functions," *Physical Review*, vol. 124, no. 2, p. 287, 1961.

[6] L. V. Keldysh *et al.*, "Diagram technique for nonequilibrium processes," *Sov. Phys. JETP*, vol. 20, no. 4, pp. 1018–1026, 1965.

[7] S. M. Reimann and M. Manninen, "Electronic structure of quantum dots," *Reviews of Modern Physics*, vol. 74, no. 4, p. 1283, 2002.

[8] C. Toher, A. Filippetti, S. Sanvito, and K. Burke, "Self-interaction errors in density-functional calculations of electronic transport," *Physical Review Letters*, vol. 95, no. 14, p. 146402, 2005.

[9] P. Mori-Sánchez, A. J. Cohen, and W. Yang, "Discontinuous nature of the exchange-correlation functional in strongly correlated systems," *Physical review letters*, vol. 102, no. 6, p. 066403, 2009.

[10] P. Darancet, A. Ferretti, D. Mayou, and V. Olevano, "Ab initio G W electron-electron interaction effects in quantum transport," *Physical Review B*, vol. 75, no. 7, p. 075102, 2007.

[11] K. S. Thygesen and A. Rubio, "Nonequilibrium GW approach to quantum transport in nano-scale contacts," *The Journal of Chemical Physics*, vol. 126, no. 9, p. 091101, 2007.

[12] X. Wang, C. D. Spataru, M. S. Hybertsen, and A. J. Millis, "Electronic correlation in nanoscale junctions: Comparison of the GW approximation to a numerically exact solution of the single-impurity Anderson model," *Physical Review B*, vol. 77, no. 4, p. 045119, 2008.

[13] W. R. Frensley, "Boundary conditions for open quantum systems driven far from equilibrium," *Reviews of Modern Physics*, vol. 62, no. 3, p. 745, 1990.

[14] P. Delaney and J. C. Greer, "Correlated electron transport in molecular electronics," *Physical review letters*, vol. 93, no. 3, p. 036805, 2004.

[15] P. Delaney and J. C. Greer, "Quantum electronic transport in a configuration interaction basis," *International journal of quantum chemistry*, vol. 100, no. 6, pp. 1163–1169, 2004.

[16] J. C. Greer, "Electronic current density expanded in natural orbitals," *Molecular Physics*, vol. 106, no. 11, pp. 1363–1367, 2008.

[17] Y. Meir and N. S. Wingreen, "Landauer formula for the current through an interacting electron region," *Physical review letters*, vol. 68, no. 16, p. 2512, 1992.

[18] A. Ferretti, A. Calzolari, R. Di Felice, and F. Manghi, "First-principles theoretical description of electronic transport including electron-electron correlation," *Physical Review B*, vol. 72, no. 12, p. 125114, 2005.

[19] B. T. Pickup and O. Goscinski, "Direct calculation of ionization energies: I. Closed shells† Supported by the Swedish Natural Sciences Research Council.," *Molecular Physics*, vol. 26, no. 4, pp. 1013–1035, 1973.

[20] E. R. Davidson, "Properties and uses of natural orbitals," *Reviews of Modern Physics*, vol. 44, no. 3, p. 451, 1972.

[21] G. Fagas, P. Delaney, and J. C. Greer, "Independent particle descriptions of tunneling using the many-body quantum transport approach," *Physical Review B*, vol. 73, no. 24, p. 241314, 2006.

[22] P.-O. Löwdin, "Quantum theory of many-particle systems. I. Physical interpretations by means of density matrices, natural spin-orbitals, and convergence problems in the method of configurational interaction," *Physical Review*, vol. 97, no. 6, p. 1474, 1955.

[23] Y. Pavlyukh and W. Hübner, "Configuration interaction approach for the computation of the electronic self-energy," *Physical Review B*, vol. 75, no. 20, p. 205129, 2007.

[24] R. J. Bartlett, I. Grabowski, S. Hirata, and S. Ivanov, "The exchange-correlation potential in ab initio density functional theory," *The Journal of chemical physics*, vol. 122, no. 3, p. 034104, 2005.

[25] A. Beste and R. J. Bartlett, "Independent particle theory with electron correlation," *The Journal of chemical physics*, vol. 120, no. 18, pp. 8395–8404, 2004.

[26] A. Beste and R. J. Bartlett, "Correlated one-particle method: Numerical results," *The Journal of chemical physics*, vol. 123, no. 15, p. 154103, 2005.

[27] R. Stadler and K. W. Jacobsen, "Fermi level alignment in molecular nanojunctions and its relation to charge transfer," *Physical Review B*, vol. 74, no. 16, p. 161405, 2006.

[28] R. Stadler, "Conformation dependence of charge transfer and level alignment in nitrobenzene junctions with pyridyl anchor groups," *Physical Review B*, vol. 81, no. 16, p. 165429, 2010.

[29] Y. Xue, S. Datta, and M. A. Ratner, "Charge transfer and "band lineup" in molecular electronic devices: A chemical and numerical interpretation," *The Journal of Chemical Physics*, vol. 115, no. 9, pp. 4292–4299, 2001.

[30] E. Ruiz, D. R. Salahub, and A. Vela, "Charge-transfer complexes: Stringent tests for widely used density functionals," *The Journal of Physical Chemistry*, vol. 100, no. 30, pp. 12265–12276, 1996.

[31] S. McDermott, C. B. George, G. Fagas, J. C. Greer, and M. A. Ratner, "Tunnel currents across silane diamines/dithiols and alkane diamines/dithiols: A comparative computational study," *The Journal of Physical Chemistry C*, vol. 113, no. 2, pp. 744–750, 2008.

[32] R. Ahlrichs, M. Bär, M. Häser, H. Horn, and C. Kölmel, "Electronic structure calculations on workstation computers: The program system turbomole," *Chemical Physics Letters*, vol. 162, no. 3, pp. 165–169, 1989.

[33] S. Brode, H. Horn, M. Ehrig, D. Moldrup, J. E. Rice, and R. Ahlrichs, "Parallel direct SCF and gradient program for workstation clusters," *Journal of computational chemistry*, vol. 14, no. 10, pp. 1142–1148, 1993.

[34] R. A. Kendall, T. H. Dunning Jr, and R. J. Harrison, "Electron affinities of the first-row atoms revisited. Systematic basis sets and wave functions," *The Journal of Chemical Physics*, vol. 96, no. 9, pp. 6796–6806, 1992.

[35] T. M. Henderson, G. Fagas, E. Hyde, and J. C. Greer, "Determination of complex absorbing potentials from the electron self-energy," *The Journal of chemical physics*, vol. 125, no. 24, p. 244104, 2006.

[36] R. Gutiérrez, G. Fagas, K. Richter, F. Grossmann, and R. Schmidt, "Conductance of a molecular junction mediated by unconventional metal-induced gap states," *EPL (Europhysics Letters)*, vol. 62, no. 1, p. 90, 2003.

[37] P. Fuentealba, H. Stoll, L. Von Szentpaly, P. Schwerdtfeger, and H. Preuss, "On the reliability of semi-empirical pseudopotentials: simulation of Hartree-Fock and Dirac-Fock results," *Journal of Physics B: Atomic and Molecular Physics*, vol. 16, no. 11, p. L323, 1983.

[38] K. S. Thygesen, "Impact of Exchange-Correlation Effects on the I V Characteristics of a Molecular Junction," *Physical review letters*, vol. 100, no. 16, p. 166804, 2008.

[39] V. Geskin, R. Stadler, and J. Cornil, "Multideterminant assessment of mean-field methods for the description of electron transfer in the weak-coupling regime," *Physical Review B*, vol. 80, no. 8, p. 085411, 2009.

[40] H. Mera, K. Kaasbjerg, Y. M. Niquet, and G. Stefanucci, "Assessing the accuracy of Kohn-Sham conductances using the Friedel sum rule," *Physical Review B*, vol. 81, no. 3, p. 035110, 2010.

Chapter 5

Conclusion

5.1   Introduction

The aim of this thesis is to benchmark the MECS method under a variety of circumstances and to validate and demonstrate the range of systems that MECS can be applied as a many body transport method in the field of molecular electronics. MECS was applied to determine charge transport properties and verify performance benchmarks across a carefully chosen set of test cases. Transport calculations were carried out with the method and compared to conventional single-particle methods and experimental data. NEGF with DFT was selected as the single-particle approximation to the transport problem to be compared with the MECS method. NEGF itself is an established method which is well documented in the literature and as such serves as a well understood, in terms of its advantages and limitations, counterpart to the MECS method.

Zeroth order electronic structure calculations were performed using Hartree Fock and Density Functional Theory methods, augmented by configuration interaction methods to systematically correct electron correlations.

5.2   Results and benchmarks

5.2.1   Conductance of point contact systems

The point contact quantum of conductance is a well characterised and understood phenomenon replicated by many single-particle transport methods. In Chapter 2, point contacts are investigated as a calibration test to the MECS method. The quantum of conductance G_0 represents the conductance of a single energy level in a junction with unity transmission. The quantum of conductance for our a model point contact MECS is $0.6 \pm 0.24 G_0$ and is well within the bounds obtained by single-particle methods (i.e. $0.3 - 1 G_0$) [1, 2, 3, 4, 5, 6, 7].

Applying MECS to point contacts with the inclusion of only single excitations in the many-electron wave function in addition to the reference state describes the quantum of conductance thirty percent higher than the conductance obtained when including higher excitations. This reduction in current (with the inclusion of many body effects) may reflect the increase of electron-electron scattering on the device region due to the improved descriptions of electron correlation. In these studies up to six excited states relative to the ground state were included. There is only a small contribution to the conductance from the first five excited states, a much larger change in conductance due to the addition of the sixth excited state is found. The results reinforce the importance of including the correct configurations with respect to the ground state to include electron correlations in the many body wave function. It also highlights that the excitations that interact the strongest with the ground state through dipole coupling are not necessarily those lowest lying in energy.

The difference in current with the transition from the single-particle basis to the many body basis via the inclusion of extra excitations demonstrates the sensitivity of even weakly correlated systems to electron correlations. This benchmark is important in determining the degree to which electron correlation affects transport in approximate single-particle weakly correlated systems.

5.2.2 Comparison of MECS with single-particle methods for correlated systems

Of additional interest is the degree to which electron correlation affects charge transport in weakly correlated systems such as alkane chains linked to gold electrodes via amines. Agreement is achieved between alkane molecular junctions for MECS and NEGF, with MECS and NEGF respectively obtaining a decay constant of $\beta = 0.76\text{Å}^{-1}$ and $\beta = 0.78\text{Å}^{-1}$ for alkanediamine. Alkanes are well

described by a single determinant (having a single reference ground state) which indicates that these systems are well described in a single-particle model.

In addition to alkanes and point contacts, MECS was applied to moderately correlated silane systems. Applying MECS to such systems of increasing correlation while simultaneously comparing with results from single-particle implementations of methods (i.e.NEGF+DFT) allows the study of the parameters affecting divergence between different approximations between the two methods giving rise to prediction of different current-voltage relationships.

these methods. MECS obtains a decay constant $\beta = 0.07\text{Å}^{-1}$ for silane diamine whereas NEGF+DFT found a $\beta = 0.35\text{Å}^{-1}$. Results from methylated oligosilane chains, i.e donor-bridge-acceptor systems, yield a experimental $\beta = 0.16\text{Å}^{-1}$ [8].

Difficulties arise when comparing MECS and NEGF methods for silanes due to the small HOMO-FERMI gap leading to sensitivity to Fermi level alignment. Therefore the degree the divergence in results due to Fermi level alignment which can be attributed electron correlation is uncertain. Despite this the divergence is considered to be primarily due to Fermi level alignment as the HOMO-Fermi gap is quite small and prone to misalignment. As a benchmark the application to silanes represents a first step in testing the capabilities of MECS on a system with significant electron correlation. Silanes are poorly represented in the experimental data, therefore having a computational many-body model of charge transport hopefully will encourage future experiments by providing a theoretical benchmark.

5.2.3   Application of MECS to various electron transport regimes

MECS was applied to various different transport regimes in its implementation. In this work both strong and weak coupling were utilised during the course of MECS

calculations. The strong coupling regime occurs when there are strong bonds and low barriers between contacts and the device region. Weak coupling in contrast is when there is weak interaction between the device and system as in molecular junctions bonded to metal electrodes by linker molecules that give rise to a large potential barrier between electrode and molecule as in alkane and silane molecular junctions. MECS experienced no complications yielding correct results for both strong and weakly coupled systems. MECS was applied to both low and moderately correlated systems in the above cases with strong agreement with experiment.

5.2.4   Comparison of MECS with experimental results

In this work MECS is benchmarked against experimentally reproducible results. Agreement between MECS and experiment is achieved for alkanes (particularly alkane diamine) and point contacts within an acceptable margin of error. Verifying results in this manner demonstrates that MECS is not just comparable to other theoretical codes and models but it can be predictive iin the study of experimental molecular junctions.

5.2.5   Modelling systems of different electronegativity

Electronegativity is a measurement of a systems affinity for electrons. An accurate treatment of electronegativity is necessary to accurately determine the correct energy level alignment at an interface. Inclusion of correlation corrections is known to be important for prediction of electronegativity as demonstrated by resulting improvement for ionisation potentials and electron affinities (see equation 5.1). Within this thesis, it is shown that electronegativity controls energy level alignment and charge transfer, and hence the current at interface or molecular junction.

Electronegativity χ is defined as

$$\chi = \frac{(E_A + E_I)}{2} \tag{5.1}$$

where E_A and E_I is the electron affinity and ionisation potential.

Underestimating the band gap as predicted within DFT leads to an overestimation of the current. In contrast the opposite overestimation of the band gap with HF leads to an underestimation of the predicted current. Accurate determination of ionisation potentials and electron affinities is hence shown to be necessary for improved descriptions of charge transport. An analytical model was implemented allowing varying degrees of electron correlation to be included and its effect on electronegativity and transport was studied. This was compared to electronic structure treatment of the same system utilising computational HF and DFT methods with different functionals (LDA,GGA and hybrid) for DFT.

From low to moderate correlation, the electron-electron self energy corrected Green's functions accurately predicts currents. These corrections break down when treating strong electron correlations as the single-particle approximation is no longer useful as a zeroth order approximation to the many body wavefunction.

By using correlated methods (in this work, by configuration interaction (CI) methods,) electronegativity is better approximated thereby yeilding improvements to the reduced density matrix, and consequently, the current. It was shown that CI improves calculation of the electronegativity by maximising the overlap to the exact reduced density matrix, implying an accurate treatment of the interacting many-electron wavefunction.

5.2.6   Modelling screening effects

The screening effect is the reduction of an applied field due to movement of opposing charges in a material. As implemented, MECS determines the voltage drop (V) between the two electrodes (i.e. $V = \xi d$ where $-\xi$ is the applied field strength and d is the distance between the electrodes). This implementation ignores the contribution from the screening effect on the electrodes, leading to ambiguity in the definition of the distance d, and hence in the value of the voltage. The screening effect can be accounted for via the inclusion of an effective distance (i.e. the equivalent in the electrodes distance that yields the induced voltage for a given applied electric field), in order to obtain the physical induced voltage drop due to electrostatic screening.

Point contacts are comprised mainly of metallic contacts and as such are affected to a considerable degree by electrostatic screening. The gap between the electrodes is effectively one atom's width. The voltage drop in point contacts occurs across the central scattering region with a surface dipole at the centre of the junction. The induced surface dipole is in agreement with theory consisting of opposing charges accumulating at the metal surface of the contacts opposing the applied electric field.

The discrepancy between the actual and naive voltage estimate (where the total distance across the molecule is assumed to be unscreened) is much less acute in typical molecular junctions as compared to point contacts, due to the wider gap distance in molecular junctions contacting "long" molecules. The screening effect is mostly of concern in MECS calculations whereby the majority of the distance between the Wigner planes is metallic, and screening reduces the actual length over which the voltage drops to the region between the electrodes.

5.2.7 Studying finite electrode effects on the Wigner distribution function

MECS implements the behaviour of semi-infinite leads via the Wigner function. By constraining the Wigner function, the effect of the semi-infinite leads can be emulated with finite sized electrodes. In this thesis we investigated the effect the finite geometry on the Wigner function as calculated within the electrodes.

In Chapter 2, the effects of finite electrodes on the stability of the Wigner function was investigated by expanding the geometry of the electrodes as a series of approximations to the semi-infinite electrodes. This was achieved via extending the electrodes in stepwise fashion towards the semi-infinite leads using repeating units that when continued, lead to a periodic semi-infinite electrode. As the Wigner function is evaluated in larger electrode models, its behaviour approaches Wigner function behaviour in an ideal electrode. In all cases the Wigner function is placed in the same location relative to the back plane of the model electrode.

Results of the Wigner stability test indicate that in spite of varying geometry, the Wigner function remains robust except for low momenta values. This applies equally to both the single sided and double sided junctions tested. Due to the relation of the Wigner function to the current $pf(p)$, the contribution of lower momenta is not critical (i.e. due to small p, where $f(p)$ is the Wigner function and p is the momentum). The resulting incoming current distribution has only minor variations with respect to the variation in geometry. This implies that the implementation of the Wigner function within MECS in the finite electrodes is relatively stable with respect to the electrode geometries.

5.3   Further observations

Based on the above results and benchmarks, it is possible to draw a number of conclusions relating to MECS method and its application to molecular systems.

Taking into consideration the variety of systems that MECS has been applied to it is possible to conclude that its application is not limited to any one transport regime. MECS has been successfully applied to both strong and weakly coupled systems, weak systems in the case of molecular junctions and strongly coupled systems in the case of point contacts including both low and moderately correlated treatments.

Subsequent analysis of the junction electrostatics confirmed that the MECS results for point contacts conform with predicted theory with the inclusion of an accurate determination of the junction voltage. The screening effect and its influence on the effective voltage drop for point contacts was studied and correctly treated. For molecular junctions, we conclude that the screening effect on molecular junctions is less due to the less polarisable molecular region comprising a large proportion of the distance separating the Wigner planes. Similarly approximations due to finite electrode geometries have little impact on the calculation of the Wigner functions used to constrain incoming electrode currents and hence MECS transport calculations. Discrepancies occur mostly at low momenta which does not significantly impact the incoming current.

MECS compares favourably with single-particle methods for systems with low correlation such as alkanes and point contacts. MECS can reproduce transport results for these systems comparable with single-particle methods. MECS also achieves agreement with experimental results for alkanes and point contacts except for giving a slightly lower conductance possibly due to electron electron interactions. Larger discrepancies in predicted currents occurs when comparisons

are made between MECS and NEGF for the moderately correlated silanes. Here the majority of the divergence between MECS and NEGF is likely due to the sensitivity of silanes to Fermi level alignment between the molecular region and the workfunction of the electrodes.

Through the course of this work MECS has been tested and compared to numerous benchmarks. This includes the modelling of electrostatics, Wigner stability tests and estimation of the quantum of conductance. The results confirm that MECS can perform well when compared with established methods and benchmarks.

5.4   Future research

Possible applications for the MECS method would be to systems with additional properties and transport regimes different to those previously studied (e.g. systems with high electron correlation, in particular, the Coulomb blockade regime). In addition, a number of modifications to MECS could accommodate descriptions of physical processes better, such as more accurate electron broadening from a better treatment of the effects of the semi-infinite leads. One such modification would be the integration of complex absorbing potentials (CAPs) into MECS method. These proposals are discussed further in the following sections.

5.4.1   Application of MECS to highly correlated systems

To date MECS has been applied to systems of increasing correlation and compared with single-particle approximations and experimental results for low and moderately correlated systems. The logical continuation of this is the further application of the MECS method to highly correlated systems including Coulomb blockade.

Highly correlated systems present a challenge to contemporary methods in determining electron transport. This is considered to be the reason for the poor agreement between theory and experiment. Such systems are in principle calculable by MECS with an appropriate treatment of electron correlation. In addition, by accounting for other physical processes (e.g. electronic band alignment in silanes), it is possible with MECS to discern the influence electron correlation has on current transport.

Previously point contacts were considered systems which are strongly coupled but weakly correlated. An interesting counterpart system for study would be an opposing weakly coupled but highly correlated system. A possible candidate for highly correlated transport is a Coulomb blockade system. Quantum dot coulomb blockade systems would therefore represent a challenging case for MECS in the highly correlated transport regime and should be the focus of future work.

5.4.2   Integration of complex absorbing potentials (CAPS)

Currently in the MECS method, as electrons leave the junction they are confronted with the unphysical end of electrode, however due to the enforced Wigner constraints they constrained upon re-entering the device region. While they cannot re-enter the junction these reflected electron momenta lead to an unphysical region within the electrodes outside the Wigner plane. While this has no direct influence on the current calculation (due to being outside the Wigner planes where the current is deduced from), however the numerical instability created hinders convergence over the entire region where the wavefunction is minimised.

Conventionally in electronic structure theory the effects of semi-infinite leads are accounted for by means of electron self energies. While useful for a wide variety of approaches electron self energies have a single-particle energy dependence which presents a difficulty when incorporating them into many body methods such as

MECS. Complex absorbing potentials (CAPs) however offer an alternative. CAPs approximates the electron self energy without an energy dependence. This allows the leads to be straightforwardly integrated into many body methods. The essence of the CAPs method is to approximate energy-dependent self-energies by energy-independent potentials. Therefore the better the CAPs mimics the self-energy over a given energy range, the better the approximation.

The inclusion of CAPs into MECS can accurately emulate the physical system connected via semi infinite leads. CAPs prevents backscattering of electrons off the edge of the electrodes effectively "absorbing" them and thereby reducing if not eliminating numerical instabilities in the region outside the Wigner planes. This potentially leads to an improvement in convergence.

During an MCCI calculation the isolated electrodes and device are considered to be an approximation to the external system (semi-infinite leads) to which it is attached. With the inclusion of CAPS the MCCI calculation yields the many-body energy levels fully accounting for semi-infinite.

In summary, integrating CAPs into MECS could provide a better description of the leads which through interaction with the device region accounts for state broadening of the device energy levels. CAPs should allow MECS to improve the effects due to broadening (broadening due to the electrodes) in current calculations.

5.4.3 Research applications

It is worth considering what are the possible applications for molecular electronics research. One such application is molecular description of photo voltaic cells. Accurate determination and description of energy absorption processes could lead to new developments and improvements in photovoltaic solar panels.

Another promising application is biological sensors. By accurately determining the

current voltage characteristics of a series of molecules a molecule specific sensor could be developed. This could lead to the development of a biorecognition sensors which could accurately detect the presence of specific molecules in a complex chemical enviroment like inside the human body. In addition is the possibility of direct electrical interface between a molecular circuit and a biological cell giving rise to the ability to measure thousands of protein and genetic signatures in real time.

References

[1] E. Scheer, N. Agraït, J. C. Cuevas, A. L. Yeyati, B. Ludoph, A. Martín-Rodero, G. R. Bollinger, J. M. van Ruitenbeek, and C. Urbina, "The signature of chemical valence in the electrical conduction through a single-atom contact," *Nature*, vol. 394, no. 6689, pp. 154–157, 1998.

[2] L. G. C. Rego, A. R. Rocha, V. Rodrigues, and D. Ugarte, "Role of structural evolution in the quantum conductance behavior of gold nanowires during stretching," *Physical Review B*, vol. 67, no. 4, p. 045412, 2003.

[3] J. L. Costa-Krämer, N. García, and H. Olin, "Conductance quantization histograms of gold nanowires at 4 k," *Physical Review B*, vol. 55, no. 19, pp. 12910–12913, 1997.

[4] V. Rodrigues and D. Ugarte, "Metal nanowires: atomic arrangement and electrical transport properties," *Nanotechnology*, vol. 13, no. 3, p. 404, 2002.

[5] A. Halbritter, S. Csonka, G. Mihály, O. I. Shklyarevskii, S. Speller, and H. van Kempen, "Quantum interference structures in the conductance plateaus of gold nanojunctions," *Physical Review B*, vol. 69, no. 12, p. 121411, 2004.

[6] A. I. Yanson, G. R. Bollinger, H. E. van den Brom, N. Agraït, and J. M. van Ruitenbeek, "Formation and manipulation of a metallic wire of single gold atoms," *Nature*, vol. 395, no. 6704, pp. 783–785, 1998.

[7] J. Kröger, H. Jensen, and R. Berndt, "Conductance of tip–surface and tip–atom junctions on Au(111) explored by a scanning tunnelling microscope," *New Journal of Physics*, vol. 9, no. 5, p. 153, 2007.

[8] M. Sasaki, Y. Shibano, H. Tsuji, Y. Araki, K. Tamao, and O. Ito, "Oligosilane chain-length dependence of electron transfer of zinc porphyrin-oligosilane-fullerene molecules," *The Journal of Physical Chemistry A*, vol. 111, no. 16, pp. 2973–2979, 2007.

Appendices

Appendix A

Electronic Structure

This appendix provides an overview of the fundamental theory and a description of the computational methods employed in this work. In particular basic concepts in electronic structure theory as applied to molecular physics are also outlined here.

A.1   Density Functional Theory

Density Functional Theory (DFT) is a formally exact many electron theory. DFT is a method of finding the ground state properties of a system without directly dealing with the many-body state wave function. In Hartree-Fock one must deal with the complex many-body wavefunction which contains 3N spatial coordinates and N spin coordinates. DFT attempts to reduce this to three coordinates by calculating the electron density (ρ).

Regarding implementation, DFT is a relatively straightforward method to apply with appropriate approximations and can in certain systems capture a high percentage of the total electronic energy at relatively low computational cost. This computational cost is approximately equal to that of Hartree-Fock and is lower than post Hartree-Fock wave function methods. Similar to wave function theory, there exists a set of post DFT improvements known as Jacobs ladder [1], however the improvements are not as systematic as in wave function based methods.

Initially motivated by the Thomas Fermi models used to calculate the Coulomb, exchange and kinetic energies, DFT was further developed into an exact theory via the Hohenberg-Kohn theory.

The first tenet of the Hohenberg-Kohn theorem upon which DFT is based states that the N electron wave function can be replaced by a density calculation. This is achieved by deducing the external electric field to within an additive constant via the electron density and as a result all other properties are determinable via the electron density. The Hohenberg-Kohn theorem utilises the variational method to

minimise the density and similar to Hartree-Fock, the calculated energy is an upper bound to the exact ground state energy.

The ground state electron density can be defined in terms of the exact ground state wave function

$$n_0(r) = \langle \psi_0 | \hat{n} | \psi_0 \rangle \qquad (A.1)$$

where $\hat{n}$ is the density operator, n_0 is the ground state density and $|\psi_0\rangle$ is the ground state wave function. Since $n_0(r)$ is dependent on the ground state wave function, both n_0 and ψ_0 are then dependent on N(the number of electrons) and V_{ext}(the external potential). The Hamiltonian (H) is defined such that $H = F + V_{ext}$. The electrostatic potential due to the nuclei is treated as an "external" potential V_{ext} with the remaining part of the Hamiltonian F given as

$$F = -\frac{1}{2}\sum_a \nabla_a^2 + \frac{1}{2}\sum_a \sum_{b \neq a} \frac{1}{|r_a - r_b|}. \qquad (A.2)$$

where $-\frac{1}{2}\sum_a \nabla_a^2$ is the kinetic energy of the electrons and $\frac{1}{2}\sum_a \sum_{b \neq a} \frac{1}{|r_a - r_b|}$ is the energy due to electron electron interactions.

F is the same for all N electron systems allowing the ground state Hamiltonian for each system to be specified by the number of electrons N and V_{ext}. $F[n]$ can be defined as a function of the density such that $F[n] = \langle \psi_0 | \hat{F} | \psi_0 \rangle$. The energy can be expressed in terms of the density $E[n]$ by the following equation

$$E[n] = F[n] + \int n(r) V_{ext}(r) d^3 r \qquad (A.3)$$

where the energy due to the external potential is determined solely by the ground-state electron density.

With the equations above its possible to formulate the Hohenberg-Kohn theorem into a variational problem with respect to the density for non-degenerate ground

states. For degenerate cases, this has been shown not to be true but these cases can be mitigated by the application of the constrained search formulation. The constrained search formulation only requires that a density be N representable, in that the density can be retrieved from an antisymmetric wave function. The ground state energy E_0 represents the lower limit in any calculation such that for all $n \neq n_0$ for N electrons in a potential V_{ext} . Thus density functional theory has a functional $F[N]$ which is independent of the external field. This formulation also limits the calculation from $3N$ variables to just three. The difficulty arises in that $F[N]$ is not explicitly known and this leads us to another development in density functional theory, i.e. Kohn-Sham density functional theory.

In Kohn-Sham DFT, the problem is treated by transforming the interacting system into a non-interacting system with the same ground state density while retaining exchange and correlation based effects. This allows approximations to the universal functional to be utilised and this greatly simplifies the form of the problem. The Kohn-Sham density can obtained from a Slater determinant. Kohn-Sham treatment of DFT incorporates electron orbitals into the density formulation. Kohn-Sham minimises the energy by varying the density in contrast to Hartree-Fock which minimises the energy with respect to variations in the single-electron orbitals. The variational solution includes a constraint on the number of electrons to N by means of a Lagrange multiplier. To proceed, Kohn-Sham DFT begins by partitioning the universal function $F[n]$ into three different components as described in the equation A.4 below;

$$F[n] = T_s[n] + \frac{1}{2} \int \frac{n(r)n(r')}{r - r'} d^3 r d^3 r' + E_{xc}[n], \qquad (A.4)$$

where $T_s[n]$ A.5

$$T_s[n] = -\frac{1}{2} \sum_{i=1}^{N} \int \psi_i^*(1) \nabla^2 \psi_i(1) d^3 r. \qquad (A.5)$$

is the kinetic energy for a non-interacting gas of density $n(r)$, and E_{xc} is the

contribution of the exchange correlation functional. The second term represents the contribution of the electrostatic Hartree energy to the system. E_{xc} contains all non-classical electrostatic potential effects and the difference in kinetic energy between interacting and non interacting systems.

The first two terms can be calculated directly with the last term requiring an approximation to the unknown form of the exchange correlation functional. By converting the system into a non interacting system the Kohn-Sham approach can solve some of the separate components exactly while treating the remaining components approximately.

Within the single-particle system, the electron density can be defined with respect to occupied orbitals as

$$n(r) = \sum_{i=1}^{N} |\psi_i(r)|^2. \tag{A.6}$$

To find the ground state density a one electron Schrodinger equation is solved. The Kohn-Sham equation is given as

$$[-\frac{1}{2}\nabla^2 + V_{KS}(r)]\psi_i(r) = \epsilon_i \psi_i(r) \tag{A.7}$$

where V_{KS} given by eq A.8 is the Kohn-Sham potential

$$V_{KS}(r) = \int \frac{n(r')}{|r - r'|}d^3r' + \frac{\partial E_{xc}[n]}{\partial n(r)} + V_{ext}, \tag{A.8}$$

and ϵ_i is the single-electron energy and $-\frac{1}{2}\nabla^2$ is kinetic energy operator. As in Hartree-Fock theory, it is possible to converge the density for the Kohn-Sham wave function using the self consistent method. V_{KS} is dependent upon the density $n(r)$ which yields a new wave function ψ_i which in turn yields a new density. This process continues until the density remains almost unchanged between iterations at which point it has converged. The density is therefore converges between successive iterations until it falls beneath a predefined threshold.

Convergence within DFT is relatively straight forward due to the presence of only one global minimum with a convex distribution [2]. The exact energy is given by below eq A.9

$$E = -\frac{1}{2}\sum_{i=1}^{N}\int \psi_i^* \bigtriangledown^2 \psi_i d^3r + \frac{1}{2}\int\int \frac{n(r)n(r')}{r-r'}d^3r d^3r' - \int n(r)V_{xc}(r)d^3r + E_{xc}[n],$$
(A.9)

where the first term is the non-interacting kinetic energy, the second term represents the contribution of the electron electron interactions, and the third term consists of correlations and the interaction correction for kinetic energy.

Due to the utilisation of matrix diagonalisation the Kohn-Sham method scales as N^3, where N is the number of basis functions when compared to the simpler Hohenberg-Kohn scaling. Accuracy for different systems can be estimated using calibration studies. Approximations to DFT, like approximations for Hartree-Fock have difficulty both in accounting for the exact correlation energy and for treating band gaps incorrectly. This leads to an underestimation by DFT of the energy gap between occupied and unoccupied energy levels rather than an overestimation as in the case of Hartree-Fock approximation.

The key shortcoming for Kohn-Sham DFT is that the functional connecting the exchange correlation energy and the electron density is not explicitly known. If the form of the exchange correlation (E_{xc}) is known then the equations can be solved precisely, but this is only known for a few simple systems. Approximations have to be created to account for E_{xc}. While there are a variety of different approximate functionals used to account for E_{xc}, the two main types are local density approximations (LDA) and general gradient approximations (GGA).

LDA is the simplest approximation and calculates the exchange correlation functional as if the local charge density was the same as a homogeneous electron gas. This also works well for inhomogeneous systems with no sharp changes in

electron density. In contrast to Hartree-Fock and for systems where LDA performs well, LDA can account for the electron correlation yielding accurate prediction for properties of many-electron systems. The typical shortcomings of LDA for molecular systems are its overestimation of charge transfer and determination of shorter bond lengths than experimentally observed. LDA performs well for systems where the density varies slowly but breaks down in highly correlated systems such as degenerate systems i.e. where the independent particle assumption no longer applies. It is often difficult to determine which systems LDA will approximate well. For example, it works well for bulk Group IV semiconductors (other than the band gap problem already mentioned) but not necessarily on their surfaces. Further limitations are seen for LDA in that it incorrectly predicts for the behaviour of Mott insulators to be semiconductors. For LDA the exchange correlation functional is defined as equation A.10:

$$E_{xc}^{LDA}[n(r)] = \int \epsilon_{xc}[n(r)]n(r)d^3r. \tag{A.10}$$

The exchange correlation functional for GGA is similar to that of LDA in that the exchange correlation functional is derived from a local density, but it also includes corrections for the density gradient. While GGA usually improves accuracy it is not systematic in that it doesn't guarantee that a GGA calculation will be an improvement over a LDA calculation. GGA exchange correlation functionals are defined by

$$E_{xc}^{GGA}[n(r)] = \int \epsilon_{xc}[n(r)]F[n(r), \bigtriangledown n(r)]d^3r, \tag{A.11}$$

where F is a correction dependent upon the gradient and the density.

Approximate DFT has a number of shortcomings in dealing with both dispersion (van der Waals forces) and with charge transfer due to the energy level alignments and band offsets.

Hybrid functionals represent a compromise between DFT exchange correlation functionals and Hartree-Fock [3]. Hybrid functionals incorporate the exact exchange functional from Hartree-Fock into the DFT formalism, mixed with the DFT exchange and correlation functional. This improves DFT orbitals in many properties such as bond length and energies. With LDA/GGA, DFT consistently underestimates the band gap and bonding distance. In contrast, Hartree-Fock does the opposite usually overestimating the band gap and bond lengths. While hybrid orbitals may provide a more accurate orbital energies than Hartree-Fock and DFT functionals individually it is not systematic, and it is difficult to determine if the band gaps are being over or underestimated and in practice are calibrated to experiment.

A.2 Configuration Interaction

Configuration interaction (CI) is a post Hartree-Fock method for improving energies and the many-electron wave function. Any set of orbitals can be used with CI, although they are usually chosen to be orthogonal. CI moves beyond the single-electron picture and uses a multi-reference wave function. It is variational in nature with the accuracy of the system moving towards the exact non-relativistic system given by a full CI for a complete many-electron basis set.

A configuration describes each independent electron in an orbital where the interactions between them are treated with an averaged field. Each configuration corresponds to a Slater determinant and interaction describes the mixing of electron configurations. In a CI calculation the system is represented as linear expansion of Slater determinants

$$|\Psi\rangle = \sum_A c_A |\psi_A\rangle \tag{A.12}$$

where $|\Psi\rangle$ is the many electron wavefunction and c_A is a coefficient representing a Slater determinant's contribution to a many-body state.

Configuration interaction improves upon a Hartee-Fock calculation by obtaining the correlation energy. Correlation energy E_{corr} is defined as the difference between the exact non-relativistic energy and the Hartree-Fock approximation, and includes all electron-electron interactions beyond the mean field approximation. This is exemplified in the equation A.13 below

$$E_{corr} = E_0 - E_{HF}, \tag{A.13}$$

where E_0 is the exact energy of a non-relativistic state.

Correlation energy arises in two distinct components, dynamic and static. Dynamical correlation energy is more easily understood as the energy difference arising out of the deficiencies of the self-consistent field (SCF) method in treating electron-electron interactions. Correct treatment of the dynamical correlation energy involves compensating for the SCF field and treating the electron-electron interactions correctly so that electrons "avoid" one another. Static correlation arises out of the inadequacy of a single determinant wave function being able to describe the state of a molecule even as a first approximation. Static correlation plays a large role in multi-reference systems with nearly degenerate states and open shell systems due to electron rearrangement. Treatment of static correlation can usually be achieved via the inclusion of a few choice configurations which strongly contribute to the wavefunction.

To improve on a single determinant HF wavefunction, the trial wavefunction is written in a multi-determinant form as in equation A.14.

$$|\Psi\rangle = c_0|\psi_0\rangle + \sum_{ia}|\psi_i^a\rangle + \sum_{i<j}\sum_{a<b}c_{ij}^{ab}|\psi_{ij}^{ab}\rangle + ... \tag{A.14}$$

Here the subscripts refer to the occupied orbitals of a single-particle ground state and the superscripts refer to the unoccupied orbitals of a single-particle state. The CI wave function can be expressed as a sum of combinations of excitations with respect to the Hartree-Fock one electron ground state wave function. The N-electron wavefunction is expanded in terms of spin-projected Slater determinants where normalisation is enforced through the constraint $\langle \Psi | \Psi \rangle = 1$. The equation A.14 can be viewed as a sum of excitation orders starting with the ground state and with each additional term representing the sum of all configurations for that level of excitation. Initially for a CI calculation the Hartree-Fock determinant is used as a reference for the start of a CI calculation. This is because the Hartree-Fock determinant is the best single approximation to the energy and as such is a good starting approximation to the many-body wave function. It holds true that not only is the CI ground state an upper bound to the exact non-relativistic ground state, but that all CI excited states represent an upper energy bound to their corresponding exact non-relativistic energies. CI is general in its implementation and can be applied to excited states.

CI can be formulated as the matrix representation of the Schrödinger equation with configuration state functions (CSFs) instead of single determinants. A CSF is a symmetry adapted linear combination of Slater determinants that can be used by CI to correctly describe spin. CSFs are constructed to have the same quantum number as the wave function. Their nature is analogous to the linear combination of atomic orbitals (LCAO) employed in a single-particle basis. CSFs have an advantage over conventional Slater determinants in that their contracted nature shortens the configuration vector of a calculation reducing the computational overhead.

CI employs a trial wave function or vector consisting of CSFs or Slater determinants with the many-electron wave function represented as a linear

combination of CSFs or Slater determinants. As the variational method converges the energy towards the exact non-relativistic energy so too does the wave function converge towards the exact many body wave function. Solving the CI problem for an N-electron Hamiltonian in a complete basis function of N-electron Slater determinants or CSF's will result in the exact eigenstates of the system. Capturing all the correlation energy with a full CI is impractical in all but the most trivial systems. The CI space expands quite rapidly with (basis function) size, with the expansion of CI space being combinatorial (worse than exponential). The size of a full CI constructed from CSFs is given by the Weyl formula [4]

$$N = \frac{M+1}{2S+1}\left(\frac{M+1}{l/2+S+1}\right)\left(\frac{M+1}{l/2-S}\right), \tag{A.15}$$

where N is the number of CSFs needed, S is the spin, M the number of orbitals and l the total number of electrons.

To compensate for the large number of configurations those configurations unlikely to contribute to the correlation are removed. One approach to limiting CI space is to ignore or "freeze" orbitals considered to be affected little by environmental changes. Typically this is applied to molecular orbitals far from the valence electrons that are the lowest lying in energy and considered tightly bound. Since the molecular orbitals are tightly bound, it is generally recommended that frozen core approximation be implemented to improve calculation times. Core correlations cancel when taking energy differences and have little effect on valence correlations. Regardless due to a lack of flexibility, the large proportion of the basis sets employed in quantum calculations are inadequate in describing the correlation of core electrons. In addition to frozen orbitals, energy cut-offs are employed, restricting the number of virtual orbitals included within a calculation. Thus virtual orbitals very high in energy and unlikely to contribute to the calculation are also excluded.

Removal of configurations alone, while reducing computational overheads, is insufficient to compensate for the large size of a full CI calculation. In practical terms, the CI space has to be truncated to carry out a calculation. Most configurations provide only a small contribution to the CI wave function, the key is in including only those with significant contributions. A common means of attempting this is excitation limited CI. This involves only including excitations within a certain excitation level with respect to the reference function. The reference function is defined as the initial configuration in a CI calculation from which excitations are applied. An example of this is CI (singles-doubles) (CI(SD)), which only includes single and double excitations with respect to the reference function. This scheme can be extended to any excitation level but in practice is usually restricted to CI(SD); CI(singles, doubles, triples) (CI(SDT)), and CI(singles, doubles, triples, quadruples) CI(SDTQ) are infrequently applied.

It is worth noting that in excitation truncated schemes, most multi-reference states will be captured. This allows excitation limited CI methods to capture the static correlation energy, but not necessarily all of the dynamical correlation energy. Considering the Hamiltonian contains only one and two body interactions, therefore only single and double excitations with respect to the reference function can interact directly with the reference function when using orthogonal molecular orbitals. However even though triple excitations and above do not interact directly with the reference function they can interact indirectly through high level excitations which do interact with the reference function.

Normally a Hartree-Fock determinant does not interact with single excitations due to Brillouin's theorem. Brillouin's theorem states that any single excitation with respect to the ground state cannot improve the energy. A general property of determinants is that if any two determinants differ by a single row or a column then any linear combination of the two can itself be expressed as a determinant. If

we take a Hartree-Fock determinant $|\psi_0\rangle$ and apply a single excitation with respect to this determinant $|\psi_1\rangle$ since it differs by only one row or column the new determinant can be expressed as a linear combination of the two as $c_i|\psi_0\rangle + c_j|\psi_1\rangle$ where c_i and c_j are coefficients. But since the Hartree-Fock determinant is the best single determinant approximation to the energy so the contribution of the single excitation is zero, or mathematically

$$\langle\psi_S|H|\psi_0\rangle = 0. \tag{A.16}$$

Any interaction between a Slater determinant which differs by any single excitation with respect to the reference determinant and the reference determinant is zero. Single excitations like higher excitations can still contribute to the wave function by interacting indirectly through other configurations.

Due to the above factors, double excitations tend to have the strongest direct interaction with the reference configuration and generally contribute the most in terms of correlation energy. For most systems (except for strongly correlated systems) excitation limited CI captures a significant proportion of the correlation energy. CI(SD) can account for up to 95% of the correlation energy for a variety of systems. Many of the configurations captured within CI(SD) contribute little in terms of energy. At non-equilibrium geometries the accuracy of CI(SD) suffers with CI(SDTQ) being a more robust alternative, but computationally orders of magnitude more expensive. Full CI is therefore relegated due to its large computational demand to the job of providing benchmarks to other truncated CI implementations on small systems.

Additionally the process of truncating CI alters the property of the CI calculation and its results. Size extensivity can be described as the scaling of energy with the number of electrons. It is expected that with size extensivity the proportion of the energy recovered scales linearly with the size of the system. This is true of full CI

but not of truncated CI. Size consistency on the other hand refers to the results of a system being equivalent to the sum of the results of its separate components (e.g. the energy of a system remains the same if it is halved and energy of each halve is calculated separately). One can view the size consistency as dissociation towards infinity. This occurs in perturbation theory which is size consistent if the reference function dissociates properly. Hartree-Fock is size extensive but not size consistent, but truncated CI is neither size extensive nor size consistent.

A.3   Monte Carlo Configuration Interaction

Monte Carlo Configuration Interaction (MCCI) is a configuration interaction based method that involves a search through Hilbert space to produce highly compact wave functions that are capable of approaching full configuration interaction, but at a greatly reduced CI vector size and computational cost [5]. In most cases except for small systems, typically on the order of ten electrons, full CI is not practical due to the computing time involved. Conventional configuration interaction based methods achieve results by increasing efficiency through truncation such as excitation limited criteria (e.g. singles, singles and doubles , single and doubles and triples etc.).

Disadvantages within excitation limited CI are that even with lower excitations with respect to the reference function many configurations with low contributions to the energy of the wave function are included. Conversely, high order excitations with large contributions are ignored due to lying outside the excitation limit. This can be compensated for by increasing the maximum excitation allowed within a scheme, but this in turn leads to an increase in the number of configurations and the problem quickly becomes computationally intractable. To counteract these limitations, with MCCI a criteria is enforced such that the vector generated is

shortened yet retains a significant proportion of the correlation energy.

MCCI achieves this via inclusion of configurations based on their contribution to the wave function. MCCI uses random (Monte Carlo) excitations with respect to the current wavefunction vector to generate configurations which are then pruned to remove those with low contribution to the wave function. This is cyclically repeated until convergence. MCCI in contrast to conventional CI truncation methods is not excitation limited and in principle capture any excitation regardless of its occupation relative to the ground state so long as its contribution to the many body wave function is significant. This allows MCCI to operate accurately on highly correlated systems which tend to have highly excited orbitals with a strong contribution to the wave function. MCCI can also achieve this at a significantly lower computational cost than conventional CI approaches. An interesting observation is that a small number of configurations can provide a large contribution to the wave function, with a large amount of configurations having little to no contribution for typical molecular problems. MCCI works within a reduced CI space of selected configurations.

MCCI starts with an initial trial vector, which is then expanded through a series of random (Monte Carlo) single and double excitations with respect to the trial vector. Initially, this can consist of one CSF but on subsequent loops can contain thousands of CSFs as a result of applying repeated excitations to the vector. MCCI applies single and double excitations to the all accumulated CSFs within the vector. Through repeated single and double excitations any part of the CI space can be reached. After the branching component the CI matrix is diagonalised using the Davidson algorithm, a modified version of the Lanczos method. This yields the contribution of each configuration to the many body wave function through their coefficients yielded by the diagonalisation. All configurations with a coefficient above a predefined fractional threshold are

Table A.1: MCCI procedure after ref. [6]

		$K = 0$.
(0)	Initialize	Define the starting vector $\lvert \Psi_0 \rangle = \sum\limits_{i=1}^{N_0} c_A \lvert \Psi_A \rangle$;
		Repeat steps (1)-(4) until convergence of the vector length N_A and the energy E
		$K = K + 1$
(1)	Branching	Generate $\lvert \Psi_R \rangle = \hat{\alpha}_R \lvert \Psi_A \rangle$ $\;\; 1 \le A \le N_A^{K-1}; \;\; N_A^{K-1}$ $+1 \le R \le N_{K-1} + N_{\text{new}}$;
		where $\hat{\alpha}_R \in \{0, \hat{a}_m^{\dagger} \hat{a}_i, \hat{a}_m^{\dagger} \hat{a}_n^{\dagger} \hat{a}_i \hat{a}_j\}$
		$\lvert \Psi^K \rangle = \sum\limits_{A=1}^{N_{K-1}+N_{\text{new}}} c_A \lvert \Psi_A \rangle$,
(2)	Matrix generation	Generate Hamiltonian $\mathbf{H}$ and overlap $\mathbf{S}$ matrices in the CSF basis.
(3)	Diagonalisation	Solve $\mathbf{Hc} = \mathbf{Sc}E$.
(4)	Pruning	IF $\lvert c_A \rvert >$ threshold THEN retain $\lvert \Psi_A \rangle$ ELSE reject $\lvert \Psi_A \rangle$;
		$\lvert \Psi^K \rangle = \sum\limits_{A=1}^{N_K} c_A \lvert \Psi_A \rangle$, where $N_K \le N_{K-1} + N_{\text{new}}$,
(5)	Converged	$E^K = \langle \Psi^K \rvert \hat{H} \lvert \Psi^K \rangle \,/\, < \Psi^K \lvert \Psi^K >$.

retained with the remaining configurations pruned from the calculation. Typically the threshold has a value of $\sim 10^{-3}$. Through modification of the threshold the precision of the calculation can be controlled. This process is outlined in table A.1.

Repeated iterations of this process yield a CI vector with an increasing number of "selected" configurations with contributions to the wave function above the predefined threshold. MCCI calculations converge when a set of convergence criteria are satisfied. Typical criteria leading to the end of the calculation are 1) the change in energy with each iteration is below a specified tolerance, and 2) the number of new configurations retained after each pruning cycle is below a specified proportion of the total number of CSFs. Once the above criteria are satisfied no significant number of new configurations will be added to the CI vector and stopping the search is justified. With this process MCCI can, in principle, capture any important configurations of the full CI space while retaining the advantage of a compact CI vector.

References

[1] J. P. Perdew and K. Schmidt, "Jacob's ladder of density functional approximations for the exchange-correlation energy," *AIP Conference Proceedings*, vol. 577, pp. 1–20, July 2001.

[2] J. P. Perdew and M. Levy, "Extrema of the density functional for the energy: Excited states from the ground-state theory," *Physical Review B*, vol. 31, pp. 6264–6272, May 1985.

[3] A. D. Becke, "A new mixing of Hartree–Fock and local density[U+2010]functional theories," *The Journal of Chemical Physics*, vol. 98, pp. 1372–1377, Jan. 1993.

[4] H. Weyl, "Theorie der Darstellung kontinuierlicher halb-einfacher Gruppen durch lineare Transformationen. I," *Mathematische Zeitschrift*, vol. 23, pp. 271–309, Dec. 1925.

[5] J. Greer, "Monte Carlo Configuration Interaction," *J. Comput. Phys.*, vol. 146, pp. 181–202, Oct. 1998.

[6] W. Gyorffy, R. J. Bartlett, and J. C. Greer, "Monte Carlo configuration interaction predictions for the electronic spectra of Ne, CH2, C2, N2, and H2o compared to full configuration interaction calculations.," *The Journal of chemical physics*, vol. 129, pp. 064103–064103, Aug. 2008.

Appendix B

Charge Transport

In this appendix an overview of the theoretical and computational methods is given. Basic concepts in electronic structure theory as applied to molecular physics are also outlined.

B.1   Non-equilibrium Green's functions

One approach for determining single-particle transport is the **Non Equilibrium Green's Function (NEGF) method** [1].

The NEGF formalism can solve the single-particle Schrödinger equation with open boundary conditions. NEGF calculates the properties of systems utilising Green's functions and allows for the determination of electron transport through a finite piece of material connected between two reservoirs. While not intrinsically a single-particle method, approximations made in its implementation make it practically so.

All molecular devices consist of a device region and two contacts (i.e. one left and one right contact). The Poisson equation and equilibrium statistical mechanics are used to analyse an electronic device in equilibrium where the Poisson equation may need to include an exchange correlation functional. When the system is in equilibrium the electronic structure of the system can be determined by Density Functional Theory (DFT). For equilibrium statistical mechanics this approach proves adequate but we need to describe non-equilibrium mechanics. For non-equilibrium mechanics each contact has a separate Fermi level associated with it which initially, are equal but are driven out of equilibrium as a voltage is applied. This requires a separate calculation of the electron density. One way to circumvent this is to partition the system into closed and open spaces where the closed spaces are treated with Gaussian basis sets and the open spaces with electron self energies.

Consider a 1-dimensional open system device that is constricted in the transverse

direction but is attached to two contacts in the longitudinal direction. An open
system in molecular electronics is when a closed system is coupled to an external
infinite system. In this case the closed system represents the device region and the
external system is the contacts. Open boundary conditions are required for
non-equilibrium states in the device region because in a closed system any
disturbance would quickly reach equilibrium. As a closed system device is coupled
to an open system with a continuum of states the discrete energy levels of the
closed system broaden and gain a finite lifetime τ.

A solution to this is Green's functions. What is a Green's function? Initially let us
consider a non-perturbed system with a hamiltonian H

$$H|\psi\rangle = E|\psi\rangle \tag{B.1}$$

$$(E - H)|\psi\rangle = 0 \tag{B.2}$$

which can be expressed as

$$(E - H)G(E) = I \tag{B.3}$$

$$G(E) = \frac{1}{E - H}. \tag{B.4}$$

Where G(E) is the Green's function. Now let's consider the same system with an
additional perturbation. For system with a perturbation v the Hamiltonian is
expressed as

$$H|\psi\rangle = |\psi\rangle + |v\rangle. \tag{B.5}$$

This is expressed in terms of the Greens function as

$$|\psi\rangle = -G(E)|v\rangle \tag{B.6}$$

The Green's function therefore describes the response of a system to a
perturbation. As a system is connected to the semi infinite leads there are two

solutions for the Green's functions, the advanced and retarded Green's functions corresponding to an outgoing and an incoming electron wave, respectively.

Now let us consider a device region described by the Hamiltonian H_D which is connected to semi-infinite leads/reservoirs described by the Hamiltonians H_L and H_R corresponding to the left and right leads respectively. The terms H_{LD}, H_{DL}, H_{RD} and H_{DR} describe the interactions between the leads and device region. It is assumed there is no interaction between the leads. This yields the system Hamiltonian:

$$\begin{bmatrix} H_L & H_{LD} & 0 \\ H_{DL} & H_D & H_{DR} \\ 0 & H_{RD} & H_R \end{bmatrix} \tag{B.7}$$

The system can be expressed in terms of Green's functions, where E is the energy, I is the identity matrix and the S matrix elements describe the corresponding terms of the overlap matrix:

$$\begin{bmatrix} ES_L - H_L & ES_{LD} - H_{LD} & 0 \\ ES_{DL} - H_{DL} & ES_D - H_D & ES_{DR} - H_{DR} \\ 0 & ES_{RD} - H_{RD} & ES_R - H_R \end{bmatrix} \begin{bmatrix} G_L & G_{LD} & G_{LR} \\ G_{DL} & G_D & G_{DR} \\ G_{RL} & G_{RD} & G_R \end{bmatrix}$$
$$= \begin{bmatrix} I & 0 & 0 \\ 0 & I & 0 \\ 0 & 0 & I \end{bmatrix} \tag{B.8}$$

The Green's functions of the leads known for the left and right contact are

$$G_R(E) = (ES_R - H_R)^{-1} \tag{B.9}$$

$$G_L(E) = (ES_L - H_L)^{-1}. \tag{B.10}$$

and are called surface Green's functions since they describe the edge of the device

region and the effect of the semi-infinite leads. For leads consisting of infinite repeating cells the periodicity of the unit cells is used to determine the surface Green's function.

Here we try and obtain a value for the device Green's function (G_D) for the system. Taking the second column of G matrix above we end up with three equations

$$(ES_L - H_L)G_{LD} + (ES_{LD} - H_{LD})G_D = 0 \tag{B.11}$$

$$(ES_{DL} - H_{DL})G_{LD} + (ES_D - H_D)G_D + (ES_{DR} - H_{DR})G_{RD} = I \tag{B.12}$$

$$(ES_R - H_R)G_{RD} + (ES_{RD} - H_{RD})G_D = 0 \tag{B.13}$$

From the top and bottom equations we can deduce

$$G_{LD} = (ES_L - H_L)^{-1}(ES_{LD} - H_{LD})G_D \tag{B.14}$$

$$G_{RD} = (ES_R - H_R)^{-1}(ES_{RD} - H_{RD})G_D \tag{B.15}$$

By substituting values for G_{LD} and G_{RD} into the central equation we can determine G_D

$$
\begin{aligned}
(ES_{DL} - H_{DL})(ES_L - H_L)^{-1}ES_{LD} - H_{LD})G_D + (ES_D - H_D)G_D \\
+ (ES_{DR} - H_{DR})(ES_R - H_R)^{-1}ES_{RD} - H_{RD})G_D = I
\end{aligned} \tag{B.16}
$$

Rearranging gives G_D as

$$G_D = (ES_D - H_D - \Sigma_L - \Sigma_R) \tag{B.17}$$

where self energies for the left and right leads are denoted by the Σ_L and Σ_R respectively.

$$\Sigma_R = -(ES_{RD} - H_{RD})g_R(ES_{DR} - H_{DR}) \tag{B.18}$$

$$\Sigma_L = -(ES_{DL} - H_{DL})g_L(ES_{LD} - H_{LD}) \tag{B.19}$$

The advantage of Green's functions approach is that one can calculate the response of a system to a perturbation without having to solve the entire eigenvalue problem. It allows for the system partitioning making it possible to either determine the Green's function of the device region exclusively, or solve the total Green's function. Such partitioning means it is possible to calculate the device Hamiltonian and include the interaction to the leads via self energies determined from the electronic structure of the contacts.

Self energies are employed in many-body physics to describe electron-electron and electron-phonon interactions. They can however, be utilised to describe the semi infinite leads with respect to a device region and in this context the electron self energies are used to treat the open boundary conditions. The self energy describes everything not included in the device region that contributes to the Hamiltonian. In essence the effects of the leads are coupled to the device region by means of a self energy.

The self energy has numerous effects on the device when it's attached to the system. For example as the self-energy is connected to the system the energy levels shift from their original position due to the interaction with the leads. The energy level shift is given by the equation:

$$H_{new} = H + \frac{\Sigma + \Sigma^\dagger}{2} \tag{B.20}$$

where H is the isolated Hamiltonian, Σ is the self energy interaction of the leads and H_{new} the resulting energy level shift to the Hamiltonian. Of more interest than the energy shift is the broadening which introduces imaginary components into the energy. Broadening adds a finite lifetime to the states of the device region consistent with charge transfer. Within the terms of the self-energy the broadening

can be defined as

$$\Gamma_{L,R} = i \left[\Sigma_{L,R} - \Sigma_{L,R}^{\dagger} \right] \tag{B.21}$$

where Σ is the self energy of the left and right electrodes respectively and Γ is the broadening matrix which describes the broadening effect of the semi infinite system on the device region.

For current **transport** of interest are the cases where there is an asymmetric (non-equilibrium) difference in the chemical potentials across the junction. For the non-equilibrium case with a potential difference induced across the junction the equilibrium electron density is no longer valid and a new non-equilibrium electron density is determined which can be used to calculate the current across the junction. With these boundary conditions, non-equilibrium Green's functions (NEGF) are appropriate. NEGF principally differs from the equilibrium Greens function approach chiefly in its treatment of the electrodes. NEGF describes the open boundary conditions by means of a self-energy. Where the equilibrium approach treats the whole structure with a universal Fermi function, NEGF treats each electrode with a separate Fermi function allowing for each electrode to be at a separate voltage and hence inducing a bias across the molecular junction. This means that only the device region has to be dealt with explicitly. Without an external field applied the NEGF method reduces to the normal case of an equilibrium Green's function.

Using the **spectral function** with Green's functions it is possible to solve the transport equation without having to solve the linear eigenvalue problem. The spectral function A gives all the solutions to the Schrodinger equation in addition to yielding the generalised density of states (multiplied by 2π) regardless of whether the states are occupied or not:

$$A(E) = i(G(E) - G(E)^{\dagger}) \tag{B.22}$$

where $A(E)$ is the spectral function and $G(E)$ is the Green's function. The left and right spectral functions $A_{L(R)}$ of each contact can be defined as

$$A_{L(R)} = G\Gamma_{L(R)}G^+. \tag{B.23}$$

where G is the device Green's function and $\Gamma_{L(R)}$ refers to the broadening matrix of the left and right contacts. The diagonal components of the spectral density yields the local density of states in a real space representation. This simple division allows for the description of a device where the Fermi levels are no longer in equilibrium with each other.

For coherent transport, without electron-electron or electron-phonon scattering the Green's function formalism becomes simpler to implement. This approximation tends to be accurate for ultra short devices with minimal scattering, such as tunnelling diodes, allowing the eigenstates to be subdivided into incident waves associated with the left and right electrodes. For coherent transport the Green's function is given by:

$$G = [EI - H - \Sigma_L - \Sigma_R]. \tag{B.24}$$

The NEGF formalism as it is applied to a device is a convenient method for evaluating the **transmission probability**.

$$T(E) = Tr(\Gamma_L G\Gamma_R G^\dagger) \tag{B.25}$$

where $T(E)$ is transmission function and G is the Green's function. The transmission function is interpreted as the probability of an electron incident from the left contact will transfer across to the right contact and depends on the occupation of states in the electrodes. Finally the current is determined via the equation

$$I = \frac{q}{h} \int dE\; T(E)(f_L - f_R) \tag{B.26}$$

where I is the current, $T(E)$ is the transmission function and f_L and f_R are Fermi functions corresponding to the left and right leads. The Fermi functions $f_{L(R)}$ are defined as

$$f_{L(R)} = \frac{1}{e^{\frac{E - \mu_{L(R)}}{kT}} + 1} \tag{B.27}$$

where E is the energy, $\mu_{L(R)}$ is the electrochemical potential of the left and right electrodes, k is Boltzmans constant and T is the temperature. Additionally at zero bias the conductance can be determined from the formula

$$g = \frac{2e^2}{h} T(E) \tag{B.28}$$

where g is the conductance and $T(E)$ the transmission function.

While not normally treated, **electron-electron scattering** can be incorporated into the NEGF formalism by means of a scattering self energy Σ_S. The relationship between Σ_S and the density matrix is dependent on the form of scattering that is occurring within the device. This modifies the Green's function to the form of

$$G = [EI - H - \Sigma_L - \Sigma_R - \Sigma_S] \tag{B.29}$$

where G is the Greens function H is the Hamiltonian and $\Sigma_{L,R}$ is the self-energy of the left and right electrode and Σ_S is the scattering self-energy. Complications arise as the scattering self-energy Σ_S is dependent on the electron density matrix and as such has to be determined self-consistently.

B.2　Many Electron Correlated Transport

Many-Electron Correlated Scattering (MECS) is a many-body method for determining current transport in nanoscale molecular systems [2, 3]. MECS, as the name implies, incorporates electron correlation (including electron-electron

scattering) into a many-body formalism to determine electron transport while avoiding common approximations to the electronic structure utilised by methods such as linear response theory, or NEGF methods (which in practice rely on a single-particle approximation). The MECS method applies a scattering based formalism to solve the open system, many body problem by modifying boundary conditions. MECS can deduce electric current from the one electron reduced density matrix obtained from a many electron wave function.

Previous work involving DFT/NEGF has led to questions over the effect of correlation energy on conductance with some conductance values differing by orders of magnitude with respect to experiment [4]. Hence deducing correlated effects on transport and comparison to conventional methods could be critical in determining the cause of divergence between experiment and theory.

While many other quantum mechanical transport codes exist they suffer from any one of a number of common assumptions:

- One of the main sources of error in DFT based codes is the error arising out of the use of approximate exchange correlation functionals such as the local density approximation (LDA) and generalised gradient approximation (GGA).

- Treating the Kohn-Sham one-electron orbitals as quasi-particles.

- The application of the Landauer-Buttiker formalism which reduces the description of conductance of the system into a one-dimensional ballistic transmission problem with reflections and transmission coefficients, ignoring the electron-electron interactions.

Traditional single-particle based methods typically employ a transmission-based formalism to deduce the current across the junction. This involves determining the correct energy levels and their seperation from the Fermi energy (where the Fermi

energy is determined from the reservoir/leads). In this context it is critical that the choice of Fermi level is correct as it can have a dramatic effect on the results of the calculations. MECS does not explicitly use a Fermi level to determine transport instead utilising a scattering based formalism. Using the CI generated configurations, MECS employs a many-electron scattering formalism to determine correlated transport across molecular junctions. MECS is valid even beyond the linear response regime.

Due to the above forementioned differences between correlated and uncorrelated electron transport, single-electron approximations break down depending on the level of correlation within the system. The principal aim of MECS is to calculate the many-body wave function for a molecular junction based system and determine the current transport across the junction for a range of applied junction voltages. Different aspects of the MECS calculation are briefly described below.

Normally, quantum transport is formulated with boundary conditions described by a single-particle picture with electron reservoirs described by Fermi levels and Fermi-Dirac distributions. In the many-body language, there is no simple analogue to the single-particle reservoir counterparts. MECS works directly with the N-particle wave function removing the direct physical interpretation of single-electron wavefunctions and eigenvalues leaving only the many-body interpretation of the system. Therefore generalisation of the conventional single-electron problem is not possible and a solution to the transport problem does not exist for many-body systems. This problem is circumvented via the employment of Wigner functions.

The Wigner function is a quasi-probability distribution that provides a phase space portrait of quantum mechanics. It has been used to define scattering boundary conditions of single-electron uncorrelated systems where it can be applied to single-particle heterogeneous systems. A classical probability distribution describes

particles with definitive momentum and position, this does not hold in quantum mechanics which is affected by the Heisenberg uncertainty principle where a particles position and energy cannot be known simultaneously. This is apparent when the Wigner function has a negative value indicating it is strictly not a probability distribution but is a momentum distribution with quantum mechanical effects. The Wigner function in the many body context cannot determine the probability of a specific electron of momentum p being at a position q but can determine the probability of finding any electron of momentum p at position q. This is due to the indistinguishability of electrons. In this work the Wigner function is applied as scattering boundary conditions to many-body correlated electron transport. Scattering boundary conditions imposed by the Wigner distribution imitate the effect of the system connected to an electron reservoir such as semi-infinite leads. The boundary conditions have to emulate the effect that any electron leaving the junction is effectively absorbed.

A Wigner plane is a two-dimensional plane that is placed within the molecular junction. This plane is the location where the Wigner function is physically implemented. To impose electron boundary conditions the Wigner plane is placed at a plane perpendicular to the principal (current carrying) axis usually behind the second to last plane of atoms in a contact as in Figure B.1. The implementation of the boundary conditions carries with it a number of assumptions (caveats),

- That there is no backscattering off the back planes so that every outgoing electron passing a Wigner plane is absorbed into the semi-infinite leads/electron reservoir.

- That the Configuration State Functions(CSFs) generated from the finite electrode geometry using configuration interaction (CI) based methods are not missing any significant contribution due to the lack of contribution to the leads/electrodes.
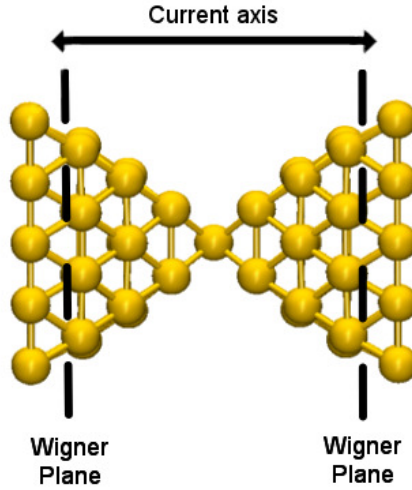
Figure B.1: Wigner planes are placed deep in junction perpendicular to current carrying axis.

By formulating the scattering boundary conditions the one electron reduced Wigner function $f(q, p)$ can be expressed in atomic units as

$$f(q,p) = N \int e^{-ip \cdot r} \psi^*(q - r/2, r_2, r_3....r_N) \times \psi(q + r/2, r_2, r_3....r_N) dr dr_2 dr_3...dr_N.$$

(B.30)

where q is the position and p is the momentum, N the number of electrons and ψ is the wavefunction. From the Wigner function the expectation value of the kinetic energy can be defined as

$$\langle \Psi | \hat{T} | \Psi \rangle = \frac{1}{(2\pi)^3} \int \frac{p^2}{2} f(q,p) dq dp$$

(B.31)

where $\hat{T}$ is the one-electron kinetic energy operator. Similar forms of the equation exist for other one electron operators. Two electron properties can be determined from the two electron reduced Wigner function. It is possible to retrieve any Nth body property from the Nth order Wigner function.

To impose boundary conditions, a reduced one-particle Wigner function is used to emulate the single-particle open boundary reservoir distribution conditions for the many-body method. MECS deduces the current using Wigner functions to emulate

the effect of electron momentum distribution incident from contact reservoirs. The Wigner functions are used to implement current transport. Wigner boundary conditions consist of fixing the Wigner function of the left and right contacts with constraints that are pointing towards the current carrying region which fixes the inward travelling momenta. At zero bias with no external field, the Wigner
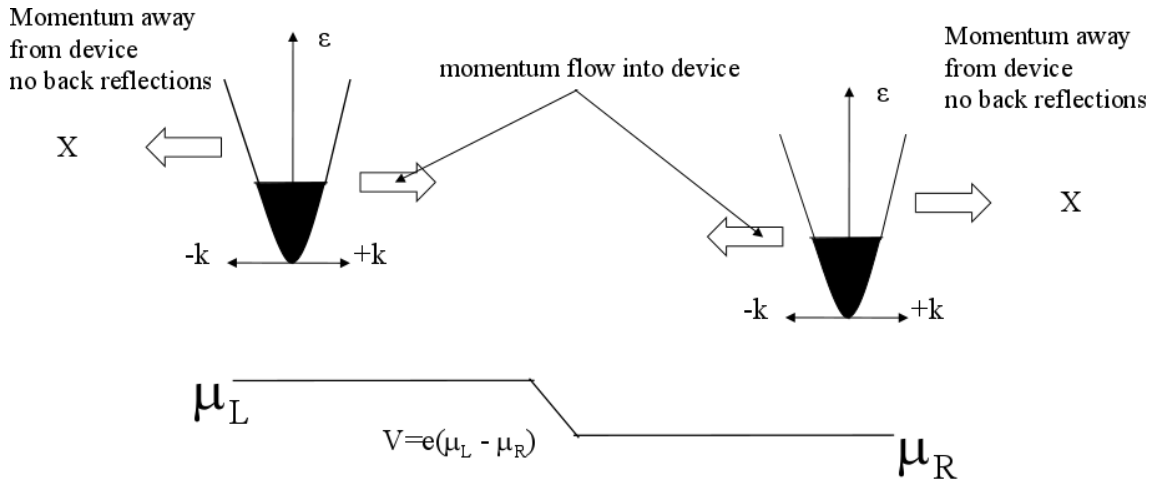
Figure B.2: Voltage difference across the junction is equivalent to $V = e(\mu_l - \mu_r)$. Incident electron momenta distributions towards the contact are equivalent with the net current across the junction determined by asymmetric backscaterring of the applied field.

function's inward momenta will be equivalent and since there is no external field there is no effect on the electrons traversing the junction the outward momenta will be equal resulting in no net current flow ($\mu_l = \mu_r \longrightarrow V = 0$). As an external field is applied the electrons traversing the junction are scattered by the applied field depending on the orientation and strength of the applied field and the direction of the incident electrons. Since the inward momenta is fixed via Wigner constraints to describe the behaviour of the reservoirs they therefore remain unchanged as a voltage is applied across the junction. The outgoing Wigner function is not constrained and allowed to move freely, leaving the current carrying region to reflect electrons out of the contact asymmetrically. This process which can be clearly seen in figure B.2 leads to an asymmetric momenta imbalance leaving the junction, resulting in a net current. In summary, current flow in the

MECS method arises not out of a direct increase in the number of electrons traversing the junction from one side to the other but purely due to asymmetric scattering in the central scattering region due to the externally applied field.

While the MECS method does not explicitly use a Fermi level (or Fermi-Dirac distribution) to determine transport we can gain insight into its transport formalism by briefly considering the Wigner function electron reservoirs from such a single-particle perspective. In figure B.3 a) the unperturbed Fermi Dirac energy dispersion for the left and right electrode with no electric field applied is displayed. Where ϵ_F is the Fermi energy, eV is the energy shift due to the applied field k_f is the momentum at the Fermi energy and $f(k)$ is the momentum distribution. As an electric field is applied the energy shifts on the right electrode from ϵ_F to $\epsilon_F + eV$ as in B.3 b). For both B.3 a) with no applied field and B.3 b) with an applied field the momentum remains unchanged and unaffected as in figure B.3 c). Thus when the electric field is applied there is an increase in potential energy of the right electrode but no corresponding increase in kinetic energy and as such the momentum profile remains unchanged as for the unperturbed case. In this regard it seems counter intuitive that the energy distribution are asymmetrical while the momentum distributions are symmetrical. This is identical to considering it to the Wigner function description previously where the incident momentum was unaffected by the applied field. The resulting current is due to asymmetric scattering of the electrons due to the applied field.

MECS determines the Wigner function from the reduced density matrix. The MECS approach utilises the reduced density matrix via the Wigner transform to determine many body correlated transport for open boundary conditions. In quantum mechanics the current $J(r)$ via the reduced density matrix is given by :

$$J(r) = \frac{1}{2i}[\nabla_r - \nabla'_r]\rho(r,r')|_{r=r'} \tag{B.32}$$
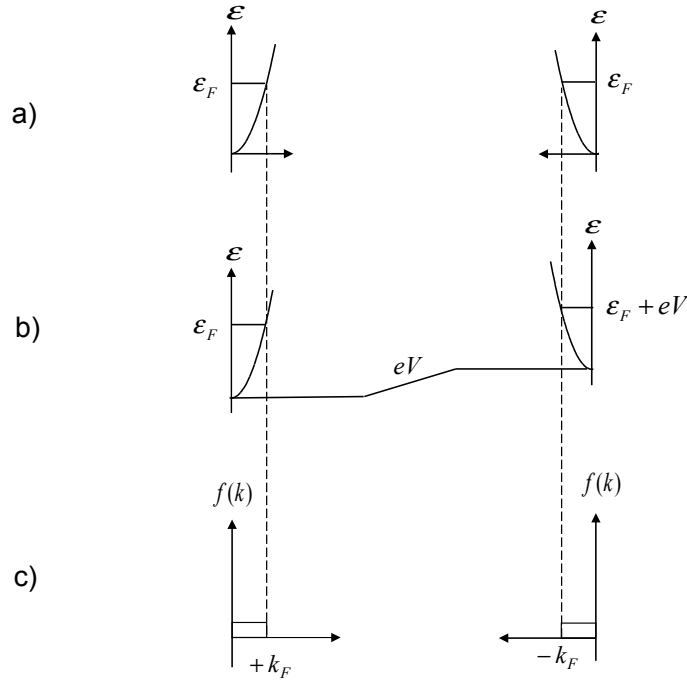
Figure B.3: Parts a) and b) contain the Fermi Dirac distribution of energy levels before and after the electric field is applied across the junction. Part c) contains the a graph of the momentum distributions corresponding to the band structures in parts a) and b). It is worth noting in comparison between parts a),b) and c) that as the total energy is increased the momentum distributions remain unperturbed.

where $\rho(r, r')$ is the density and r the position. From the above equation it is clear that for a real $\rho(r', r)$ no current will flow. CI coefficients have to be complex to describe a semi infinite system (due to broadening) that is necessary for current transport. MECS uses the CI method Monte Carlo Configuration Interaction (MCCI) to calculate the electronic structure of the junction, and transport properties are calculated using the Wigner function within open boundary conditions under constraints.

MECS will typically employ not just a many body ground state but also many body excited states in the course of a calculation to provide a good many body basis. In this case the perturbation is about the many body ground state and

couples to the many-body excited states via the dipole matrix elements (electric field coupling). Without the addition of excited states the wave function would lack the necessary flexibility to describe the polarisation of the electron scattering region of the wave function. Single excitations relative to the ground state are included to describe the system as an electric field is applied. Initially the wave function of the unperturbed system is given by the equation:

$$\langle \Psi_0 | H | \Psi_0 \rangle = E\Psi_0 \tag{B.33}$$

As an electric field is applied the Schrödinger equation becomes

$$\langle \Psi | H + \epsilon z | \Psi \rangle = E\Psi + b.c.'s \tag{B.34}$$

where ϵ is the electric field, b.c.'s are boundary conditions and z is the axis orientation of the electric field. When an electric field is applied the zero field ground state CI vector Ψ_0 no longer represents the CI ground state of the perturbed system Ψ. This underlines the necessity of including excited states in the current carrying wave function.

Normally CI variational problems are solved by treating it as an eigenvalue problem. There is no linear eigenvalue problem with which to transform the MECS variant of the many body problem. Conventional linear optimisation problems are trivial to solve, of greater difficulty to solve are the non-linear optimisation problems of which MECS is one. Typically non-linear optimisation problems can be solved by different methods such as Newton method, steepest descent or the conjugate gradient method. The non linear optimisation approach implemented within MECS is the conjugate gradient method which converges to the solution in at most N steps where N is the dimension of the matrix. This limits the maximum number of steps whereas in the method of steepest descent no such upper bound

exists.

A requirement of the minimisation of the energy in any formalism involves that at the minimum point that it's gradient is zero. Non-convex problems have the additional difficulty of converging to a local and not a global minima. Due to the non-convex nature of the minimisation problem convergence criteria is enforced to ensure minimisation only converges to the global minimum.

There are also additional constraints that MECS imposes in the non linear optimisation problem. The normalisation constraint is one such criteria where $\langle \Psi | \Psi \rangle = 1$. This is a constraint qualification. Finally the Wigner constraints are imposed on the inward pointing (that is the portion of the Wigner function with electrons projected towards the device region) portion ofthe Wigner function to fix the inward electron momenta from each Wigner function. Constraining the Wigner function in this way freezes the inward momenta such that it remains unaffected by the externally applied field. This boundary condition arises out of the assumption that the leakage current from the reservoir is small and as such will not perturb the incoming momenta distribution. A requirement is that the gradient of the energy is parallel to the gradient of the constraint function. This ensures that not only is the energy minimised but that all applied constraints are satisfied.

Typically in CI the Hamltonian operator is in a many body basis and diagonalised to solve the variational problem. A penalty function is included over the bare Lagrangian multipliers to improve convergence [5, 6].The penalty function approach is a constrained optimisation method which penalises points which do not obey the constraints and turns the constrained minimisation problem into an unconstrained variational problem. The Lagrange penalty function utilised in MECS is

$$L(\Psi, \lambda_i, \sigma) = \langle \Psi | H + \epsilon z | \Psi \rangle - \sum_{i=1}^{n} \lambda_i c_i(\Psi) + \frac{1}{2}\sigma \sum_{i=1}^{n} c_i^2(\Psi) \qquad \text{(B.35)}$$

where Ψ is the wavefunction, ϵ is the electric field, λ the Lagrangian constraints

coefficients , σ is the penalty term. $\langle\Psi|H + \epsilon z|\Psi\rangle$ is the energy of the system with the applied field $\sum_{i=1}^{n}\lambda_i c_i(\Psi)$ is the constraint term and $\sum_{i=1}^{n} c_i^2(\Psi)$ is the penalty function. The Lagrange multipler penalty function is a modified penalty function approach which is more numerically stable, improves convergence and avoids the ill conditioning problem (Severe slopes near convergence caused by very high $\sigma(\sigma = 10^{12})$.

Within MECS constraints are imposed by means of Lagrange multipliers, one for each constraint. Initially the Lagrange multipliers are guessed whereby the unconstrained conjugate gradient method converges to a solution and the Lagrange multipliers are updated. This process is iteratively repeated until the penalty constraints are within a predefined tolerance. Convergence over the unconstrained component is performed with the conjugate gradient method.

With the wave function determined via the constrained minimisation problem the current can be determined from the reduced density matrix using the equation

$$J(r) = \frac{1}{2i}[\nabla_r - \nabla_r']\rho(r, r')|_{r=r'}. \tag{B.36}$$

where $J(r)$ is the one electron current density, $\rho(r, r')$ is the density and r is the position. The resulting current is deduced from the difference in momenta from the perturbed Wigner function and the unperturbed reference Wigner function calculated initially. The first convergence loop occurs on the unperturbed system which serves as a reference state for the application of the electric field. In order to generate a current (I) versus voltage $(V)(IV)$ curve calculations are repeated by increasing the applied field ϵ in steps. At each step the wave function is minimised with respect to the energy and the current determined from the one electron density matrix. The base calculation (i.e.with no applied electric field) is treated as a zero reference point for the applied field calculations with the current determined from the difference between them.

Is it important to note that when the energy is being minimised it is a global quantity however the wave function can vary locally leading to discrepancies in current density. Due to ECPs (Effecitve core potentials) and finite basis the current does not obey the continuity equation and can therefore vary locally across the junction. Despite the fact that the current is variable at any point in the current carrying region, the ECPs nevertheless yield the correct transmission coefficients. Therefore the total current across the device region is correctly described. Current constraints also mitigate the effect of the local variations across a junction.

The MECS in it's numerical implementation utilises a sequence of programs in the course of a transport calculation. The programs typically used in the course of a MECS calculation are TURBOMOLE, MCCI, and VICI (Voltage Current Configuration Interaction). The initial part of the MECS method performs a conventional Hartree Fock (HF) or DFT calculation. This involves running a single-particle code such as TURBOMOLE to generate the one and two electron integrals. (Note: TURBOMOLE can be replaced with any other HF or DFT code. The only stringent requirement is the that molecular orbitals should be orthogonal and the set of one and two electron integrals be available to generate the CI Hamiltonian matrix elements). The next step is that MCCI utilises the one and two electron integrals to generate the many-body Hamiltonian Configuration State Functions (CSFs)using configuration interaction. Finally the VICI program determines the current from the CSFs and integrals.

The MECS method is modular and not tied to any code so long as it can produce the required CSFs and electron integrals. While in principle any CI code can be used so long as it generates a CSF vector, MCCI combines a high proportion of the correlation energy with a compact CI vector. MCCI achieves this by only using highly contributing CSFs thereby increasing efficency for a given vector size.

References

[1] S. Datta, *Electronic Transport in Mesoscopic Systems*. Cambridge University Press, May 1997.

[2] P. Delaney and J. C. Greer, "Quantum electronic transport in a configuration interaction basis," *International Journal of Quantum Chemistry*, vol. 100, pp. 1163–1169, Dec. 2004.

[3] P. Delaney and J. C. Greer, "Correlated Electron Transport in Molecular Electronics," *Physical Review Letters*, vol. 93, p. 036805, July 2004.

[4] T. Kudernac, N. Katsonis, W. R. Browne, and B. L. Feringa, "Nano-electronic switches: Light-induced switching of the conductance of molecular systems," *J. Mater. Chem.*, vol. 19, pp. 7168–7177, Oct. 2009.

[5] R. Fletcher, *Practical Methods of Optimization*. Chichester: Wiley, 2 edition ed., May 2000. bibtex: fletcher_practical_2000.

[6] D. P. Bertsekas, *Constrained Optimization and Lagrange Multiplier Methods*. Belmont, Mass: Athena Scientific, Jan. 1996. bibtex: bertsekas1996.

Appendix C

Supporting information: Tunnel Currents across Silane Diamines/Dithiols and Alkane Diamine/Dithiols

Table C.1: Contact resistances calculated from experiment and obtained from NEGF/DFT and MECS results for alkane dithiols and diamines.

End group	Reference		$R_C(k\Omega)$
Amine	ref [1]	HC†	350
		LC	4000
	ref [2]		430
	MECS (ref [3])		140
	NEGF/DFT (this work ref [4])		180
Thiol	ref [1]	HC	20
		LC	59
	ref [5]		72
	ref [6]	HC	27
		MC	160
		LC	12000
	ref [7]		10
	MECS (ref [8])		140

† For experimental data with multiple peaks in the conductance histogram, the peaks are separated as HC for high conductance, MC for medium conductance, and LC for low conductance.
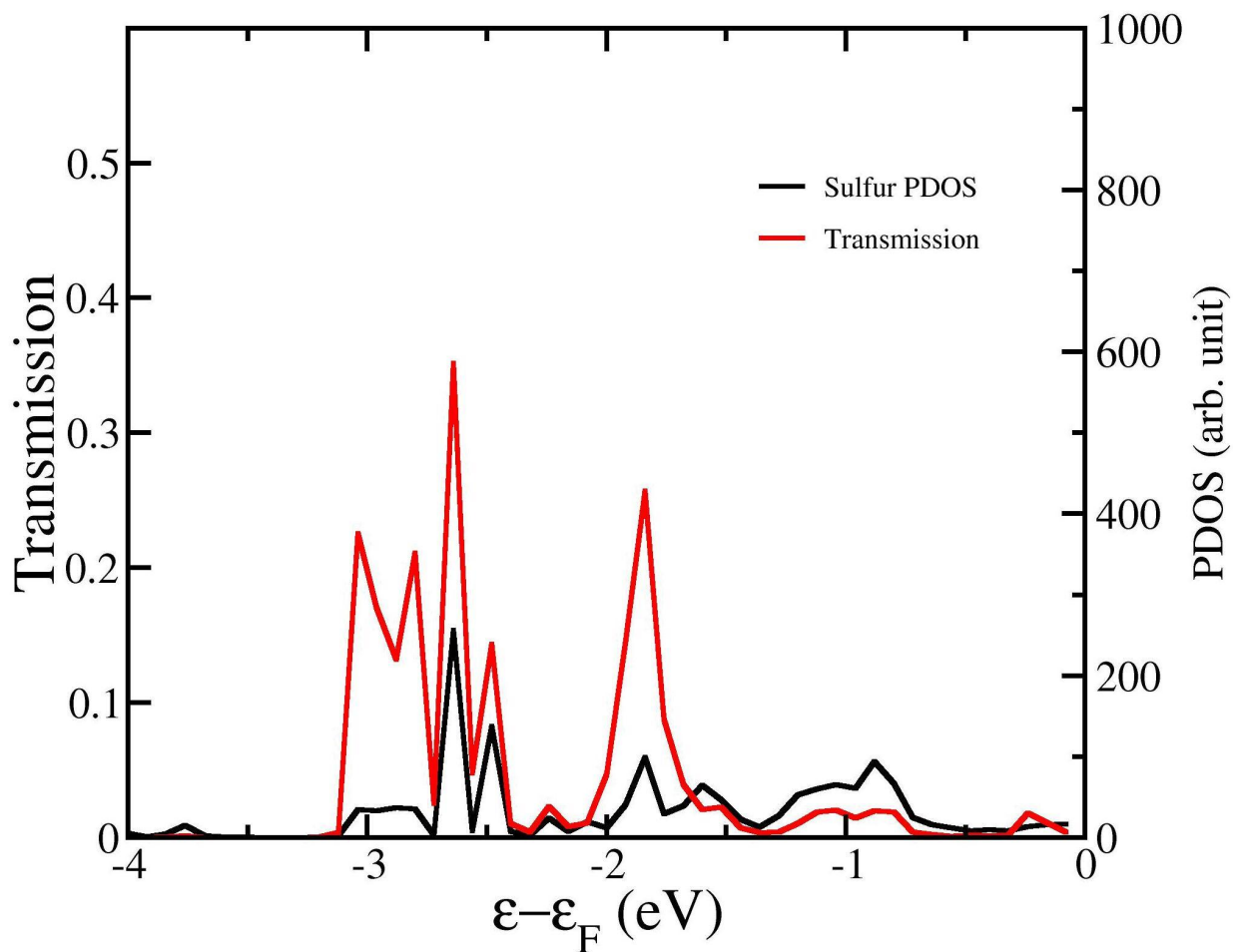
Figure C.1: Transmission and partial density of states (PDOS) projected on a
sulfur atom in the hexanedithiol junction versus energy shifted by
the Fermi energy. The lineup of the PDOS peak with the HOMO
transmission peak near -1.8 eV demonstrates the non-negligible con-
tribution of the sulfur to the molecular HOMO which could affect the
accuracy of the complex band structure calculations for the alkane
dithiol structures.

References

[1] F. Chen, X. Li, J. Hihath, Z. Huang, and N. Tao, "Effect of Anchoring Groups on Single-Molecule Conductance: Comparative Study of Thiol-, Amine-, and Carboxylic-Acid-Terminated Molecules," *Journal of the American Chemical Society*, vol. 128, pp. 15874–15881, Dec. 2006.

[2] L. Venkataraman, J. E. Klare, C. Nuckolls, M. S. Hybertsen, and M. L. Steigerwald, "Dependence of single-molecule junction conductance on molecular conformation," *Nature*, vol. 442, pp. 904–907, Aug. 2006.

[3] G. Fagas and J. C. Greer, "Tunnelling in alkanes anchored to gold electrodes via amine end groups," *Nanotechnology*, vol. 18, no. 42, p. 424010, 2007.

[4] S. McDermott, C. B. George, G. Fagas, J. C. Greer, and M. A. Ratner, "Tunnel currents across silane diamines/dithiols and alkane diamines/dithiols: A comparative computational study," *The Journal of Physical Chemistry C*, vol. 113, no. 2, pp. 744–750, 2008.

[5] S.-Y. Jang, P. Reddy, A. Majumdar, and R. A. Segalman, "Interpretation of stochastic events in single molecule conductance measurements," *Nano letters*, vol. 6, no. 10, pp. 2362–2367, 2006.

[6] C. Li, I. Pobelov, T. Wandlowski, A. Bagrets, A. Arnold, and F. Evers, "Charge transport in single Au| alkanedithiol| Au junctions: coordination

geometries and conformational degrees of freedom," *Journal of the American Chemical Society*, vol. 130, no. 1, pp. 318–326, 2008.

[7] B. Xu and N. J. Tao, "Measurement of single-molecule resistance by repeated formation of molecular junctions," *Science*, vol. 301, no. 5637, pp. 1221–1223, 2003.

[8] G. Fagas, P. Delaney, and J. C. Greer, "Independent particle descriptions of tunneling using the many-body quantum transport approach," *Physical Review B*, vol. 73, no. 24, p. 241314, 2006.

Appendix D

Supporting information: Electronegativity and Electron Currents in Molecular Tunnel Junctions

D. Supporting information:
Electronegativity and Electron
Currents in Molecular Tunnel
Junctions

*D.1 ONE-ELECTRON REDUCED
DENSITY MATRIX AND GREEN'S
FUNCTION*

D.1 ONE-ELECTRON REDUCED DENSITY MATRIX AND GREEN'S FUNCTION

Electron currents may be calculated from the one-electron reduced density matrix [1, 2, 3] as

$$J(r) = \frac{1}{2i}[\nabla_r - \nabla'_r]\rho(r,r')|_{r=r'} \tag{D.1}$$

with J the current density, r a position vector, and ρ the one-electron reduced density matrix (RDM); atomic units are implied unless otherwise given. As the current density operator is a one-body differential operator, to obtain accurate predictions for electron currents it is necessary to obtain accurate predictions of the RDM; the error in calculating currents with an approximate RDM has recently been explored [4]. From another viewpoint, calculation of the current can also proceed through computation of the one electron retarded and advanced Green's functions $G_{r,a}$ and application of a Landauer-type formula [5, 6]:

$$I = \frac{1}{\pi}d\omega[f_L(\omega;\mu_L) - f_R(\omega;\mu_R)]Tr[\Gamma_L(\omega)G_a(\omega)\Gamma_R(\omega)\Lambda G_r(\omega) \tag{D.2}$$

with electron energy ω, $\Gamma_{L,R}$ spectral densities, $f_{L,R}$ energy distributions with $\mu_{L,R}$chemical potentials in the left (L) and right (R) electron reservoirs, and Λ is the correction due to correlations weighted by the spectral density of the electrodes and electron-electron spectral density on the molecule. The causal Green's function is related to the RDM via the relation

$$\rho(r,r) = \frac{1}{2\pi i}\oint d\omega G(r,r';\omega), \tag{D.3}$$

with the complex integration performed along the Coulson contour. We begin by pointing out that the reduced density matrix obtained from a many-electron wavefunction corrected to second order in electron correlation is equivalent to the

D. Supporting information:
Electronegativity and Electron
Currents in Molecular Tunnel
Junctions

*D.1 ONE-ELECTRON REDUCED
DENSITY MATRIX AND GREEN'S
FUNCTION*

reduced density matrix arising from correcting IPs and EAs in the Green's function to second order in the electron self-energy [7]. To proceed, the energy operator for a molecule within a tunnel junction is written in the form

$$\hat{H}(\lambda) = \int dr\hat{\psi}^\dagger(r)h(r)\hat{\psi}(r) + \int drdr'\hat{\psi}^\dagger(r)v_{HF}(r,r')\hat{\psi}(r') +$$
$$\lambda[\frac{1}{2}\int drdr'\hat{\psi}^\dagger(r)\hat{\psi}(r')v(r,r')\hat{\psi}^\dagger(r')\hat{\psi}(r) - \int drdr'\hat{\psi}^\dagger(r)v_{HF}(r,r')\hat{\psi}(r')]$$

(D.4)

with v the electron-electron interaction on the molecular region, v_{HF} the Hartree-Fock potential and $\hat{\psi}^\dagger, \hat{\psi}$ are second quantized electron field operators. It is assumed that the Fock equations have been solved with electrode self-energies $\Sigma^{L,R}$ to describe the interaction between the molecular region electrons and electrons in the reservoirs; external potentials are also included in the Fock operator. For $\lambda = 0$, the Hamiltonian reduces to the Fock operator

$$\hat{H}(0) = \hat{F} = \sum_p \epsilon_p \hat{a}_p^\dagger \hat{a}_p$$

(D.5)

with $\hat{a}^\dagger, \hat{a}$ creation and annihilation operators for Hartree-Fock states. For $\lambda = 1$, the many-electron Hamiltonian is restored. A perturbation expansion in λ is written for the many-electron wavefunction:

$$|\Psi\rangle = |\Psi^{(0)}\rangle + \lambda|\Psi^{(1)}\rangle + \lambda^2|\Psi^{(2)}\rangle + ...$$

(D.6)

For our choice of 0th order approximation, Brillouin's theorem insures that the first order wavefunction consists of only double electron excitations, on the other hand the second order term includes single through quadruple excitations. From

$$\rho(r,r') = \langle\Psi|\hat{\psi}^\dagger(r')^\dagger\hat{\psi}(r)|\Psi\rangle$$

(D.7)

D. Supporting information:
Electronegativity and Electron
Currents in Molecular Tunnel
Junctions

*D.1 ONE-ELECTRON REDUCED
DENSITY MATRIX AND GREEN'S
FUNCTION*

to first order in λ the correction to the 0th order density matrix vanishes [8]. The density matrix to second order is

$$\rho \approx \rho^{(0)} + \lambda^2 \rho^{(2)}. \tag{D.8}$$

The RDM may be represented as an infinite expansion over single-electron states ϕ

$$\rho(r,r') = \sum_{pq} \rho_{pq} \phi_q^*(r') \phi_p(r). \tag{D.9}$$

Explicit calculation of the density matrix coefficients from eq. D.6 through second order in λ yields

$$\rho_{ij} = \delta_{ij} - \frac{1}{2} \sum_{abk} \frac{<ab||ik><jk||ab>}{(\epsilon_i + \epsilon_k - \epsilon_a - \epsilon_b)(\epsilon_j + \epsilon_k - \epsilon_a - \epsilon_b)} \tag{D.10}$$

$$\rho_{ab} = \frac{1}{2} \sum_{ijc} \frac{<ij||ac><bc||ij>}{(\epsilon_i + \epsilon_j - \epsilon_c - \epsilon_a)(\epsilon_i + \epsilon_j - \epsilon_c - \epsilon_b)} \tag{D.11}$$

$$\rho_{ia} = \frac{1}{2} \sum_{abj} \frac{<ab||ij><aj||ab>}{(\epsilon_i - \epsilon_a)(\epsilon_i + \epsilon_j - \epsilon_a - \epsilon_b)} - \frac{1}{2} \sum_{ijb} \frac{<ij||ib><ab||ij>}{(\epsilon_i - \epsilon_a)(\epsilon_i + \epsilon_j - \epsilon_a - \epsilon_b)} \tag{D.12}$$

with $\langle pq||rs \rangle = \langle pq|v|rs \rangle - \langle pq|v|sr \rangle$. We use the convention whereby indices $i, j, k, ...$ label occupied, $a, b, c, ...$ label unoccupied, and $p, q, r, ...$ are used to label general (occupied or unoccupied) states in $|\Psi^{(0)}\rangle$.

Transmission resonances are given through the poles of the Green's functions and can be identified as IPs and EAs. It is known that introduction of correlation corrections beyond independent particle models for the Green's function improves the prediction of IPs and EAs. Hence, it is reasonable to assume that if an independent particle picture is chosen to optimize IPs and EAs, it follows that prediction of currents from the NEGF approach will be improved. In this context, a model for transport is measured in terms of reproducing the molecular electronegativity.

D. Supporting information:
Electronegativity and Electron
Currents in Molecular Tunnel
Junctions

D.1 ONE-ELECTRON REDUCED
DENSITY MATRIX AND GREEN'S
FUNCTION

The Green's function with second order self-energies has been studied by Pickup and Goscinski [7] leading to the following approximation

$$
\begin{aligned}
[G^{(2)}\omega]_{pq}^{-1} =& [G^{(0)}\omega]_{pq}^{-1} + \Sigma^{(2)}(\omega)_{pq} \\
=& (\omega - \epsilon_p)\delta_{pq} - \frac{1}{2}\sum_{iab}\frac{<ab||pi><qi||ab>}{\omega + \epsilon_i - \epsilon_a - \epsilon_b} - \frac{1}{2}\sum_{ija}\frac{<ij||pa><qa||ij>}{\omega + \epsilon_a - \epsilon_i - \epsilon_j}
\end{aligned}
\tag{D.13}
$$

The lowest order improvement to Koopmans' IPs and EAs are obtained from the poles of the diagonal elements of $G(\omega)$. It is found the self-energy corrects Koopmans' IP ϵ_i through terms describing orbital relaxation and pair correlations; a similar interpretation holds for corrections to the EAs [7]. Within this approximation, it is also possible to determine the density matrix directly from eq. D.3 ; the resulting density matrix coincides exactly with the density matrix calculated from eq. D.6 through $O(\lambda^2)$. Hence calculating the density matrix through second order in electron correlation and correcting IPs and EAs with second order self-energies $\Sigma^{(2)}$ will lead to the same predictions for electron current. For moderate electron correlations, improving spectra for independent particle models or explicitly including correlations in the RDM are equivalent.

A criterion for selecting an independent particle model for quantum electronic transport was given as the set of single-particle states yielding an approximate density matrix with maximal overlap to the exact RDM [9]. The single-electron states diagonalizing the RDM are natural orbitals (NOs) [10] and their eigenvalues ρ_i are known as natural occupations. If one asks what is the best finite expansion approximation $\tilde{\rho}$ to the exact RDM

$$
\int |\rho - \tilde{\rho}|^2 dr dr' = min,
\tag{D.14}
$$

it is found that including the first n natural orbitals with the largest occupancies for a truncated expansion eq. D.9 fulfills the least squares condition [8]. We

D. Supporting information:
Electronegativity and Electron
Currents in Molecular Tunnel
Junctions

*D.1 ONE-ELECTRON REDUCED
DENSITY MATRIX AND GREEN'S
FUNCTION*

consider the couplings between density matrix coefficients in eq. D.10 by writing

$$\rho = \begin{bmatrix} \rho_{ij} & \rho_{ia} \\ \rho_{ai} & \rho_{ab} \end{bmatrix} \tag{D.15}$$

with (ij), (ab), and (ia) denoting occupied-occupied, unoccupied-unoccupied, and occupied-unoccupied spaces respectively, with occupations referred to the 0th order wavefunction. The natural orbitals to second order in electron correlation are given by the eigenfunctions of eq. D.15. Constructing the "best" independent particle picture in the sense of eq. D.14 implies occupying a single Slater determinant by the first n e natural orbitals. We have previously shown numerically that a single determinant composed of the largest occupation number NOs can lead to essentially the same results as a full many-body treatment for tunneling through alkanes [9]. For a single determinant approximation, the density matrix is idempotent $\rho^2 = \rho$ which occurs since the first n_e occupations are equal to 1 with all others 0. Hence a measure for the quality of a single determinant approximation is how well the eigenvalues of eq. D.15 approximate the idempotency condition. As the ρ_{ia} couplings between the occupied and unoccupied spaces becomes stronger, the occupations of the $0th$ order states can become significantly less than unity. From many-body theory it is well understood what this condition implies: a single determinant or independent particle picture is no longer useful as a 0th order wavefunction. For weak to moderate correlations, the Green's function approach can achieve improved IPs and EAs by a low order approximation to the electron self-energy. As natural occupancies in the 0th order wavefunction become very much less than unity, a perturbation expansion about an independent particle picture loses meaning and even higher order corrections to $|\psi^{(0)}>$ will not correct IPs and EAs on the molecular region. In a similar context, this is seen as the failing of the GW approximation for systems with multi-determinantal ground states [11] or in strongly correlated electron transport

D. Supporting information:
Electronegativity and Electron
Currents in Molecular Tunnel
Junctions

*D.2 DFT and HF TRANSPORT FOR
HEXATRIENE DITHIOL*

[12, 13, 14]. For strong electron correlations coupled-cluster theory offers a

convenient nonperturbative framework from which higher order approximations to

the density matrix follow [15], alternatively correlated one particle methods

[16, 17] to infinite order can be chosen to yield correct IPs and EAs.

D.2 DFT and HF TRANSPORT FOR HEXATRIENE DITHIOL
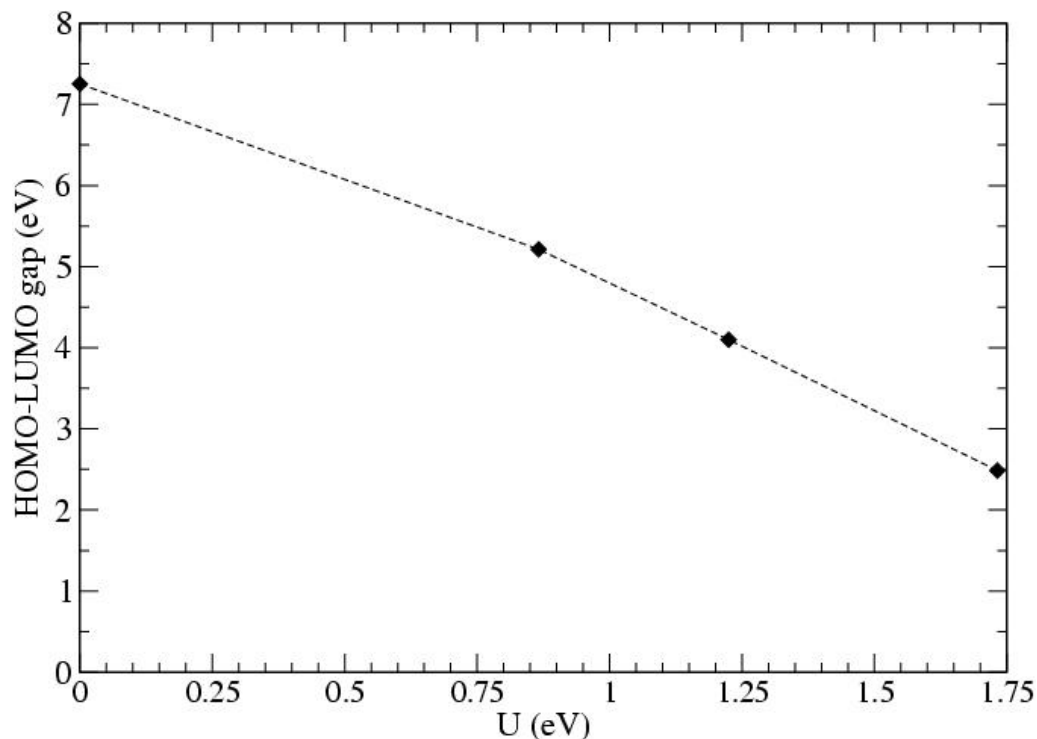
Figure D.1: HOMO-LUMO gap for the tight binding model system as a function
of the electron-electron self energy as varied through the interaction
parameter U. The reduction in the gap demonstrates the effect of
electron-electron self-energy on the molecular electronegativity.

D. Supporting information:
Electronegativity and Electron
Currents in Molecular Tunnel
Junctions

D.2 DFT and HF TRANSPORT FOR
HEXATRIENE DITHIOL

(a)

(b)

D. Supporting information:
Electronegativity and Electron
Currents in Molecular Tunnel
Junctions

D.2 DFT and HF TRANSPORT FOR
HEXATRIENE DITHIOL
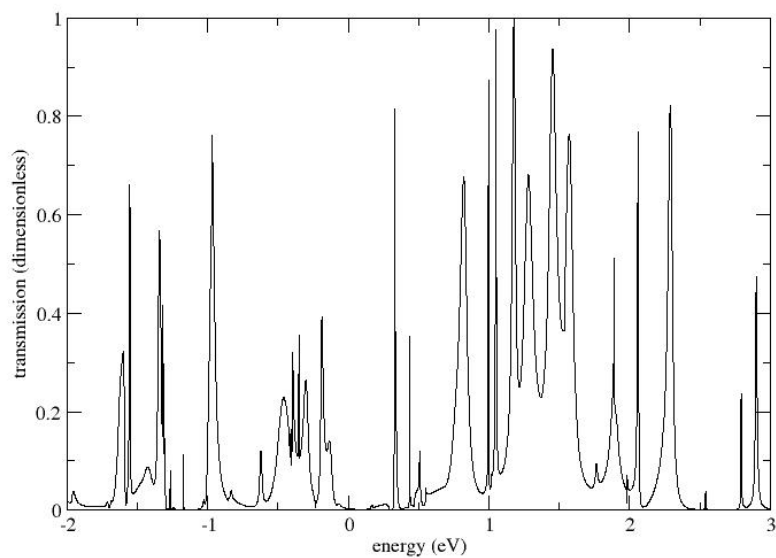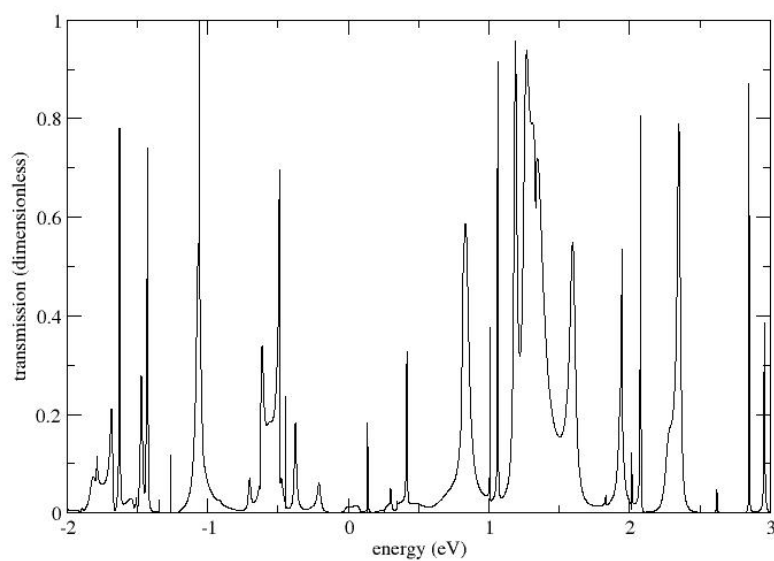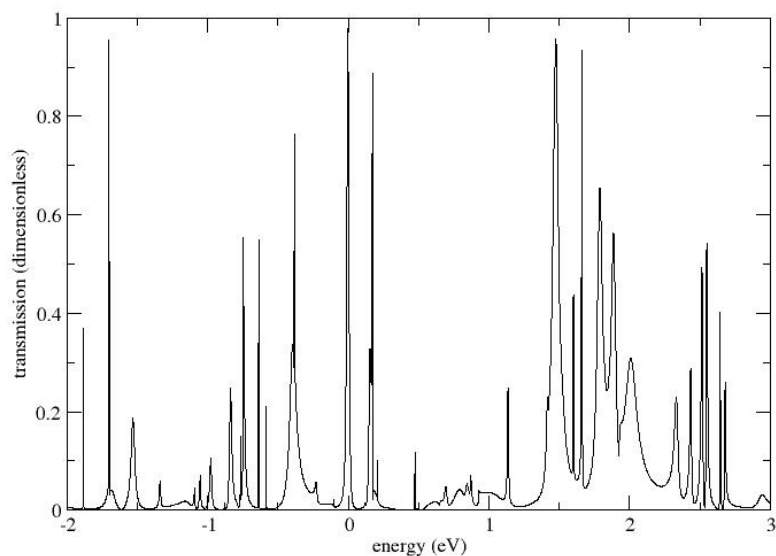
(c)
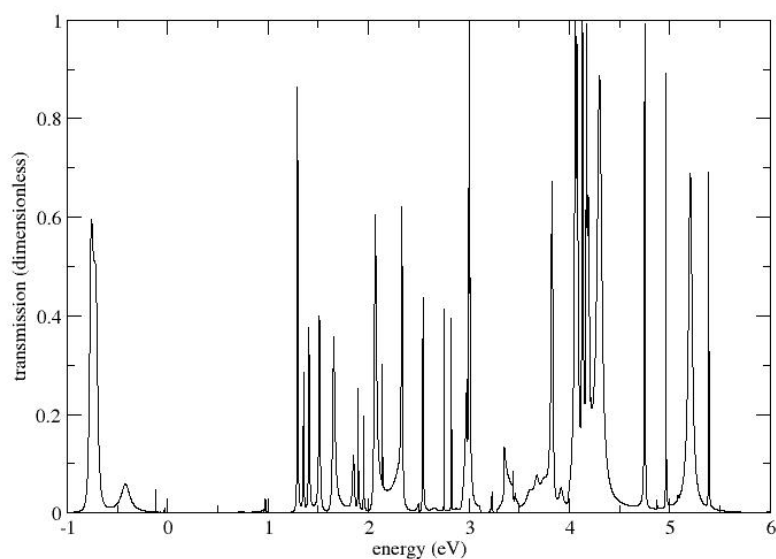
(d)

Figure D.2: Comparison of electron transmission calculated from different electron structure treatments for the hexatriene dithiol molecular junction. Transmission (dimensionless) is plotted versus energy in electron volts, E_F denotes the Fermi energy and is taken to be the energy of the highest occupied state in the left lead (a) DFT/LDA, $E_F = -1.85eV$ (b) DFT/GGA, $E_F = -2.08eV$ (c) DFT/hybrid, $E_F = -1.87eV$ (d) Hartree-Fock, $E_F = -1.57eV$

D. Supporting information:
Electronegativity and Electron
Currents in Molecular Tunnel
Junctions

D.2 DFT and HF TRANSPORT FOR
HEXATRIENE DITHIOL

References

[1] W. R. Frensley, "Boundary conditions for open quantum systems driven far from equilibrium," *Reviews of Modern Physics*, vol. 62, pp. 745–791, July 1990.

[2] P. Delaney and J. C. Greer, "Correlated Electron Transport in Molecular Electronics," *Physical Review Letters*, vol. 93, p. 036805, July 2004.

[3] P. Delaney and J. C. Greer, "Quantum electronic transport in a configuration interaction basis," *International Journal of Quantum Chemistry*, vol. 100, pp. 1163–1169, Dec. 2004.

[4] J. C. Greer, "Electronic current density expanded in natural orbitals," *Molecular Physics*, vol. 106, pp. 1363–1367, June 2008.

[5] Y. Meir and N. S. Wingreen, "Landauer formula for the current through an interacting electron region," *Physical Review Letters*, vol. 68, pp. 2512–2515, Apr. 1992.

[6] A. Ferretti, A. Calzolari, R. Di Felice, and F. Manghi, "First-principles theoretical description of electronic transport including electron-electron correlation," *Physical Review B*, vol. 72, no. 12, p. 125114, 2005.

[7] B. T. Pickup and O. Goscinski, "Direct calculation of ionization energies: I. Closed shells† Supported by the Swedish Natural Sciences Research Council.," *Molecular Physics*, vol. 26, no. 4, pp. 1013–1035, 1973.

[8] E. R. Davidson, "Properties and uses of natural orbitals," *Reviews of Modern Physics*, vol. 44, no. 3, p. 451, 1972.

[9] G. Fagas, P. Delaney, and J. C. Greer, "Independent particle descriptions of tunneling using the many-body quantum transport approach," *Physical Review B*, vol. 73, no. 24, p. 241314, 2006. Note the condition for a single particle theory to have maximal overlap to the exact reduced density matrix for 2 electron systems is the same as requiring a single determinant to have maximum overlap to the exact wavefunction. The determinant maximizing the overlap $\langle \Psi_B | \Psi \rangle$ for any number of electrons is the Brueckner determinant. For many-electron systems, the density matrix obtained from the Brueckner determinant provides a good approximation to the exact RDM; see refs. [16, 17].

[10] P.-O. Löwdin, "Quantum theory of many-particle systems. I. Physical interpretations by means of density matrices, natural spin-orbitals, and convergence problems in the method of configurational interaction," *Physical Review*, vol. 97, no. 6, p. 1474, 1955.

[11] Y. Pavlyukh and W. Hübner, "Configuration interaction approach for the computation of the electronic self-energy," *Physical Review B*, vol. 75, no. 20, p. 205129, 2007.

[12] P. Darancet, A. Ferretti, D. Mayou, and V. Olevano, "Ab initio G W electron-electron interaction effects in quantum transport," *Physical Review B*, vol. 75, no. 7, p. 075102, 2007.

[13] K. S. Thygesen and A. Rubio, *Nonequilibrium GW approach to quantum transport in nano-scale contacts.* AIP, 2007.

[14] X. Wang, C. D. Spataru, M. S. Hybertsen, and A. J. Millis, "Electronic correlation in nanoscale junctions: Comparison of the GW approximation to a

numerically exact solution of the single-impurity Anderson model," *Physical Review B*, vol. 77, no. 4, p. 045119, 2008.

[15] R. J. Bartlett, I. Grabowski, S. Hirata, and S. Ivanov, "The exchange-correlation potential in ab initio density functional theory," *The Journal of chemical physics*, vol. 122, no. 3, p. 034104, 2005.

[16] A. Beste and R. J. Bartlett, "Independent particle theory with electron correlation," *The Journal of chemical physics*, vol. 120, no. 18, pp. 8395–8404, 2004.

[17] A. Beste and R. J. Bartlett, "Correlated one-particle method: Numerical results," *The Journal of chemical physics*, vol. 123, no. 15, p. 154103, 2005.

Appendix E

Computational Contribution

In this chapter we discuss the code developed during the course of this PHD.

E.1   Atomic orbital extraction and partition

The code takes a system from a TURBOMOLE calculation in the molecular orbital basis and transforms it into an atomic orbital basis. In addition it can partition the system into different components such as the leads and the device region necessary to describe semi-infinite systems. This code was the primary contribution to chapter 4 where it facilitated the necessary partition and localisation in the atomic orbital basis of the electronic structure of hexetrienedithiol required for NEGF transport.

```fortran
program fock_calc
IMPLICIT NONE

integer :: i,j,k,size,mov,sumof,no_unitcell
integer :: info,ldz,Devicesize,contactsize,principalsize
double precision ,allocatable :: fock(:,:),cmat(:,:),overlap(:,:),energy(:,:)
double precision ,allocatable :: RCONDE(:),RCONDV(:),WORK(:),comp_e(:),comp_c1(:),comp_c2(:),VL
    (:,:),VR(:,:),Lscale(:),Rscale(:)
double precision :: switch,ab,bb
Integer ,allocatable :: Iwork(:)
Logical ,allocatable :: Bwork(:)
Integer :: ilo,ihi,Lwork

character (len=80) ::line  ,rubbish

open(unit = 1,  File = 'Device.txt',status = 'replace')
open(unit = 2,  File = 'Deviceoverlap.txt',status = 'replace')

open(unit = 3,  File = "contactleft.txt",status = 'replace')
open(unit = 4,  File = "Scontactleft.txt",status = 'replace')
open(unit = 30, File = "contactright.txt",status = 'replace')
open(unit = 7,  File = "Scontactright.txt",status = 'replace')

open(unit = 8,  File = "Wireleft.txt",status = 'replace')
open(unit = 9,  File = "Sleft.txt",status = 'replace')
open(unit = 10, File = "Wireright.txt",status = 'replace')
open(unit = 11, File = "Sright.txt",status = 'replace')

open(unit = 12, File = "Devicecontactleft.txt",status = 'replace')
open(unit = 13, File = "SDevicecontactleft.txt",status = 'replace')
open(unit = 14, File = "Devicecontactright.txt",status = 'replace')
open(unit = 15, File = "SDevicecontactright.txt",status = 'replace')

open(unit = 16, File = "contactleftwireleft.txt",status = 'replace')
open(unit = 17, File = "Scontactleftwireleft.txt",status = 'replace')
```

```fortran
open(unit = 18, File = "contactrightwireRight.txt",status = 'replace')
open(unit = 19, File = "ScontactrightwireRight.txt",status = 'replace')


open(unit = 20, file = 'Fockout.txt',status = 'replace')
open(unit = 21, file = 'soverlap.txt', status = 'old')
open(unit = 22, file = "extraval.txt",status = 'replace')
open(unit = 23, file = 'mos', status = 'old')
open(unit = 24, file = "devicemos.txt",status = 'replace')
open(unit = 25, file = "energyvals.txt",status = 'replace')
open(unit = 26, file = "overextraval.txt",status = 'replace')
open(unit = 27, file = "Dataconst.txt",status = 'replace')
open(unit = 28, file = "H0f.txt",status = 'replace')
open(unit = 29, file = "H1f.txt",status = 'replace')
open(unit = 31, file = "S0f.txt",status = 'replace')
open(unit = 32, file = "S1f.txt",status = 'replace')
open(unit = 33, file = "molecs.txt",status = 'replace')
open(unit = 34, file = "overlapvals.txt",status = 'replace')


do while (rubbish(3:5).ne.'SCF')            ! start a loop to find the line where scf is stated in
      the mos file
read(23,fmt = '(a30)') rubbish              !  first data line is two lines below.
end do
read(23,fmt = '(a30)')                       !skipping line
read(23,fmt = '(a26,d20.14,a9,I9)') rubbish , switch , rubbish , size  !read in first energy
    eigenvalue as switch and matrix size as size

                                                        ! while ignoring other text
Print *  , 'a'
allocate(fock(1,sumof(size)),overlap(size,size))    ! allocate fock matrix to be an array of the
      size necassary to read in the triangular overlap Matrix


do while (rubbish(13:24).ne.'OVERLAP(CAO)')        ! start a loop to find the line where overlap(
      cao) is stated in the soverlap.txt file
Read(21,fmt='(a30)') rubbish                             ! Matrix values start two lines below.
end do
read(21,fmt='(a30)')                              !skipping line
print *  , ' b'
i = 0
do while (i.lt.(sumof(size)))                    !start loop which reads in overlap values max 3
      per line and terminates when finished
if ((sumof(size) - i) .lt.3) then               ! If less then 3 elements left to read then only
      read in required amount
line = Achar((48+(sumof(size)-i)))
line(2:)='(d26.14)'
read(21, fmt=line) (fock(1,j),j = i+1,sumof(size))
Print *  , (fock(1,j), j =i+1,sumof(size))
else
read(21, fmt='(3d26.14)') (fock(1,j),j = i+1,i+3) !if more then 3 elements left to read then raed
      in a max of 3
Print *  , (fock(1,j),j = i+1,i+3)
end if
i = i + 3                                        !if more then 3 elements left loop will continue
      else loop will terminate as all values have been read
end do
print *  , 'c'
overlap(1,1)=fock(1,1)                            ! transfering initial balue from fock array to overlap
      Matrix
do j = 2 , size                                 !loop fills in upper triangle of overlap matrix
```

```fortran
do i = 1 , j
overlap(i,j) = fock(1,(sumof(j-1)+i))
end do
end do

do j = 2 , size                    !loop mirrors upper triangle onto lower triangl as overlap is
     symmetric
do i = 1 , (j-1)
overlap(j,i)=overlap(i,j)
end do
end do
print * , ' d'
Lwork = 2*size*size+12*size+16
Deallocate (Fock)                  !Deallocating Fock
allocate(fock(size,size),energy(size,size),cmat(size,size),comp_e(size),comp_c1(size),comp_c2(
     size),VL(size,size),VR(size,size)) !allocating values
allocate (Lscale(size),Rscale(size),RCONDE(size),RCONDV(size),WORK(Lwork))
allocate (Iwork((size+6)),Bwork(size))

energy(1,1) = switch !  setting the initial energy value already read in

do i = 1,size      ! this loop reads in the eigen vectors and energy eigen values
j=0
do while( j .lt. size)             ! read
if ((size - j) .ge. 4) then
mov = 4
else
mov = (size - j)
end if


line='( d20.14)'
line(2:2)= Achar((48+mov))
write(*,*) "line",line
write(*,*) "j",j
Read(unit = 23,FMT = line) (cmat(k,i),k=(j+1),(j+mov))
write(*,*) (cmat(k,i),k=j+1,(j+mov))

j = j + mov
end do

if (i .ne. size) then
read(23,fmt ='(a26,d20.14,a26)') rubbish,energy(i+1,i+1),rubbish
end if
end do
Print * , 'overlap '
Print * , overlap
print * , 'cmat '
Print * , cmat

fock = matmul(overlap,cmat)
fock = matmul(fock,energy)
fock = matmul(fock,transpose(cmat))
fock = matmul(fock,overlap)
Print * , "fock"
Print * , fock
```

```fortran
do i=1,size
do j=1,size
write(unit = 20 , FMT = '(d20.14)') fock(i,j)
write(unit = 33 , FMT = '(d20.14)') cmat(i,j)
write(unit = 34 , FMT = '(d20.14)') overlap(i,j)
end do
end do

do j=1,size
write(unit = 25 , FMT = '(d20.14)') energy(j,j)
end do

Print *, " input Device size :"
read(*,*) j
Devicesize = j
Print *," eh "

Print *, " input Contact size :"
read(*,*) j
contactsize = j
Print *," eh "

Print *, " input Principal size :"
read(*,*) j
principalsize = j
Print *," eh "

no_unitcell = (size - Devicesize - contactsize*2)/(2*principalsize)

write(unit = 27 , FMT = '(I10,I10,I10)') Devicesize,contactsize,principalsize,size
write(unit = 6 , FMT = '(I10,I10,I10)') Devicesize,contactsize,principalsize,size

write(unit = 6 , FMT = '(I10)') Devicesize
write(unit = 6 , FMT = '(I10)') contactsize
write(unit = 6 , FMT = '(I10)') principalsize
write(unit = 6 , FMT = '(I10)') size

!device fock being written
DO j = 1 , (Devicesize)
DO k = 1 , (Devicesize)
write (1,fmt = '(d20.14)') Fock(k,j)
write (2,fmt = '(d20.14)') overlap(k,j)
write (24,fmt = '(d20.14)')cmat(k,j)
end do
end do

!left contact
DO j = Devicesize+1, (Devicesize+contactsize)
DO k = Devicesize+1 , (Devicesize+contactsize)
write (3,fmt = '(d20.14)') Fock(k,j)
write (4,fmt = '(d20.14)') overlap(k,j)
end do
end do

!right contact
DO j = (1+(contactsize+Devicesize)), (2*contactsize+Devicesize)
DO k = (1+(contactsize+Devicesize)), (2*contactsize+Devicesize)
```

```fortran
write (30,fmt = '(d20.14)') Fock(k,j)
write (7,fmt = '(d20.14)') overlap(k,j)
end do
end do

!right principal layer
DO j = (2*contactsize+Devicesize)+1,(2*contactsize+Devicesize+principalsize)
DO k = (2*contactsize+Devicesize)+1,(2*contactsize+Devicesize+principalsize)
write (10,fmt = '(d20.14)') Fock(k,j)
write (11 ,fmt = '(d20.14)') overlap(k,j)
end do
end do

!left principal layer
DO j = (2*contactsize+Devicesize+no_unitcell*principalsize)+1,(2*contactsize+Devicesize+(
       no_unitcell+1)*principalsize)
DO k = (2*contactsize+Devicesize+no_unitcell*principalsize)+1,(2*contactsize+Devicesize+(
       no_unitcell+1)*principalsize)
write (8 ,fmt = '(d20.14)') Fock(k,j)
write (9 ,fmt = '(d20.14)') overlap(k,j)
end do
end do

write (6,*)" device left contact interaction"
DO j = Devicesize+1,(Devicesize+contactsize)
DO k =  1,Devicesize
write (12,fmt = '(d20.14)') Fock(k,j)
write (13,fmt = '(d20.14)') overlap(k,j)
end do
end do

write (6,*)" device right contact interaction"
DO j =  (1+(contactsize+Devicesize)), (2*contactsize+Devicesize)
DO k =  1,Devicesize
write (14,fmt = '(d20.14)') Fock(k,j)
write (15,fmt = '(d20.14)') overlap(k,j)
end do
end do

write (6,*)"right principal contact interaction"
Do j  =(2*contactsize+Devicesize)+1,(2*contactsize+Devicesize+principalsize)
DO k =  (1+(contactsize+Devicesize)), (2*contactsize+Devicesize)
write (18,fmt = '(d20.14)') Fock(k,j)
write (19,fmt = '(d20.14)') overlap(k,j)
end do
end do

write (6,*)"left principal contact interaction"
DO j = (2*contactsize+Devicesize+no_unitcell*principalsize)+1,(2*contactsize+Devicesize+(
       no_unitcell+1)*principalsize)
DO k =  1 + Devicesize , contactsize+Devicesize
write (16,fmt = '(d20.14)') Fock(k,j)
write (17,fmt = '(d20.14)') overlap(k,j)
end do
end do

!extravals
```

```fortran
write (22,*)"device extravals"
write (26,*)"device extravals"
DO j = (Devicesize+contactsize+1),size
DO k = 1,Devicesize
write (22,fmt = '(d20.14)') Fock(k,j)
write (26,fmt = '(d20.14)') overlap(k,j)
end do
end do


write (22,*)"right contact extravals"
write (26,*)"right contact extravals"
DO j = (Devicesize+2*contactsize+Principalsize+1),size
DO k = 1+devicesize + contactsize ,(Devicesize+2*contactsize)
write (22,fmt = '(d20.14)') Fock(k,j)
write (26,fmt = '(d20.14)') overlap(k,j)
end do
end do


write (22,*)"left contact extraval"
write (26,*)"left contact extraval"
DO j = (Devicesize+2*contactsize+(no_unitcell+1)*principalsize+1),size
DO k = devicesize+1,devicesize+contactsize
write (22,fmt = '(d20.14)') Fock(k,j)
write (26,fmt = '(d20.14)') overlap(k,j)
end do
end do


if(no_unitcell.ge.2) then

DO j = (Devicesize+2*contactsize+1),(Devicesize+2*contactsize+(no_unitcell)*principalsize)
DO k = devicesize+1,devicesize+contactsize
write (22,fmt = '(d20.14)') Fock(k,j)
write (26,fmt = '(d20.14)') overlap(k,j)
end do
end do


DO j = (Devicesize+2*contactsize+principalsize+1), (Devicesize+2*contactsize+2*principalsize)
DO k = (Devicesize+2*contactsize+principalsize+1), (Devicesize+2*contactsize+2*principalsize)
write (28,fmt = '(d20.14)') Fock(k,j)
write (31,fmt = '(d20.14)') overlap(k,j)
end do
end do


DO j = (Devicesize+2*contactsize+(no_unitcell+1)*principalsize+1),(Devicesize+2*contactsize+(
    no_unitcell+2)*principalsize)
DO k = (Devicesize+2*contactsize+(no_unitcell+1)*principalsize+1),(Devicesize+2*contactsize+(
    no_unitcell+2)*principalsize)
write (28,fmt = '(d20.14)') Fock(k,j)
write (31,fmt = '(d20.14)') overlap(k,j)
end do
end do


DO j = (Devicesize+2*contactsize+principalsize+1), (Devicesize+2*contactsize+2*principalsize)
DO k = 1+devicesize + 2*contactsize ,(Devicesize+2*contactsize+principalsize)
```

```fortran
write  (29,fmt = '(d20.14)') Fock(k,j)
write  (32,fmt = '(d20.14)') overlap(k,j)
end do
end do


DO j = (Devicesize+2*contactsize+(no_unitcell+1)*principalsize+1),(Devicesize+2*contactsize+(
      no_unitcell+2)*principalsize)
DO k = (Devicesize+2*contactsize+no_unitcell*principalsize+1),(Devicesize+2*contactsize+(
      no_unitcell+1)*principalsize)
write  (29,fmt = '(d20.14)') Fock(k,j)
write  (32,fmt = '(d20.14)') overlap(k,j)
end do
end do
end if


if(no_unitcell.ge.3) then
write  (22,*)"right principal extraval"
write  (26,*)"right principal extraval"
DO j = (Devicesize+2*contactsize+2*principalsize+1),size
DO k = 1+devicesize + 2*contactsize ,(Devicesize+2*contactsize+principalsize)
write  (22,fmt = '(d20.14)') Fock(k,j)
write  (26,fmt = '(d20.14)') overlap(k,j)
end do
end do


write  (22,*)"left principal extraval"
write  (26,*)"left principal extraval"
DO j = (Devicesize+2*contactsize+(no_unitcell+2)*principalsize+1),size
DO k = (Devicesize+2*contactsize+no_unitcell*principalsize+1),(Devicesize+2*contactsize+(
      no_unitcell+1)*principalsize)
write  (22,fmt = '(d20.14)') Fock(k,j)
write  (26,fmt = '(d20.14)') overlap(k,j)
end do
end do


DO j = Devicesize+2*contactsize+1  ,Devicesize+2*contactsize+(no_unitcell)*principalsize
DO k = (Devicesize+2*contactsize+no_unitcell*principalsize+1),(Devicesize+2*contactsize+(
      no_unitcell+1)*principalsize)
write  (22,fmt = '(d20.14)') Fock(k,j)
write  (26,fmt = '(d20.14)') overlap(k,j)
end do
end do


end if

close(1,status =  'keep')
close(2,status =  'keep')
close(3,status =  'keep')
close(4,status =  'keep')
close(30,status =  'keep')
close(7,status =  'keep')
close(8,status =  'keep')
close(9,status =  'keep')
close(10,status = 'keep')
close(11,status = 'keep')
close(12,status = 'keep')
```

```fortran
close(13,status = 'keep')
close(14,status = 'keep')
close(15,status = 'keep')
close(16,status = 'keep')
close(17,status = 'keep')
close(18,status = 'keep')
close(19,status = 'keep')
close(20,status = 'keep')
close(21,status = 'keep')
close(22,status = 'keep')
close(23,status = 'keep')
close(24,status = 'keep')
close(25,status = 'keep')
close(26,status = 'keep')
close(27,status = 'keep')
close(28,status = 'keep')
close(29,status = 'keep')
close(26,status = 'keep')
close(31,status = 'keep')
close(32,status = 'keep')
close(33,status = 'keep')
close(34,status = 'keep')


Call DGGEVX( 'N','V','V','B',size ,fock ,size ,overlap ,size ,comp_c1 ,comp_c2 ,comp_e ,VL,size ,VR,size ,
     ilo ,ihi ,Lscale ,Rscale ,ab ,bb ,Rconde ,Rcondv ,work ,Lwork ,iwork ,bwork ,info )

Print * , "cmat"
print * , (cmat)
Print * , "VL"
Print * , VL
Print * , "VR"
Print * , VR


Print * , "Energy"
print * , (energy)
comp_c2 = (comp_c1/comp_e)
Print * , "En_func"
Print * , comp_c2



end program fock_calc

integer function sumof(I)
IMPLICIT NONE
Integer :: I,j
sumof = I*(I+1)/2
end function sumof
```

E.2 Preliminary work on CAPS in atomic and molecular basis

The preliminary coding on CAPs continued from earlier work on CAPs involving a model system [1]. Building upon this model the overlap matrix was incorporated to initially describe systems in the local atomic orbital basis (so real systems can be described) using the output from a TURBOMOLE program. This code utilses the local atomic Hamiltonian and its interaction with the leads to calculate the self-energy. It subsequently determines the CAPs in a molecular orbital basis and the resulting transmission across the junction with both the CAPs and self-energy.

```fortran
module accuracy
IMPLICIT NONE
integer , parameter :: prec = selected_real_kind (P=15,R=307)
end module accuracy

program selfenergy
use accuracy
IMPLICIT NONE


Real (kind=Prec),External :: Icon
integer :: i,j,k,l,t,size,mov,no_unitcell
integer :: Devicesize,contactsize,principalsize
real (kind=prec) :: lambda,prev,threshold,thresh,minval,S0,S1,H0,H1,funkyn,last
real (kind=prec) ,allocatable :: PR(:,:),SPR(:,:),PL(:,:),SPL(:,:),energy(:,:)
real (kind=prec) , allocatable :: D(:,:),SD(:,:),CL(:,:),SCL(:,:),CR(:,:),SCR(:,:),devicemos(:,:)
real (kind=prec) ,allocatable :: DCL(:,:),SDCL(:,:), DCR(:,:),SDCR(:,:)
real (kind=prec) ,allocatable :: CLPL(:,:),SCLPL(:,:),CRPR(:,:),SCRPR(:,:)
COMPLEX (kind=prec) ,allocatable :: selfPL(:,:),selfPR(:,:),selfCR(:,:),selfCL(:,:)
COMPLEX (kind=prec) ,allocatable :: selfD(:,:),energyoutput(:),selfdl(:,:),selfdr(:,:)


CHARACTER :: JOBVL, JOBVR
INTEGER :: INFO, LDA, LDB, LDVL, LDVR, LWORK, N,M
real (kind=prec),allocatable :: RWORK( : ),norm(:)
COMPLEX (kind=prec),allocatable :: A(:,:), ALPHA(:), B( :,:), BETA(:), VL( :,:), VR( :,:),WORK(:)
     ,resonanced(:,:),newfunc(:,:),UL(:,:),UR(:,:),WL(:,:),WR(:,:),CAP(:,:),specL(:,:),SPecr(:,:)
     ,transmission(:),UD(:,:),resonanceL(:,:),resonanceR(:,:),VECT(:),comp(:,:)
COMPLEX (kind=prec) :: greens,epsilon,out


integer, allocatable :: IPIV(:)
logical :: Flag


open(unit = 21, file = "energyvals.txt",status = 'old')
open(unit = 22, file = "Dataconst.txt",status = 'old')
open(unit = 27, file = "CAP.txt",status = 'replace')
open(unit = 32, file = "graphselfL.txt",status ='replace')
open(unit = 31, file = "graphgreens.txt",status ='replace')
open(unit = 33, file = "graphselfimagL.txt",status ='replace')
```

```fortran
open(unit = 34, file = "graphgreensimag.txt",status ='replace')
open(unit = 35, file = "graphselfR.txt",status ='replace')
open(unit = 36, file = "graphselfimagR.txt",status ='replace')

read(unit = 22, FMT = '(I10,I10,I10)')  Devicesize,contactsize,principalsize
read  (unit = 22, FMT = '(I10)')  size

allocate(D(devicesize,devicesize),SD(Devicesize,Devicesize),CL(contactsize,contactsize),SCL(
    contactsize,contactsize))
allocate(CR(contactsize,contactsize),SCR(contactsize,contactsize))
allocate(DCL(Devicesize,contactsize),SDCL(Devicesize,contactsize),DCR(Devicesize,contactsize),
    SDCR(devicesize,contactsize))
allocate(Pl(principalsize,principalsize),PR(principalsize,Principalsize),SPL(principalsize,
    Principalsize),SPR(principalsize,Principalsize))
allocate(CLPl(contactsize,principalsize),CRPR(contactsize,Principalsize),SCLPL(contactsize,
    Principalsize),SCRPR(contactsize,Principalsize))
allocate(selfPL(principalsize,principalsize),selfPR(principalsize,principalsize),selfCR(
    contactsize,contactsize),selfCL(contactsize,contactsize))
allocate(selfD(devicesize,devicesize),energy(size,size))
allocate(resonanced(devicesize,devicesize),selfdl(devicesize,devicesize),selfdr(devicesize,
    devicesize))
allocate(UL(devicesize,devicesize),UR(devicesize,devicesize),UD(devicesize,devicesize),WL(
    devicesize,devicesize),WR(devicesize,devicesize),specl(devicesize,devicesize),specr(
    devicesize,devicesize))



allocate(resonanceL(devicesize,devicesize),resonanceR(devicesize,devicesize))
allocate(vect(devicesize))
Allocate(A(devicesize,devicesize),B(devicesize,devicesize),VR(devicesize,devicesize),energyoutput
    (devicesize))
allocate(norm(devicesize),Comp(devicesize,devicesize),newfunc(devicesize,devicesize),CAP(
    devicesize,devicesize),Devicemos(devicesize,devicesize),energyoutput(Devicesize))


CALL readinputdata(size,principalsize,contactsize,devicesize,H0,H1,S0,S1,D,SD,devicemos,CL,SCL,CR
    ,SCR,DCL,SDCL,DCR,SDCR,PL,SPL,PR,SPR,CLPL,SCLPL,CRPR,SCRPR,energy)

SD = 0
do i = 1  ,devicesize
sd (i,i)=1
end do

H0 = D(1,1)
H1 = D(1,2)
S0 = SD(1,1)
S1 = SD(1,2)

D = 0
do i = 1  , devicesize−1,1

D(i,i)= H0
if ((i.eq.((devicesize/2)+1)).or.(i.eq.((devicesize/2)+1)))then
D(i+1,i)=H1
D(i,i+1)=H1
else
D(i+1,i)=H1
```

```fortran
D(i,i+1)=H1
end if
end do
D(devicesize,devicesize)= H0


scr=1
scl=1
spl = 1
spr = 1
sclpl = 0
scrpr = 0
sdCL = 0
sdcR = 0

DCL = 0
SDCL = 0
DCR = 0
SDCR = 0

CR = H0
SCR = SD(1,1)
CL = H0
SCL = SD(1,1)
DCL(1,1) = H1/2
DCR(devicesize,1) = H1/2
PL = H0
SPL = SD(1,1)
PR = H0
SPR = SD(1,1)
CLPL = H1
CRPR = H1


do i = 1,size
Print *, energy(i,i)
end do
A = D
B = SD

call diagonalise(A,B,devicesize,VR,energyoutput)

resonanceL = 0
resonanceR = 0
do i = 1 , devicesize

resonanceL(i,i)=energyoutput(i)
resonanceR(i,i)=energyoutput(i)
end do

flag = .false.
do j = 1, devicesize
do lambda = 0.01 ,1 ,0.01

if ((1-lambda).lt.0.0000001) then
flag =.true.
end if
```

```
CALL selfconsistent(resonanceL(j,j),S0,H0,S1,H1,D,SD,DCl,SDCl,Pl,SPl,Cl,SCl,ClPl,SClPl,
     principalsize,contactsize,devicesize,lambda,Vect,out)
resonanceL(j,j)=out

if (flag.eq..true.)then
do i = 1,devicesize
UL(i,j)=VECT(i)
end do
end if


CALL selfconsistent(resonanceR(j,j),S0,H0,S1,H1,D,SD,DCR,SDCR,PR,SPR,CR,SCR,CRPR,SCRPR,
     principalsize,contactsize,devicesize,lambda,Vect,out)


resonanceR(j,j)=out

if (flag.eq..true.)then

do k = 1 ,devicesize
UR(k,j)=VECT(k)
end do

end if
flag = .false.
end do !lambda end do



end do !J end do




CALL normalification (UL,SD,devicesize)

CALL normalification (UR,SD,devicesize)

deallocate(A)
allocate(A(devicesize,devicesize))

call sort (UL,devicesize,resonanceL)
call sort (UR,devicesize,resonanceR)



call removedegen(UL,resonanceL,D,S0,H0,S1,H1,SD,DCL,SDCL,PL,SPL,CL,SCL,CLPL,SCLPL,principalsize,
     contactsize,devicesize)
call removedegen(UR,resonanceR,D,S0,H0,S1,H1,SD,DCR,SDCR,PR,SPR,CR,SCR,CRPR,SCRPR,principalsize,
     contactsize,devicesize)

call buildW(UL,SD,D,resonanceL,devicesize,WL)

CAll inverse(UL,devicesize,A)


call buildW(UR,SD,D,resonanceR,devicesize,WR)
CAll inverse(UR,devicesize,A)
```

```fortran
CAP=WL+WR

deallocate(A)
allocate(A(devicesize,devicesize))


A = D+WL
B = SD

call diagonalise(A,B,devicesize,VR,energyoutput)

A = D+WR
B = SD

call diagonalise(A,B,devicesize,VR,energyoutput)

A = D+CAP
B = SD

call diagonalise(A,B,devicesize,VR,energyoutput)


UD = VR

do i = 1,devicesize
resonanced(i,i)=energyoutput(i)
end do


deallocate(A)
allocate(A(devicesize,devicesize))


call sort(VR,devicesize,resonanced)


do j = 1,devicesize
do i = 1,devicesize
write(27,*)CAP(i,j)
end do
end do


do i = 1 ,100
minval = -1 + 0.02*i

CALL selfenergycalc(minval,selfD,S0,H0,S1,H1,D,SD,DCL,SDCL,PL,SPL,CL,SCL,CLPL,SCLPL,principalsize
      ,contactsize,devicesize)
funkyn = ((S0*minval-H0)/(2*(S1*minval-H1)))
if ((funkyn*funkyn).gt.1) then
greens = (S1*(minval)-H1)*(funkyn-Dsqrt(funkyn*funkyn-1))
else
greens = cmplx(real((S1*minval-H1)*(real(funkyn))),-((S1*minval-H1)*(Dsqrt(1-funkyn*funkyn))))
end if
write(32,*)(-1 + 0.02*i),"    ",real(selfD(1,1))
write(33,*)(-1 + 0.02*i),"    ",icon(selfD(1,1))
```

```fortran
write(31,*)(-1 + 0.02*i),"    ",real(greens)
write(34,*)(-1 + 0.02*i),"    ",icon(greens)


CALL selfenergycalc(minval,selfD,S0,H0,S1,H1,D,SD,DCR,SDCR,PR,SPR,CR,SCR,CRPR,SCRPR,principalsize
     ,contactsize,devicesize)


write(35,*)(-1 + 0.02*i),"    ",real(selfD(devicesize,devicesize))
write(36,*)(-1 + 0.02*i),"    ",icon(selfD(devicesize,devicesize))


end do



Print *,'enter number of vals'


read (*,*) j


CALL Transmissionrun (D,S0,H0,S1,H1,SD,DCL,SDCL,PL,SPL,CL,SCL,CLPL,SCLPL,DCR,SDCR,PR,SPR,CR,SCR,
     CRPR,SCRPR,principalsize,contactsize,devicesize,WL,WR,j)


close(21,status = 'keep')
close(22,status = 'keep')
close(27,status = 'keep')
close(31,status = 'keep')
close(32,status = 'keep')
close(33,status = 'keep')
close(34,status = 'keep')
close(35,status = 'keep')
close(36,status = 'keep')
end program selfenergy


Subroutine inverse(U,size,A)
use accuracy


integer, INTENT(IN):: size
complex (KIND=PREC) , INTENT(IN)::U(size,size)
complex (KIND=PREC) , INTENT(out)::A(size,size)


COMPLEX (kind=prec),allocatable :: WORK(:)
integer, allocatable :: IPIV(:)
integer M,N,lda,Lwork


M = size
N = size
LDA = M
Lwork = N


allocate(WORK(size))
allocate(IPIV(N))


A = U
CAll ZGETRF(M, N, A,lda , IPIV, INFO)


Call ZGETRI(N, A, LDA, IPIV, WORK, LWORK, INFO)



END subroutine
```

```fortran
subroutine diagonalise(T,S,size,VR,energyoutput)
use accuracy

integer, INTENT(IN):: size
complex (KIND=PREC), INTENT(IN)::T(size,size),S(size,size)
complex (KIND=PREC), INTENT(out)::VR(size,size),energyoutput(size)
COMPLEX (kind=prec) ,allocatable :: WORK(:)
real (kind=prec),allocatable::  RWORK(:),Z(:,:)
COMPLEX (kind=prec),allocatable::alpha(:),beta(:),A(:,:),B(:,:),Test(:,:),VL(:,:)
integer ::i,j

N = size
LDA = size
LDB = size
LDVL = N
LDVR = N
Lwork = 2*N

allocate(ALPHA(size),BETA(size),WORK(Lwork),RWORK(8*size),B(size,size),A(size,size),Z(size,size),
    Test(size,size),VL(size,size))

A=T
B=S

call ZGGEV( "V","V", N, A,LDA, B, LDB, ALPHA, BETA,VL, LDVL, VR, LDVR, WORK, LWORK, RWORK , INFO)

CALL normalification (VR,S,size)

energyoutput = alpha/beta


end subroutine

subroutine selfenergycalc(energy,selfD ,S0,H0,S1,H1,D,SD,DC,SDC,P,SP,C,SC,CP,SCP,principalsize,
    contactsize ,devicesize)
use accuracy

integer ,INTENT(IN):: principalsize ,contactsize ,devicesize
real (kind=prec),intent(IN) :: D(devicesize ,devicesize ),SD(devicesize ,devicesize ),C(contactsize ,
    contactsize ),SC(contactsize ,contactsize )

real (kind=prec),intent(IN) :: H0,H1,S0,S1
COMPLEX (kind=prec):: selfP(Principalsize ,Principalsize ),selfC(contactsize ,contactsize ),greens
COMPLEX (kind=prec),Intent(out):: selfd(devicesize ,devicesize )
COMPLEX (kind=prec),allocatable ::A(:,:)
real (kind=prec)  ::renergy ,funkyn

real (kind=prec),intent (IN):: energy
real (kind=prec),intent(IN) :: DC(devicesize ,contactsize ),SDC(devicesize ,contactsize ),P(
    Principalsize ,Principalsize ),SP(PRincipalsize ,Principalsize )
real (kind=prec),intent(IN) :: CP(contactsize ,Principalsize ),SCP(contactsize ,Principalsize )

renergy = real(energy)
funkyn = ((S0*renergy−H0)/(2*(S1*renergy−H1)))
if ((funkyn*funkyn).gt.1) then
greens = (S1*(renergy)−H1)*(funkyn)−abs(S1*(renergy)−H1)*Dsqrt(funkyn*funkyn−1)
else
```

```fortran
greens = cmplx(real((S1*renergy-H1)*(real(funkyn))),-abs(S1*renergy-H1)*(Dsqrt(1-funkyn*funkyn)))
end if


selfP = P + greens

allocate(A(principalsize,principalsize))
call inverse ((renergy*SP - selfP),principalsize,A)


selfC = C + matmul((renergy*SCP-CP),matmul(A,transpose(renergy*SCP-CP)))

deallocate (A)
allocate(A(contactsize,contactsize))
call inverse ((renergy*SC - selfC),contactsize,A)
selfD = matmul(((renergy*SDC-DC)),matmul(A,transpose((renergy*SDC-DC))))
deallocate(A)



end subroutine



subroutine selfconsistent(energyin,S0,H0,S1,H1,D,SD,DC,SDC,P,SP,C,SC,CP,SCP,principalsize,
     contactsize,devicesize,lambda,Vect,out)
use accuracy
IMPLICIT NONE

Real (kind=Prec),External :: Icon

integer,intent(IN)::principalsize,contactsize,devicesize
real (kind=prec),intent(IN) :: D(devicesize,devicesize),SD(devicesize,devicesize),C(contactsize,
     contactsize),SC(contactsize,contactsize)
real (kind=prec),intent(IN) :: DC(devicesize,contactsize),SDC(devicesize,contactsize),P(
     Principalsize,Principalsize),SP(PRincipalsize,Principalsize)
real (kind=prec),intent(IN) :: CP(contactsize,Principalsize),SCP(contactsize,Principalsize)
real (kind=prec),intent(IN) :: H0,H1,S0,S1
real (kind=PREC),intent(in) :: lambda
integer :: k,i,l
real (kind=prec) ::last,thresh,funkyn,minval

COMPLEX (kind=prec),INTENT(IN) :: energyin
COMPLEX (kind=prec):: selfd(devicesize,devicesize),selfP(Principalsize,Principalsize),selfC(
     contactsize,contactsize)
COMPLEX (kind=prec) ::B(devicesize,devicesize),energyoutput(devicesize),VR(devicesize,devicesize)
     ,energy,greens,V(devicesize)
COMPLEX (kind=prec),INTENT(out) :: out,Vect(devicesize)
COMPLEX (kind=prec),allocatable ::A(:,:)

allocate(A(devicesize,devicesize))

energy=energyin
thresh = 0.00000001

last = energyin-thresh*3
k = 1

do while(abs(real(energy)-last).gt.thresh)

Last= (real(energy))
```

```fortran
CALL selfenergycalc(last,selfD,S0,H0,S1,H1,D,SD,DC,SDC,P,SP,C,SC,CP,SCP,principalsize,contactsize
     ,devicesize)

A = D + lambda * selfD

B = SD

CALL diagonalise(A,B,devicesize,VR,energyoutput)


minval=1
Do i = 1 ,devicesize
if ((abs(real(energyoutput(i))-last)).lt.minval) then
minval = abs(energyoutput(i)-last)
l = i
end if
end do

if (l.ne.k) then

end if
k=l
energy = energyoutput(l)

end do

out = energy
do i = 1,devicesize
Vect(i)=VR(i,l)
end do

end subroutine

subroutine readinputdata(size,principalsize,contactsize,devicesize,H0,H1,S0,S1,D,SD,devicemos,CL,
     SCL,CR,SCR,DCL,SDCL,DCR,SDCR,PL,SPL,PR,SPR,CLPL,SCLPL,CRPR,SCRPR,energy)
use accuracy

integer, INTENT(IN)::size,principalsize,contactsize,devicesize

REAL(kind=Prec),INTENT(INout):: D(devicesize,devicesize),SD(Devicesize,Devicesize),CL(contactsize
     ,contactsize),SCL(contactsize,contactsize),energy(size,size)
REAL(kind=Prec),INTENT(INout)::Devicemos(devicesize,devicesize),CR(contactsize,contactsize),SCR(
     contactsize,contactsize)
REAL(kind=Prec),INTENT(INout)::DCL(Devicesize,contactsize),SDCL(Devicesize,contactsize),DCR(
     Devicesize,contactsize),SDCR(devicesize,contactsize)
REAL(kind=Prec),INTENT(INout)::Pl(principalsize,principalsize),PR(principalsize,Principalsize),
     SPL(principalsize,Principalsize),SPR(principalsize,Principalsize)
REAL(kind=Prec),INTENT(INout)::CLPl(contactsize,principalsize),CRPR(contactsize,Principalsize),
     SCLPL(contactsize,Principalsize),SCRPR(contactsize,Principalsize)
REAl(kind=PRec),Intent(Inout)::H0,H1,S0,S1

open(unit = 1, File = 'Device.txt',status = 'old')
open(unit = 2, File = 'Deviceoverlap.txt',status = 'old')

open(unit = 3, File = "contactleft.txt",status = 'old')
```

```fortran
open(unit = 4, File = "Scontactleft.txt",status = 'old')
open(unit = 28, File = "contactright.txt",status = 'old')
open(unit = 7, File = "Scontactright.txt",status = 'old')

open(unit = 8, File = "Wireleft.txt",status = 'old')
open(unit = 9, File = "Sleft.txt",status = 'old')
open(unit = 10, File = "Wireright.txt",status = 'old')
open(unit = 11, File = "Sright.txt",status = 'old')

open(unit = 12, File = "Devicecontactleft.txt",status = 'old')
open(unit = 13, File = "SDevicecontactleft.txt",status = 'old')
open(unit = 14, File = "Devicecontactright.txt",status = 'old')
open(unit = 15, File = "SDevicecontactright.txt",status = 'old')

open(unit = 16, File = "contactleftwireleft.txt",status = 'old')
open(unit = 17, File = "Scontactleftwireleft.txt",status = 'old')
open(unit = 18, File = "contactrightwireRight.txt",status = 'old')
open(unit = 19, File = "ScontactrightwireRight.txt",status = 'old')

open(unit = 20, file = "devicemos.txt",status = 'old')

open(unit = 23, file = "H0f.txt",status = 'old')
open(unit = 24, file = "H1f.txt",status = 'old')
open(unit = 25, file = "S0f.txt",status = 'old')
open(unit = 26, file = "S1f.txt",status = 'old')

read (23,fmt = '(d20.14)')H0
read (24,fmt = '(d20.14)')H1
read (25,fmt = '(d20.14)')S0
read (26,fmt = '(d20.14)')S1


DO j = 1 , (Devicesize)
DO k = 1 , (Devicesize)
read (1,fmt = '(d20.14)')D(k,j)
read (2,fmt = '(d20.14)')SD(k,j)
read (20,fmt = '(d20.14)')devicemos(k,j)
end do
end do

DO j = 1 ,contactsize
DO k = 1 ,contactsize
read (3,fmt = '(d20.14)')CL(k,j)
read (4,fmt = '(d20.14)')SCL(k,j)
read (28,fmt = '(d20.14)')CR(k,j)
read (7,fmt = '(d20.14)')SCR(k,j)
end do
DO k = 1 , (Devicesize)
read (12,fmt = '(d20.14)')DCL(k,j)
read (13,fmt = '(d20.14)')SDCL(k,j)
read (14,fmt = '(d20.14)')DCR(k,j)
read (15,fmt = '(d20.14)')SDCR(k,j)
end do
end do

DO j = 1 ,principalsize
DO k = 1 ,principalsize
```

```fortran
read (8,fmt = '(d20.14)')PL(k,j)
read (9,fmt = '(d20.14)')SPL(k,j)
read (10,fmt = '(d20.14)')PR(k,j)
read (11,fmt = '(d20.14)')SPR(k,j)
end do

DO k = 1 ,contactsize
read (16,fmt = '(d20.14)')CLPL(k,j)
read (17,fmt = '(d20.14)')SCLPL(k,j)
read (18,fmt = '(d20.14)')CRPR(k,j)
read (19,fmt = '(d20.14)')SCRPR(k,j)
end do
end do

DO j = 1 ,size
read (21,fmt = '(d20.14)')energy(j,j)
end do

close(1,status =  'keep')
close(2,status =  'keep')
close(3,status =  'keep')
close(4,status =  'keep')
close(7,status =  'keep')
close(8,status =  'keep')
close(9,status =  'keep')
close(10,status = 'keep')
close(11,status = 'keep')
close(12,status = 'keep')
close(13,status = 'keep')
close(14,status = 'keep')
close(15,status = 'keep')
close(16,status = 'keep')
close(17,status = 'keep')
close(18,status = 'keep')
close(19,status = 'keep')
close(20,status = 'keep')
close(23,status = 'keep')
close(24,status = 'keep')
close(25,status = 'keep')
close(26,status = 'keep')

end subroutine

Real (Selected_real_kind(P=15,R=307)) function Icon(m)
use accuracy
implicit NONE
complex (kind=prec),intent(in)::m
Icon =  real((m-real(m))*cmplx(0,-1))
end function Icon

subroutine buildW(U,SD,D,resonance,devicesize,W)
use accuracy

integer  , intent(in)::devicesize
REAL (kind=prec),intent(in),dimension(devicesize,devicesize)::SD,D
complex (kind=prec),intent(in),dimension(devicesize,devicesize)::U,resonance
complex (kind=prec),intent(out),dimension(devicesize,devicesize)::W
```

```fortran
complex (kind=prec),dimension(devicesize,devicesize)::A

W=matmul(SD,U)
W=matmul(W,resonance)
call inverse(U,devicesize,A)

W=matmul(W,A)

W=W-D
end subroutine

subroutine Printmat(T,devicesize)
use accuracy
Real (kind=Prec),External :: Icon
integer,intent(in)::devicesize
complex (kind=prec),intent(in),dimension(devicesize,devicesize)::T
complex (kind=prec),dimension(devicesize,devicesize)::U
integer ::i,j

U=T

do i = 1 ,devicesize
do j = 1 ,devicesize
if ((real(U(j,i)).lt.0.000001).and.(real(U(j,i)).gt.-0.000001))then
 U(j,i)=U(j,i)-real(U(j,i))
end if

if ((icon(U(j,i)).lt.0.000001).and.(icon(U(j,i)).gt.-0.000001))then
U(j,i)=U(j,i)-cmplx(0,1)*icon(U(j,i))
end if
end do
end do


end subroutine

subroutine Sort(U,N,energy)
use accuracy
Integer ,intent(in)::N
Complex (kind=Prec),intent(inout),dimension(N,N)::U,energy
Complex (kind=Prec)::tmp,vect(N)
integer ::j,k

Do k = 2 ,N
Do j = k,2,-1
If(Real(energy(J,J)).lt.Real(energy(J-1,J-1))) Then
Tmp = energy(J,J)
Vect   = U(:,J)
Energy(J,J)    = Energy(J-1,J-1)
U(:,J) = U(:,J-1)
Energy(J-1,J-1)    = Tmp
U(:,J-1) =Vect
Else
GoTo 50
end if
end do
50 end do
```

```fortran
end subroutine

subroutine SortL(U,N,energy)
use accuracy
Integer ,intent(in)::N
Complex (kind=Prec),intent(inout),dimension(N,N)::U
Complex (kind=Prec),intent(inout),dimension(N)::energy
Complex (kind=Prec)::tmp,vect(N)
integer ::j,k

Do k = 2,N
Do j = k,2,-1
If(Real(energy(J)).lt.Real(energy(J-1))) Then
Tmp = energy(J)
Vect    = U(:,J)
Energy(J)    = Energy(J-1)
U(:,J) = U(:,J-1)
Energy(J-1)    = Tmp
U(:,J-1) =Vect
Else
GoTo 50
end if
end do
50 end do
end subroutine

subroutine Transmissionrun (D,S0,H0,S1,H1,SD,DC,SDC,P,SP,C,SC,CP,SCP,DCR,SDCR,PR,SPR,CR,SCR,CRPR,
     SCRPR,principalsize,contactsize,devicesize,WL,WR,j)
use accuracy
Real (kind=Prec),External :: Icon

integer,intent(IN)::principalsize,contactsize,devicesize,j
real (kind=prec),intent(IN) :: D(devicesize,devicesize),SD(devicesize,devicesize),C(contactsize,
     contactsize),SC(contactsize,contactsize)
real (kind=prec),intent(IN) :: DC(devicesize,contactsize),SDC(devicesize,contactsize),P(
     Principalsize,Principalsize),SP(PRincipalsize,Principalsize)
real (kind=prec),intent(IN) :: CP(contactsize,Principalsize),SCP(contactsize,Principalsize)
real (kind=prec),intent(IN) :: H0,H1,S0,S1
complex (kind=prec),intent(IN),dimension(devicesize,devicesize)::WL,WR

complex (kind=prec),dimension(devicesize,devicesize) :: selfd,specLself,SpecRself,CAP,SpecL,specR
Real (kind=Prec)::energy,Id(devicesize,devicesize)
complex (kind=Prec),dimension(devicesize,devicesize)::A,B ,comp,selfL,selfR
complex (kind=Prec)val
integer ::i,k
Complex (kind=Prec), allocatable ::transmission(:)

open(unit = 50, file = "trans.txt",status = 'replace')
open(unit = 51, file = "Gimag.txt",status = 'replace')
open(unit = 52, file = "transself.txt",status = 'replace')
open(unit = 53, file = "Gimagself.txt",status = 'replace')

Id = 0
do i = 1, devicesize
Id(i,i) = 1
end do
```

```
Comp = 0
do i= 1,j
energy = 2*i
energy = (energy/j)−1


CALL selfenergycalc(energy,selfD,S0,H0,S1,H1,D,SD,DC,SDC,P,SP,C,SC,CP,SCP,principalsize,
     contactsize,devicesize)
SpecLself=cmplx(0,1)*(selfD−transpose(conjg(selfD)))
selfL = selfD


CALL selfenergycalc(energy,selfD,S0,H0,S1,H1,D,SD,DC,SDC,P,SP,C,SC,CP,SCP,principalsize,
     contactsize,devicesize)

SpecRself=cmplx(0,1)*(selfD−transpose(conjg(selfD)))
selfR = selfd


selfD = selfL + selfR
B= (energy)*SD
B= B − (D+selfd)

call inverse(B,devicesize,A)


val = 0
do k = 1 , devicesize
Val=val+A(k,k)
end do
write(53,*)real((energy)),"␣␣␣␣",icon(val)

comp = matmul(specLself,A)
comp = matmul(comp,specRself)
comp = matmul(comp,transpose(conjg(A)))

val=0
do k = 1 , devicesize
Val=val+comp(k,k)
end do
write(52,*)real(energy),"␣␣␣␣",real(val)
end do


SpecL=cmplx(0,1)*(WL−transpose(conjg(WL)))
SpecR=cmplx(0,1)*(WR−transpose(conjg(WR)))
CAP = WL + WR
Comp = 0
do i= 1,j
energy = 2*i
energy = (energy/j)−1
B = (energy)*SD
B = B − (D+CAP)

call inverse(B,devicesize,A)

val = 0
do k = 1 , devicesize
Val=val+A(k,k)
```

```fortran
end do
write(51,*) real((energy)-1.0),"    ",icon(val)
comp = matmul(specL,A)
comp = matmul(comp,specR)
comp = matmul(comp,transpose(conjg(A)))


val=0
do k = 1 , devicesize
Val=val+comp(k,k)
end do
write(50,*) real(energy),"    ",real(val)
end do


close(50)
close(51)
close(52)
close(53)
end subroutine

subroutine normalification (VR,S,size)
use accuracy


integer , intent(in):: size
complex (kind=prec),intent(inout),dimension(size,size)::VR
real (kind=prec),intent(in),dimension(size,size)::S
integer :: i,j
Real (kind=prec)::normy(size,size)
complex (kind=prec),dimension(size,size)::test


normy=(Matmul(MAtmul(transpose(conjg(VR)),S),VR))


do j = 1,size
do i = 1,size


VR(i,j)=VR(i,j)/dsqrt(normy(j,j))
end do
end do


end subroutine

Subroutine removedegen(VR,resonance,D,S0,H0,S1,H1,SD,DC,SDC,P,SP,C,SC,CP,SCP,principalsize,
     contactsize,devicesize)
use accuracy


integer , intent(in)::devicesize,principalsize,contactsize
complex (kind=prec),intent(inout),dimension(devicesize,devicesize)::VR,resonance
real (kind=prec),intent(IN):: D(devicesize,devicesize),SD(devicesize,devicesize),C(contactsize,
     contactsize),SC(contactsize,contactsize)
real (kind=prec),intent(IN):: DC(devicesize,contactsize),SDC(devicesize,contactsize),P(
     Principalsize,Principalsize),SP(PRincipalsize,Principalsize)
real (kind=prec),intent(IN):: CP(contactsize,Principalsize),SCP(contactsize,Principalsize)
real (kind=prec),intent(IN):: H0,H1,S0,S1
integer :: i,j,k
complex (kind=prec),dimension(devicesize,devicesize)::A,B,TR,selfD,temp
```

```fortran
complex (kind=prec),dimension(devicesize)::energyoutput
real (kind=prec) :: tolerence,energy
logical :: degenerate

degenerate = .false.
tolerence = 0.00001


i = 0
j = 1



do
i = 0
do while(abs(real(resonance(j,j))-real(resonance((j+i+1),(j+i+1)))).lt.tolerence)

i = i+1
end do


if (i.gt.0) then


degenerate = .true.
energy = real(resonance(J,J))

CALL selfenergycalc(energy,selfD,S0,H0,S1,H1,D,SD,DC,SDC,P,SP,C,SC,CP,SCP,principalsize,
     contactsize,devicesize)


A = D + selfD
B = SD


CALL diagonalise(A,B,devicesize,TR,energyoutput)

temp=0
do k =1,devicesize
temp(k,k)=energyoutput(k)
end do


call sort(TR,devicesize,temp)



do k = j , j+i
resonance(k,k)=temp(k,k)
VR(:,k) = TR(:,k)
end do
end if



j= j+i+1
if (j.gt.devicesize-1)exit
end do



end subroutine
```

References

[1] T. M. Henderson, G. Fagas, E. Hyde, and J. C. Greer, "Determination of complex absorbing potentials from the electron self-energy," *The Journal of chemical physics*, vol. 125, no. 24, p. 244104, 2006.

List of Acronyms

BDT Benzene dithiol

CAPs Complex absorbing potentials

CI Configuration interaction

CSF Configuration state function

D-B-A Donor bridge acceptor

DFT Density functional theory

EA Electron affinity

ECP Effective core potential

GGA General gradient approach

GS Ground state

HC High conductance

HF Hartree Fock

HOMO Highest occupied molecular orbital

IP Ionisation potential

LC Low conductance

LDA Local density approximation

LUMO Lowest unoccupied molecular orbital

MC Medium conductance

MCCI Monte carlo configuration interaction

MECS Many electron correlated scattering

MIGS Metal induced gap states

NEGF Non equilibrium Greens function

NO Natural orbitals

PDOS Partial density of states

RAM Random access memory

RDM Reduced density matrix

SCF Self consistent field

VICI Voltage current configuration interaction